Accept-reject decision-making revealed via a quantitative and ethological study of *C. elegans* foraging

Authors: Jessica A. Haley[1,2], Tianyi Chen[2], Mikio Aoi[3,4]*, and Sreekanth H. Chalasani[2]**[Lead Contact]

Affiliations:

[1] Neurosciences Graduate Program, University of California San Diego, La Jolla, CA, USA.

[2] Molecular Neurobiology Laboratory, Salk Institute for Biological Studies, La Jolla, CA, USA.

[3] Halıcıoğlu Data Science Institute, University of California San Diego, La Jolla, CA, USA.

[4] Department of Neurobiology, University of California San Diego, La Jolla, CA, USA.

*Correspondence: maoi@ucsd.edu

**Correspondence: schalasani@salk.edu

ORCID: 0000-0001-6282-7124 (J.A.H), 0009-0003-7572-2155 (T.C.), 0000-0002-7052-880X (M.A.), 0000-0003-2522-8338 (S.H.C.)

Abstract

Decision-making is a ubiquitous component of animal behavior that is often studied in the context of foraging. Foragers make a series of decisions while locating food (food search), choosing between food types (diet or patch choice), and allocating time spent within patches of food (patch-leaving). Here, we introduce a framework for investigating foraging decisions using detailed analysis of individual behavior and quantitative modeling in the nematode *Caenorhabditis elegans*. We demonstrate that *C. elegans* make *accept-reject* patch choice decisions upon encounter with food. Specifically, we show that when foraging amongst small, dispersed, and dilute patches of bacteria, *C. elegans* initially *reject* several bacterial patches, opting to prioritize exploration of the environment, before switching to a more exploitatory foraging strategy during subsequent encounters. Observed across a range of bacterial patch densities, sizes, and distributions, we use a quantitative model to show that this decision to *explore* or *exploit* is guided by available sensory information, internal satiety signals, and learned environmental statistics related to the bacterial density of recently encountered and *exploited* patches. We behaviorally validated model predictions on animals that had been food-

deprived, animals foraging in environments with multiple patch densities, and null mutants with defective chemosensation. Broadly, we present a framework to study ecologically relevant foraging decisions that could guide future investigations into the cellular and molecular mechanisms underlying decision-making.

Keywords

decision-making, foraging, exploration, exploitation, dietary choice, *C. elegans*, quantitative modeling

Introduction

Decision-making is frequently defined as the selection of a course of action among several alternatives. The ubiquity and importance of decision-making has led to its use in describing a broad range of behaviors from taxes of unicellular organisms to economics and politics in human society [1, 2]. In decision neuroscience, laboratory experiments have investigated the behavioral choices of animals in well-controlled environments or tasks [3]. While these experiments have led to key insights into mechanisms underlying decision-making and related cognitive processes [4], a comprehensive understanding of decision-making remains elusive. Many researchers have advocated for a more neuroethological approach – suggesting that experiments designed to understand problems the brain evolved to solve offer a more rigorous framework [3, 5, 6]. Thus, one approach to enrich our understanding of decision-making is to look at the decisions made by animals foraging in naturalistic environments.

Foraging animals make a hierarchy of decisions to locate food (food search), choose between different food types (diet or patch choice), and allocate time spent within patches of food items (patch-leaving) [5, 7-10]. These foraging decisions often require that an animal *exploit* an environment for known resources or *explore* it for potentially better opportunities elsewhere [9, 11]. This exploration-exploitation trade-off requires cognitive computations such as learning the spatiotemporal distribution of food, route planning, estimation of food availability, and decision-making [12, 13]. According to optimal foraging theory, foragers may seek to maximize their rate of net energy gained over time [8, 9, 14] by using internal and external information to guide decision-making, especially in environments where resources are sparsely distributed or fluctuating. Although many studies have provided insight into the motivations, behavioral implementations, and genes associated with foraging decisions [9, 10], a more rigorous framework for exploring the neuronal mechanisms underlying foraging decisions is essential to establish a comprehensive understanding of decision-making.

The microscopic nematode *Caenorhabditis elegans* is well suited for investigating the cellular and molecular basis of foraging decisions [15]. A myriad of genetic tools, behavioral assays, and neuronal imaging techniques have been developed to take advantage of the species' quick reproductive cycle, isogeneity, optical transparency, and ease of maintenance [16-18]. While *C. elegans* typically feed upon a diversity of bacterial types in the wild [19], they are commonly maintained in the laboratory on agar plates containing large patches of the bacteria *Escherichia coli* as a food source

[16]. However, even in these simplified laboratory conditions and despite having a numerically simple nervous system of only 302 neurons [16, 20], *C. elegans* display complex and robust species-typical behaviors [21] involving learning and memory [22-25], and decision-making [26-31]. Recent studies have demonstrated that ecologically focused environmental enrichment permits identification of novel behaviors and gene functions in *C. elegans* and other animals [32-35].

Foraging animals often must make one of two types of decisions: *stay-switch* or *accept-reject*. *Stay-switch* decisions refer to scenarios where an individual experiences diminishing returns with the current action and must decide when to switch to a new action (e.g., patch-leaving and area-restricted search) [5, 7-10]. In contrast, *accept-reject* decisions refer to situations where an individual must decide between engaging with an option or ignoring it in search of a better one (e.g., diet or patch choice) [5, 8, 9]. *Stay-switch* decisions have been well described in *C. elegans* [25, 26, 36-41] and enable them to successfully explore an environment and exploit the bacteria within [28, 42-44]. However, to our knowledge, *accept-reject* decisions have not yet been demonstrated in *C. elegans*. While *C. elegans* have been shown to alter food preferences in a diet choice assay, this behavior has only been described by a set of *stay-switch* decisions [31, 36, 44]. The ability to make *accept-reject* decisions is likely advantageous for foraging in fluctuating or variable environments as rejecting an encountered food item of low quality creates the opportunity for a subsequent encounter with preferred food. Thus, while *C. elegans* can successfully forage in patchily distributed environments, it is not known whether *C. elegans* make decisions to *exploit* a patch of food upon encounter and how this decision-making process changes over a series of patch encounters.

In this study, we aimed to identify if *C. elegans* make *accept-reject* decisions upon encounter with bacterial patches. To answer this question, we performed a detailed analysis of the behavior of individual animals foraging in an ecologically relevant environment where bacterial patches were dilute and dispersed. In conditions where the bacterial density was much lower than that of previously visited patches, animals first explored the environment before *accepting* patches for exploitation. This explore-then-exploit strategy persists even when only one bacterial patch is present in the environment. Using a theoretical framework, we found that this initial exploration reflects a series of *accept-reject* decisions guided by signals related to the bacterial density of current and recently *explored* and *exploited* patches as well as the animal's state of satiety.

Results

103 ***C. elegans* forage in patchy environments with an explore-then-exploit strategy**

104 To investigate whether *C. elegans* make *accept-reject* decisions upon encounter with bacterial
105 patches, we observed the behavior of animals foraging on an agar surface containing an isometric
106 grid of small, low density bacterial patches (Figure 1A, Video 1-2). Animals were confined to an
107 arena where their behavior was recorded and tracked for 60 minutes (Figure 1A, Figure 1 –
108 supplement 1, Video 3). During this time, animals were observed to move about the arena (Figure
109 1A-C, Figure 1 – supplement 2, Video 4) with each animal encountering, on average, ~8.4 total
110 patches and ~5.3 unique patches during the one-hour recording (Figure 1D). These patch
111 encounters ranged in duration from seconds to tens of minutes and could be classified as either
112 short or long (2+ minutes) using a Gaussian mixture model (Figure 1E, Figure 1 – supplement 3).
113 Notably, animals were significantly more likely to stay on patch for longer durations at later time
114 points (Figure 1F) which corresponded to an overall increase in their probability of residing on
115 patch (Figure 1G, Figure 1 – supplement 4). Specifically, we found that while animals initially resided
116 on bacterial patches at levels close to those predicted by chance, an animal's probability of residing
117 on a bacterial patch increased significantly after ~10 minutes. These findings, that patch duration
118 and residence increased over time, suggest that animals are more likely to exploit an encountered
119 patch as time goes on.

120 Given that the bacterial density of the experimental patches was approximately 20 times
121 more dilute than that of conditions animals experienced during development and immediately
122 preceding the assay, it was possible that the initial delay in exploitation could be due to animals'
123 inability to detect the presence of bacteria in these more dilute patches. We therefore set out to
124 determine if animals detected patches at all time points. Previous studies have shown that *C. elegans*
125 display an immediate and marked slowdown upon encounter with the edge of a food patch and
126 sustain these slower speeds on food [28, 45]. Therefore, velocity can be used as a proxy for an
127 animal's ability to sense a bacterial patch. Following this precedent, we quantified the instantaneous
128 velocity of individuals in our assay (Figure 1H). We observed significant deceleration of an animal's
129 instantaneous velocity upon encounter with the patch edge (Figure 1I), with no obvious difference
130 between short duration, early time point (Figure 1J) and long duration, late time point (Figure 1K)
131 encounters. Animals consistently displayed marked slowdown when approaching the patch edge
132 (Figure 1L), achieving an average deceleration of -19.5 $\mu m/s^2$ upon encounter with the bacterial
133 patch (Figure 1M, Figure 1 – supplement 5). This slowdown was statistically significant for both long
134 and short duration encounters (Figure 1M). Further, consistent with *C. elegans* behavior on larger and

135 more densely seeded patches in other studies [46], animals in our assay maintained significantly lower
136 average velocities on patch (~52 μm/s) compared to off patch (~198 μm/s) (Figure 1N,O). These
137 results suggest that, despite detecting the availability of food during early patch encounters, *C. elegans*
138 opt to initially prioritize exploration of the environment before switching to a more exploitatory
139 foraging strategy during subsequent patch encounters.
140

141 **The timing of the switch from exploration to exploitation varies with bacterial density**

142 To determine whether this explore-then-exploit foraging strategy is dependent upon food-
143 related characteristics of the environment, we varied the density of the bacterial patches. By diluting
144 bacterial stocks and controlling growth time, we created 12 bacterial density conditions with relative
145 density ranging from 0 to ~200 (Figure 2A, Figure 2 – supplement 1-3). At the low end of this range
146 (densities less than ~0.5), animals do not appear to detect bacterial patches as indicated by on-patch
147 velocities matching those of animals foraging on bacteria-free (density 0) patches (Figure 2B,C). At
148 the high end of the range (density ~200), bacterial density is comparable to the environments
149 animals experienced during development and immediately prior to the assay (Figure 2 – supplement
150 2-3).

151 Previous studies have shown that in diet choice assays where animals are given the option
152 between patches of varying quality or density, animals spend more time on preferred patches [31, 36,
153 44]. We hypothesized that even when all patches in the environment are of equal density, an efficient
154 forager should still modulate the amount of time spent on the bacterial patches in a density-
155 dependent manner. To test this, behavior was recorded and tracked for one hour as animals foraged
156 in patchy environments matching one of the bacterial density conditions (Figure 2D, Figure 2 –
157 supplement 4). Consistent with our hypothesis, we found that the total time animals spent on
158 bacterial patches increased monotonically with increasing bacterial density following a sigmoidal
159 trend (Figure 2E). Further, the probability of an animal residing on patch as a function of time was
160 highly dependent on the bacterial density (Figure 2F, Figure 2 – supplement 5). At the highest
161 densities (50 and 200), animals spent nearly 100% of time in the assay on bacterial patches, while at
162 the lowest densities (0 to 0.3), animals spent chance levels of time on patch for the duration of the
163 experiment. At intermediate densities (0.5 to 10) animals initially resided on patches at rates
164 predicted by chance, later transitioning to more time spent on patch. Notably, this delayed increase
165 in patch residence is density dependent with animals switching earlier in environments with patches
166 of greater density.

Consistent with our previous observation that animals reside on patches for either short or long durations (Figure 1E), we observed two distinct patch encounter types: 1) short (less than 2 minute) patch visits and 2) long (often tens of minutes) patch visits (Figure 2G). Using a two-component Gaussian mixture model (GMM), we classified all encounters based on the duration of these patch visits and animals' average velocity during the encounter (Figure 2H, Figure 2 – supplement 6). We identified two behaviorally distinct clusters: 1) short duration and fast velocity (*explore*), and 2) long duration and slow velocity (*exploit*) encounters. The *explore* encounters suggest that an animal has *rejected* a patch, opting to continue exploration of the environment. In contrast, the *exploit* encounters suggest that an animal has *accepted* a patch and is consuming the bacteria within.

While we previously found that animals consistently slowed down upon encounter with the patch edge when foraging in relative density ~10 (Figure 1J-M), we observed that a large portion of short duration, exploratory encounters were not accompanied by this slow down (Figure 2 – supplement 7A-B), especially for the lowest bacterial densities tested. Therefore, to determine which exploratory encounters displayed evidence that the patch was detected by the animal, we further classified encounters by an animal's minimum velocity on patch, deceleration upon patch entry, and maximum change in the animal's velocity upon encounter (i.e., the difference between the peak velocity immediately before the patch encounter and the minimum velocity achieved during the patch encounter) (Figure 2I, Figure 2 – supplement 7, Video 5). We again observed two behaviorally distinct clusters: 1) large slow-down and slow on-patch velocity, and 2) small slow-down and fast on-patch velocity. We classified these encounters as *sensing* and *non-sensing*, respectively, using a semi-supervised quadratic discriminant analysis (QDA) approach. The presence of a slow-down and the subsequent continuation of slower on-patch velocity suggest that an animal sensed the bacteria, while the absence of a slowdown suggests that the animal likely did not perceive the encounter. For simplicity, we refer to 1) *non-sensing* encounters as *searching* (i.e., on-patch behavior that matches off-patch behavior where an animal appears to be searching for food); 2) *sensing*, short duration encounters as *sampling* (i.e., evaluating a patch's suitability as a food source, but ultimately *rejecting* the patch and continuing to explore the environment); and 3) *sensing*, long duration encounters as *exploiting* (i.e., *accepting* a patch and consuming its bacteria) (Figure 2J). Consistent with our interpretation of *searching* encounters, the average velocities that animals achieved during *search* on (~200 μm/s) and off (~207 μm/s) patch were similar, especially when compared to markedly slower on-patch velocities during *sample* (~114 μm/s) and *exploit* (~57 μm/s) encounters (Figure 2K). In

summary, we have identified three distinct patch encounter types: encounters that were not detected (*search*) and encounters that were detected with the animal subsequently deciding to *reject* (*sample*) or *accept* (*exploit*) the patch.

We next characterized how the frequency of encounter types varied as a function of time and patch density. The behavior of 443 animals (20-50 worms per condition) was tracked and classified at each time point (Figure 2L, Video 6). In low density conditions (0 to 0.3), animals spent nearly all of their time *searching* on or off patch. With increasing bacterial patch density, animals spent less time *searching* and more time *sampling* and *exploiting*. Animals foraging in medium density patches (0.5 to 10) initially spent most of their time *sampling* patches upon encounter. However, animals eventually switched to mostly *exploiting* patches. Animals foraging on high density patches (50 and 200) almost exclusively *exploited*. Classification of on-patch behavior across all densities tested revealed a consistent switch from *exploratory* behaviors (*searching* and *sampling*) to *exploitation* (Figure 2M) with the timing of the switch occurring earlier for animals foraging in environments with higher bacterial patch density (Figure 2N). The delay in exploitation corresponded to a comparatively large number of initial exploratory encounters with animals on medium density conditions (0.5 to 10) *exploiting* after an average of 4.8 to 18.7 exploratory encounters (Figure 2O). To summarize, for densities similar to those experienced immediately preceding the experiment (50 and 200), animals immediately *exploit* available bacteria. On the other hand, for bacterial densities that appear to be below an animal's sensory threshold (0 to 0.3), animals never *exploit* patches and spend the entire 60-minute assay *searching* for food. When foraging in medium density patches (0.5 to 10), animals initially explore the environment via a combination of *searching* and *sampling* encounters and eventually switch to *exploiting*. Notably, the timing of this switch is density-dependent with animals switching earlier when foraging on higher density patches.

Animals explore before exploiting even when only one patch is available

Given that bacterial patches within an environment were relatively invariable and that bacterial growth during the experiment was negligible (Figure 2 – supplement 3), it was surprising that animals were often willing to *reject* 10+ patches before *exploiting* a patch of the same density as those previously *rejected* (Figure 2O). This *sampling* behavior may be beneficial when food is patchily distributed in the environment as exploiting a dilute patch may result in a lost opportunity for future encounter with a higher quality patch. Thus, we hypothesized that an animal's willingness to *accept* a patch whose density matched that of a previously *rejected* patch could be a specific feature of a

patchily distributed environment where numerous observations of individual patches could contribute to learning the features of a changing environment. To address this, we observed whether animals were willing to *reject* a patch numerous times before *accepting* it even when only one patch is available in the environment. We created environments with single large (~8.3 mm) or small (~1.8 mm) diameter patches with relative density ranging from 0 to ~400 (Figure 3A-C). Behavior was tracked for 60 minutes as animals foraged in these environments (Figure 3D-E, Figure 3 – supplement 1-2). We found that even in these single patch environments, animals initially *explore* (*search* and *sample*) before *exploiting* (Figure 3F-G) in a density-dependent manner. Just as when foraging in a patchily distributed environment (Figure 2N), animals *explored* (*search* and *sample*) the small and large single patches numerous times prior to *exploiting* with the timing of this switch occurring significantly earlier with increasing bacterial density (Figure 3H-I). These results suggest that the explore-then-exploit strategy employed by *C. elegans* is not specific to a patchily distributed environment. Rather, animals may *sample* the same patch numerous times before deciding to *exploit*, especially when foraging on dilute patches. The decision of when to stop *exploring* and start *exploiting* is highly dependent upon the density of bacteria within a patch with the switch occurring earlier when animals encounter patches of higher density.

External and internal sensory information guide the decision to explore or exploit

While our behavioral analysis demonstrated that *C. elegans* modulate their decision to *explore* or *exploit* in a density-dependent manner, it remains unclear whether these animals use more complex cognitive processes such as learning and memory to guide their foraging decision. It is plausible that animals are making decisions using simple heuristics given only available sensory information about the current patch. However, previous studies have shown that food-related behaviors in *C. elegans* can be driven by internal states [31] as well as memories of the environment [25, 36, 42]. Thus, to better understand the factors driving the exploitation decision, we implemented a generalized linear model (GLM) to test how foraging decisions are influenced by the density of the current patch as well as additional food-related factors such as an animal's level of satiety and prior experience (Figure 4A).

We considered that the probability of exploiting a patch upon any given encounter can be described by a logistic function:

$$p(y_k = 1|\boldsymbol{\beta} \cdot \boldsymbol{x}_k) = \frac{1}{1 + e^{-\boldsymbol{\beta} \cdot \boldsymbol{x}_k}}$$

where $p(y_k = 1|\boldsymbol{\beta} \cdot \boldsymbol{x}_k)$ represents the conditional probability that an animal exploited during patch encounter k; $\boldsymbol{x}_k \in R^n$ is a vector of covariates; and $\boldsymbol{\beta} \in R^n$ is a vector of weights that describes how much each covariate influences the animal's choice. In models compared here, $\boldsymbol{x}_k$ includes a combination of a constant element and covariates that may empirically influence the decision to *exploit*. We considered the simplest model where every encounter is independent with fixed probability of *exploiting* (i.e., $p(y_k = 1|\beta_0)$) where β_0 represents the average animal's propensity to *exploit*. We compared this null model against a set of nested models containing covariates that vary from encounter to encounter and relate to: 1) the relative density of the encountered patch k (ρ_k), 2) the duration of time spent off food since departing the last *exploited* patch (τ_s), 3) the relative density of the patch encountered immediately before encounter k (ρ_h), and 4) the relative density of the last *exploited* patch (ρ_e). Using this model design (i.e., $\boldsymbol{\beta} \cdot \boldsymbol{x}_k = \beta_0 + \beta_k \rho_k + \beta_s \tau_s + \beta_h \rho_h + \beta_e \rho_e$), we assessed how each of these covariates influences the probability of *exploitation* at each patch encounter k (Figure 4A).

Given that our aim is to understand what factors influence an animal's decision to *explore* or *exploit*, we rationalized that encounters where the animal did not detect the presence of bacteria were unlikely to contribute to decision-making. Therefore, we excluded *searching* encounters from our analysis where the bacterial patch was not *sensed*. To account for the uncertainty in our classification of *sensing*, we probabilistically included patch encounters with frequency equal to the probability that the bacterial patch was *sensed* (Figure 4B) as previously estimated by semi-supervised QDA (Figure 2I, Figure 2 – supplement 7). In doing so, we simulated sets of observations of *sensed* (*sample* and *exploit*) encounters. Further, to account for the uncertainty in our classification of patch encounters as *exploration* or *exploitation*, we fit our GLM to the probability of *exploiting* $p(y_k = 1|\boldsymbol{z}_k)$ as previously estimated by GMM (Figure 2H, Figure 2 – supplement 6) rather than fitting to direct observations of exploitation y_k (see Models of exploitation probability).

When selecting covariates for our model, we calculated the Bayesian information criterion (BIC) – a model selection test to avoid overfitting by penalizing increases in the number of parameters – and observed improved model performance upon addition of each covariate (Figure 4 – supplement 1A). Further, we found that all covariates (i.e., ρ_k, τ_s, ρ_h, and ρ_e) significantly contribute to the decision to *exploit* $p(y_k = 1|\boldsymbol{\beta} \cdot \boldsymbol{x}_k)$ as indicated by coefficient values significantly greater than or less than zero (Figure 4C, Figure 4 – supplement 1B). Specifically, we found that β_k and β_s are significantly greater than zero which suggests that animals are more likely to *exploit*

patches with increasing patch density ρ_k and duration of food-deprivation τ_s. On the other hand, β_h and β_e are significantly negative, which suggests that the greater the density of a recently encountered or *exploited* patch, ρ_h and ρ_e, the less likely an animal should be willing to *exploit* the current patch.

In order to better understand how each of the covariates in our model affect the *exploitation* decision, we examined the probability of observing *exploitation* for the first time as a function of the cumulative number of patches an animal encountered. Exploitation events were simulated from a Bernoulli distribution with probability estimated by the model (i.e., $y_k|\boldsymbol{x}_k \sim \mathrm{Bern}\big(p(y_k = 1|\boldsymbol{\beta} \cdot \boldsymbol{x}_k)\big)$) or observed from our classification of *exploitation* (i.e., $y_k|\boldsymbol{z}_k \sim \mathrm{Bern}\big(p(y_k = 1|\boldsymbol{z}_k)\big)$). Although the probability of *exploiting* for the first time was not expressly fit by our model, this derived metric highlights the model's ability to predict the delay in *exploitation* observed for animals foraging on low to medium density bacterial patches in our experiments (Figure 4D, Figure 4 – supplement 2). For the simplest model where every encounter is independent with fixed probability of *exploiting* $p(y_k = 1|\beta_0)$, we find that the probability of *exploiting* for the first time is greatest for the first encounter and decreases for every subsequent encounter (Figure 4D, Figure 4 – supplement 2), fitting a geometric distribution.

We next considered whether the observed delay in *exploitation* could be explained by a simple density-dependent model (i.e., $p(y_k = 1|\beta_0 + \beta_k\rho_k)$). This model predicts that animals are more likely to *exploit* bacterial patches of greater density with probability proportional to the relative density of the current patch ρ_k. While this density-dependent model accurately predicted that the first *exploitation* occurs earlier on average for higher density patches, it also predicted that, regardless of patch density, the first *exploitation* is most frequently observed on the first encounter which did not match the observed distribution (Figure 4D, Figure 4 – supplement 2). We subsequently considered that the onset of food-deprivation during *exploration* of these low-density environments could drive the observed time-dependent delay in *exploitation*. We assume that animals become satiated during *exploitation* and use the duration of time an animal spent searching off-food since the last *exploitation* event (i.e., τ_s) as a proxy for the animal's likely decrease in satiety. With the addition of this satiety-related signal (i.e., $p(y_k = 1|\beta_0 + \beta_k\rho_k + \beta_s\tau_s)$), we observed a slight delay in when animals are predicted to first *exploit* for the lowest density conditions tested (Figure 4D, Figure 4 – supplement 2). To validate our finding that animals use a satiety-related signal to inform decision making, we applied our model to observations of animals foraging in patchily distributed

environments following 3 hours of food-deprivation (Figure 4 – supplement 3A-B). We found that only with the inclusion of a satiety-related covariate in our model, were we able to reliably predict the immediate *exploitation* that food-deprived animals exhibit (Figure 4 – supplement 3C). Altogether, these results suggest that animals use available external and internal sensory information to guide the decision to *exploit*.

Prior experience guides the decision to *explore* or *exploit*

Although the current patch density and satiety covariates significantly influence the decision to *exploit*, this model (i.e., $p(y_k = 1|\beta_0 + \beta_k\rho_k + \beta_s\tau_s)$) does not accurately predict the extent that *exploitation* was delayed. We hypothesized that because animals had experienced very densely seeded bacterial patches immediately prior to the assay, animals may have built an expectation that high density bacterial patches are available in the new environment. We would therefore expect an initial suppression in the probability of *exploiting* while animals updated their expectation using information learned from *sampling* patches in the current environment. To test whether the decision to *exploit* could be influenced by prior experience, we added a history-dependent covariate to our model (i.e., $p(y_k = 1|\beta_0 + \beta_k\rho_k + \beta_s\tau_s + \beta_h\rho_h)$ where ρ_h is the relative density of the patch encountered immediately before encounter k). We find that inclusion of the density of the most recently encountered patch significantly improves our prediction of *exploitation* (Figure 4D, Figure 4 – supplement 2). We then considered whether the animal's expectation of bacterial density in the environment might be a longer lasting memory. Specifically, we considered if the relative density of the most recently *exploited* patch ρ_e could have influenced the animal's decision to *exploit*. The addition of this second history-dependent term to our model (i.e., $p(y_k = 1|\beta_0 + \beta_k\rho_k + \beta_s\tau_s + \beta_h\rho_h + \beta_e\rho_e)$) further improved the fit of our model (Figure 4D, Figure 4 – supplement 2) suggesting that *C. elegans* use recent experiences of encountered and *exploited* patches to guide their decision to *exploit*. Animals may use this learned information to create and update an expectation for the relative density of bacterial patches available in their environment and compare that estimate against the density of a subsequently encountered patch. Altogether, these results suggest that animals use prior experience to keep track of available resources and modulate their decision to *explore* or *exploit*, a strategy that is highly beneficial for behavioral adaptation in a changing environment.

To validate the role of prior experience in guiding foraging decisions, we observed animals foraging in environments with multiple patch densities (Figure 4E, Figure 4 – supplement 4A-C).

355 Our model predicts that the lower the density of recently encountered and/or *exploited* patches, the
356 more likely an animal should be to *exploit* a subsequent patch. Without the history-dependent terms
357 ρ_h and ρ_e, our model predicts that no relationship should exist between prior experience and the
358 probability of *exploiting* the current patch. To test which model best fit the animals' behavior, we
359 calculated the conditional probabilities of *exploiting* $p(y_k = 1|\boldsymbol{\beta} \cdot \boldsymbol{x}_k)$ for this new multi-density,
360 multi-patch data set with more nuanced combinations of current (ρ_k) and recent patch (ρ_h and ρ_e)
361 density using the coefficients $\boldsymbol{\beta}$ learned previously (Figure 4C, Figure 4 – supplement 4D). We
362 observed significantly better predictions of *exploitation* probability for the model including prior
363 experience as compared to the model without the terms ρ_h and ρ_e (Figure 4F) as confirmed by a
364 likelihood-ratio test. We observed an augmentation in *exploitation* when animals move from low to
365 high density (e.g., 1 to 4 or 1 to 7) as predicted by the model with history-dependence, but not the
366 model without. It is important to note, that this improvement in prediction was achieved without
367 fitting the model to this new multi-density data set. In summary, our modeling results suggest that
368 animals evaluate bacterial density, monitor internal signals of satiety, and leverage prior experience to
369 drive their decision to *exploit* a bacterial patch upon encounter.
370

371 **Chemosensation is required for the evaluation of patch density**

372 The quantitative modeling applied in this study provides a useful framework for testing the
373 influence of behaviorally relevant features on decision-making. To validate this approach and further
374 elucidate how animals evaluate current and recent patch density, we assessed the foraging behavior
375 of mutants deficient in a sensory modality (Figure 4 – supplement 5). We found that animals with
376 reduced function of non-ciliated mechanoreceptor neurons due to a null mutation in the *mec-4* gene
377 behave similarly to wild-type N2 animals, displaying increasingly delayed *exploitation* as patch density
378 decreases (Figure 4G, Figure 4 – supplement 5). Contrastingly, animals with reduced function of
379 ciliated chemoreceptor neurons due to a null mutation in the *osm-6* gene displayed immediate
380 *exploitation* even while foraging on low density patches (Figure 4G, Figure 4 – supplement 5). These
381 results indicate altered decision-making in the chemosensory mutants. Specifically, it appears that the
382 influence of patch density on the *exploitation* decision is reduced in *osm-6* mutants and that these
383 animals are more likely to *accept* a patch by default.

384 To further elaborate on these findings, we fit our GLM to each of the three data sets (i.e.,
385 N2, *mec-4*, *osm-6*) and assessed the difference in the estimated distributions of coefficients $\boldsymbol{\beta}$ between

386 mutant and wild-type models (Figure 4H). We hypothesized that the density-related covariates (ρ_k,
387 ρ_h, and ρ_e) would have smaller magnitude (i.e., less influence on decision-making) for animals with
388 reduced sensation of bacterial density. Consistent with this hypothesis, we found a significant
389 reduction in the magnitude of the influence of current patch density (i.e., β_k) on the decision to
390 exploit in *osm-6* mutants. Further, we found a significant increase in the intercept β_0 in *osm-6* mutants
391 which corresponds to the overall increase in *exploitation* observed in these animals (Figure 4G, Figure
392 4 – supplement 5). These results suggest that chemosensation plays an important role in evaluating
393 the density of the current patch and that when this sensory modality is impaired, animals modify
394 their default behavioral strategy to prioritize *exploitation*. We also observed a marginal increase in our
395 estimate of the influence of recently *exploited* patches (i.e., β_e) in *osm-6* mutants which suggests that
396 reduced efficacy in the evaluation of current patch density also affects learning and memory of
397 patch density. No significant changes were detected in the *mec-4* mutants. Although we cannot rule
398 out a role for mechanosensation in contributing to the assessment of patch density, this modality
399 likely provides less salient information than chemosensation. Altogether, these results suggest that
400 chemosensation is necessary for the evaluation of patch density and that when this modality is
401 impaired, animals prioritize *exploitation*. Further, these results demonstrate that this quantitative
402 modeling approach can be used to probe mechanisms underlying decision-making.
403

404 **Discussion**

405

406 Like all foraging animals, *C. elegans* must choose between *exploiting* an environment for known
407 resources and *exploring* it for potentially better opportunities elsewhere [5, 7-11]. Previous studies
408 have shown that *C. elegans* use *stay-switch* decisions to efficiently explore a patchily distributed
409 environment and exploit the bacteria within [28, 42-44]. In this study, we show that *C. elegans* also
410 make *accept-reject* decisions while foraging. Specifically, we observe that animals often initially *reject* low
411 density bacterial patches, opting to prioritize exploration of the environment, before switching to a
412 more exploitatory foraging strategy during subsequent encounters. This explore-then-exploit
413 strategy was consistent across a range of bacterial patch densities, sizes, and distributions. In order
414 to better understand this phenomenon and identify the factors that contribute to the decision to
415 *exploit*, we leveraged a quantitative modeling approach to hypothesis testing. We found that animals
416 do not employ a default explore-then-exploit strategy; rather, this behavior reflects a series of *accept-*

417 *reject* decisions guided by multimodal information related to an animal's environment and internal
418 state. Specifically, we show that each decision to *explore* or *exploit* is informed by available sensory
419 information, internal satiety signals, and learned environmental statistics related to the bacterial
420 density of recently encountered and *exploited* patches.
421

422 **_C. elegans_ make _accept-reject_ foraging decisions**

423 While *C. elegans* have been shown to alter food preferences in a diet choice assay, this
424 behavior has only been described by a set of *stay-switch* decisions [31, 36, 44]. Specifically, *C. elegans*
425 were found to modulate their patch-leaving frequency to *stay* on high quality bacterial patches and
426 *switch* with declining food quality and quantity [26, 36, 40, 41]. The overall effect of leaving low
427 quality patches more frequently is that animals are more likely to reside on high quality patches.
428 Thus, *stay-switch* decision-making enables *C. elegans* to efficiently allocate time spent between
429 exploring or exploiting in a manner consistent with optimal foraging theory [5, 7-11]. However,
430 optimal foraging theory also predicts that an animal should never exploit (i.e., always *reject*) a low
431 density patch if higher density patches are sufficiently abundant as inclusion of the low density
432 patch type in the animals' diet decreases the overall rate of energy gained [5, 9]. Thus, while leaving
433 low density patches more frequently drives an overall increase in the rate of energy gained, it can still
434 result in sub-optimal foraging behavior.

435 Here, we demonstrate that *C. elegans* are capable of making *accept-reject* decisions upon
436 encounter with bacterial patches. We employed unbiased and quantitative methods – GMM and
437 semi-supervised QDA – to estimate whether animals *sensed* a patch and, if they did, whether they
438 *accepted* or *rejected* it. We found that animals initially *rejected* low density patches, opting to continue
439 exploration of the environment, and that this *reject* decision did not reflect an animal's inability to
440 detect the presence of bacteria in these dilute patches. Further, we found that the decision to *explore*
441 or *exploit* is density-dependent and robust across a range of bacterial densities, distributions, and
442 sizes. The initial preference for *exploration* during foraging on low density patches suggests that
443 animals may be *searching* for denser bacterial patches such as those experienced immediately
444 preceding the assay and throughout development. This explore-then-exploit strategy is advantageous
445 for animals when bacterial patch density is low or variable. On the other hand, we observed
446 immediate exploitation of high density patches. In these environments, an explore-then-exploit
447 strategy is disadvantageous, as delaying exploitation when patch density is already high results in
448 spending more energy on food search with no expected increase in energy gained during *exploitation*

449 of a subsequently encountered patch. Thus, consistent with an energy maximizing optimal forager,
450 *C. elegans explores* first when bacterial patch density is low, but immediately *exploits* when bacterial
451 patch density is sufficiently high. Altogether, our results demonstrate that *C. elegans* make a distinct
452 decision to either *explore* or *exploit* a patch upon encounter and that the density-dependence of this
453 decision is consistent with predictions from optimal foraging theory.
454 Our finding that *C. elegans* are willing to *reject* numerous encountered patches is somewhat
455 surprising, especially given that *C. elegans* likely possess limited spatial memory [25] and do not
456 appear to detect the presence of bacterial patches prior to encounter as slow-down only occurs
457 within one body-length of the patch edge (Figure 2B). Further, *C. elegans* are likely unaware of how
458 many patches are in the environment as evidenced by their willingness to *reject* a patch even when
459 only one patch is available. Taken together, this suggests that animals are "knowingly" passing up an
460 opportunity to *exploit* an immediately available food source for the potential opportunity to *exploit*
461 preferred food later. This type of behavior has been described min humans and other animals in the
462 context of delayed gratification [47, 48], intertemporal choice [47, 49, 50], self-control [51, 52], and
463 optimal stopping [53, 54]. Notably, few animals display the capacity for delayed gratification when
464 given the option between eating an immediately available but less preferred food item and waiting
465 for a preferred food item [55-58]. Even fewer animals are willing to wait if the delayed reward is not
466 visible or increases in quantity rather than quality [59, 60]. Our observation that *C. elegans* can exhibit
467 delayed gratification suggests that this and similar processes require less complex cognition than
468 previously considered or that we may have underestimated the cognitive capacity of *C. elegans*.
469

470 **Prior experience and satiety guide foraging decision-making**

471 *Stay-switch* decisions in *C. elegans* are strongly modulated by a variety of internal and external
472 sensory cues over a range of behavioral timescales. For example, patch-leaving frequency can be
473 modulated by an animal's prior experience [25, 42], metabolic status, arousal state [31], as well as the
474 presence of pathogens [61, 62], chemorepellents [63], predators [64, 65], and varying levels of
475 environmental O_2 and CO_2 [40, 66].
476 Here, we used a quantitative framework to show that prior experience (i.e., the density of
477 current and recently encountered and *exploited* bacterial patches) guides *accept-reject* decision-making.
478 According to early models in optimal foraging theory, foragers behave as if they have *complete*
479 *information* about the environment (e.g., animals are assumed to know the average density of bacterial
480 patches) [9]. Later theoretical and empirical work expanded models of patch choice to accommodate

481 situations where animals have *incomplete information* (e.g., environments with fluctuating resources)
482 and, therefore, must both acquire information and forage [8, 10, 67]. This work suggests that
483 animals may continuously sample areas in their environment to keep track of resource availability.
484 Here, we found that animals initially choose to *sample* patches and that the duration of this period of
485 *sampling* is correlated with the degree of mismatch between current and recently experienced and
486 *exploited* patches (i.e., animals spend more time *sampling* as the magnitude of difference between the
487 patch density experienced immediately before and during the experiment increases). When there is
488 no difference between current and prior experience (i.e., animals foraging on patches of relative
489 density 200), animals rarely *sample*. These results suggest that *C. elegans* use *sampling* as a way of re-
490 evaluating the overall quality of patches available in the environment when a change is detected.
491 Further, the results of our model suggest that animals likely use the information learned during
492 *sampling* encounters to guide their decision to *explore* or *exploit* on subsequent patch encounters. We
493 behaviorally validated this hypothesis by applying our model predictions to animals foraging in
494 environments with multiple patch densities. We predicted and observed that the lower the density of
495 recently encountered or *exploited* patches and the higher the density of the current patch, the more
496 likely an animal would be to *exploit*. These results suggest that *C. elegans* can learn and remember
497 features of recent experiences and use that learned information to guide efficient decision-making.
498 Incorporating prior experience into the decision to *explore* or *exploit* currently available food is highly
499 beneficial when foraging in a fluctuating environment. *C. elegans* thus may have evolved this ability to
500 maximize foraging in the wild where animals experience a boom-and-bust environment [68].
501 In addition to prior experience, internal state signals serve a critical role in modifying
502 decision-making in *C. elegans* [31, 69]. For example, food-deprived animals are more likely to cross an
503 aversive barrier (e.g., copper, primaquine, glycerol) in search of food as compared to well-fed
504 controls [69, 70]. Here, we find that a satiety-related signal likely drives the decision to *exploit*.
505 Specifically, our model suggests that as animals' satiety decreases, their willingness to accept a lower
506 quality patch increases. We confirmed this prediction by analyzing the behavior of food-deprived
507 animals, which immediately *exploit* even when bacterial patches are very dilute. Combined with the
508 effect of prior experience, these results suggest that the decision to *explore* or *exploit* likely requires
509 integration of food-related internal and external cues. Future studies should probe if additional
510 factors related to the animal's biotic and abiotic environment [35, 71-74] as well as alternative
511 motivations (e.g., reproduction and predatory avoidance) [75-78] further modify these foraging
512 decisions.

513

514 **Quantitative and ethological approach to investigating decision-making**

515 Naturalistic observations of *C. elegans* behavior are necessary to achieve a more complete
516 cellular, molecular, and genetic understanding of how the nervous system has evolved to drive
517 animal behavior. For example, large patches of densely seeded bacteria have primarily been used in
518 experiments assessing *C. elegans* foraging [20, 21, 79-81]. However, wild nematodes experience a
519 boom-and-bust environment [68] that may be more consistent with sparse, patchily distributed
520 bacteria [28]. Thus, just as quiescence is only observed on high quality bacterial patches [82],
521 additional behavioral states may be discovered when assessing foraging in dilute patchy
522 environments. By conducting detailed analyses of ecologically inspired foraging behaviors in
523 individual animals, we discovered that *C. elegans* make *accept-reject* decisions upon encounter with
524 bacterial patches. By studying foraging in these environments containing small, dilute bacterial
525 patches, we increased the frequency of opportunities for *accept-reject* decision-making (i.e., patch
526 encounters and patch-leaving events are more frequent) and decreased the condition-specific bias
527 towards *accept* decisions (i.e., animals are less likely to *accept* patches when moved between
528 environments of differing bacterial density). We expect that further investigation into naturalistic
529 behaviors could reveal additional insights into more complex behaviors and decision-making in *C.*
530 *elegans* and other animals.

531 In this study, we fine-tuned an assay that enables observation of ecologically relevant
532 decision-making in freely moving animals. We posit that future studies can leverage this assay to
533 investigate the neuronal mechanisms underlying decision-making. The frequency of decision-making
534 opportunities (i.e., numerous *accept-reject* decisions could be observed in the span of minutes) and
535 consistency of patch choice decisions across hundreds of animals and a range of environmental
536 conditions tested supports this claim. Further, we anticipate that the *accept-reject* decision occurs
537 during a narrow time window – possibly at the time of encounter with the patch edge or shortly
538 thereafter. Therefore, we expect that this assay could be adapted for experiments utilizing calcium
539 imaging in freely-moving animals [17, 30, 83-87] to monitor neuronal activity as animals make these
540 decisions.

541 Finally, we used simple quantitative models to dissect and validate the components
542 underlying decision-making. Specifically, we employed a logistic regression GLM which we adapted
543 to accommodate our uncertainty in classification of *sensing* and *exploitation* for each encounter. The
544 GLM enabled us to conduct a sequence of hypothesis tests probing the influence of food-related

signals on the decision to *exploit*. Further, the GLM enabled us to identify the simplest model that could explain the observed delay in *exploitation*. While even the null model predicted that, on average, numerous *exploratory* encounters were likely to occur before the first *exploitation*, models including satiety and prior experience significantly better predicted the extent of this delay. We demonstrated that we could validate these model predictions in food-deprived animals, animals exploring multiple patch densities, and animals with sensory deficiencies. We propose that this approach to investigating behavior and decision-making is incredibly powerful for refining hypotheses and enables subsequent investigation leveraging the diversity of cellular, molecular, and genetic tools available in *C. elegans*.

Abbreviations

Bayesian information criterion (BIC), Gaussian mixture model (GMM), generalized linear model (GLM), kernel density estimate (KDE), Kullback-Leibler (KL) divergence, lysogeny broth (LB), nematode growth medium (NGM), optical density at 600 nm (OD_{600}), quadratic discriminant analysis (QDA)

Acknowledgements

We thank members of the Chalasani lab for comments on the manuscript and James Fitzgerald for advice on modeling. This research was funded by grants from the National Science Foundation (J.A.H.), UCSD Undergraduate Summer Research Award (T.C.), NIH RO1 MH096881, Dorsett Brown Foundation, and Salk Innovation Grant (S.H.C.).

Author Contributions

Jessica Haley: Conceptualization, Methodology, Software, Validation, Formal analysis, Investigation, Resources, Data Curation, Writing – Original Draft, Writing – Reviewing & Editing, Visualization, Supervision, Project administration, Funding acquisition. **Tianyi Chen:** Investigation, Data Curation, Writing – Reviewing & Editing. **Mikio Aoi:** Methodology, Formal analysis, Writing – Reviewing & Editing, Visualization, Supervision. **Sreekanth Chalasani:** Conceptualization, Resources, Writing – Reviewing & Editing, Supervision, Funding acquisition.

Declaration of Interests

The authors declare no competing interests.

576 ## Materials and Methods

577

578 **Key Resources Table**

Reagent type (species) or resource	Designation	Source or reference	Identifier
bacterial strain (*Escherichia coli*)	OP50	Caenorhabditis Genetics Center	WBStrain00041969
bacterial strain (*Escherichia coli*)	OP50-GFP	Caenorhabditis Genetics Center	WBStrain00041972
organism/strain (*Caenorhabditis elegans*)	N2: wild isolate	Caenorhabditis Genetics Center	WBStrain00000001
organism/strain (*Caenorhabditis elegans*)	PR811: [osm-6(p811) V]	Caenorhabditis Genetics Center	WBStrain00030796
organism/strain (*Caenorhabditis elegans*)	TU253: [mec-4(u253) X]	Caenorhabditis Genetics Center	WBStrain00035037
software, algorithm	StreamPix 8	NorPix	RRID:SCR_015773
software, algorithm	WormLab	MBF Bioscience	RRID:SCR_017669
software, algorithm	MATLAB 2024a	Mathworks	RRID:SCR_001622
software, algorithm	Photoshop 2024	Adobe	RRID:SCR_014199
software, algorithm	Illustrator 2024	Adobe	RRID:SCR_010279
software, algorithm	Code for analysis	https://github.com/shreklab/Haley-et-al-2024	

579

580 **Data and Code Availability**

581 All data reported in this paper will be shared by the lead contact upon request. All original
582 code has been uploaded to GitHub (https://github.com/shreklab/Haley-et-al-2024) and are publicly
583 available as of the date of publication. Any additional information required to reanalyze the data
584 reported in this paper is available from the lead contact upon request. Source data files contain the
585 summarized data for all plots.

586

587 **Bacterial cultures**

588 Stock liquid cultures of the OP50 strain of *Escherichia coli* were prepared via inoculation of a
589 single colony in sterile lysogeny broth (LB) grown overnight at room temperature. Stock liquid
590 cultures were subsequently stored at 4°C for up to 6 weeks.

591 Solutions of OP50 for each experiment were prepared via a series of dilutions in LB (Figure
592 1 – supplement 1A). 50 mL of OP50 stock solution was centrifuged at 3000 rpm for 5 minutes.
593 After removal of supernatant, approximately 500 to 1000 μL of saturated liquid culture remained.

594 The bacterial density of this saturated solution was estimated by measuring the optical density at 600
595 nm (OD_{600}) of a 1:50 dilution of the homogenized solution on a spectrophotometer (Molecular
596 Devices SpectraMax Plus 384). The saturated solution was subsequently diluted to achieve an OD_{600}
597 of ~10 (μ = 10.22, σ = 0.31). Measurements of the number of colony forming units in the "10"
598 solution estimated 13.1×10^9 cells per mL on average. Additional densities (OD_{600} = {0.05, 0.1, 0.5, 1,
599 2, 3, 4, 5}) were prepared via dilution of the "10" solution with LB and kept on ice to prevent
600 bacterial growth. A "0" density solution was prepared with just LB.
601 For all experiments, these density solutions were seeded onto cold, low-moisture nematode
602 growth medium (NGM) plates (3% agar) to facilitate pipetting of small, circular, quick-drying
603 patches. Unless otherwise noted, seeded plates were immediately returned to 4°C after patches dried
604 to prevent bacterial growth. Plates were stored at 4°C for an average of 6 days before
605 experimentation.
606 For experiments using an OP50 strain expressing green fluorescent protein (OP50-GFP)
607 [88], cultures were prepared as above, but with the addition of 100 μg/mL of carbenicillin to the
608 liquid LB. All bacterial strains used in this study are listed in the Key Resources table.
609
610 **Nematode cultures**
611 *Caenorhabditis elegans* strains were maintained under standard conditions at 20°C on NGM
612 plates (1.7% agar) seeded with stock liquid culture of OP50 [16]. All experiments were performed
613 on young adult hermaphrodites, picked as L4 larvae the day before the experiment (μ= 24.6 hours, σ
614 = 3.4). Unless otherwise indicated, well-fed animals of the standard *C. elegans* strain N2 Bristol were
615 used for experiments. Transgenic strains were always compared to matched controls tested in parallel
616 on the same days. All *C. elegans* strains used in this study are listed in the Key Resources table.
617
618 **Assay preparation and recording**
619 ***Single-density, multi-patch assay***
620 Several days before the experiment, condition and acclimation plates were prepared (Figure 1
621 – supplement 1A). For the condition plates, a large circular arena (30 mm in diameter) made of clear
622 transparency film (6 mil, PET) was cut using a computer-controlled cutting machine (Cricut Maker
623 3) and placed in the center of a 10 cm petri dish filled with 25 mL of NGM (3% agar). These arenas
624 function to corral animals with a low probability of escape [89]. A pipetting template made of the
625 same material was designed and cut with an isometric grid consisting of 19 circular holes spaced 6

626 mm apart from center-to-center. The pipetting template was overlaid on top of the arena and 0.5 μL
627 of OP50 solution (OD_{600} = {0, 0.05, 0.1, 0.5, 1, 2, 3, 4, 5, 10}) was pipetted into each hole. After
628 drying, the template was immediately removed, and the petri dish lid replaced to prevent
629 contamination and dehydration. For two conditions ("1 (12H)" and "1 (48H)"), plates were seeded
630 with OD_{600} = 1 and then left at room temperature for 12 or 24 hours, respectively, prior to storage at
631 4°C. For all other conditions, plates were immediately stored at 4°C after drying. Acclimation plates
632 were prepared by seeding NGM (3% agar) plates with one large patch of 200 μL of OD_{600} = 1
633 grown for 24 hours at room temperature.
634 Approximately 24 hours before the experiment, acclimation plates and "1 (48H)" condition
635 plates were transferred from 4°C to room temperature. After plates warmed to room temperature
636 (~1 hour), 30-60 L4 animals were picked onto the acclimation plates. Plates were then stored at
637 20°C until the experiment for a combined bacterial growth time of approximately 48 hours (24
638 hours from freshly seeded to 4°C; 24 hours from 4°C to experiment). The combined bacterial
639 growth time for all condition plates was approximately 1 hour (μ= 1.16 hours, σ = 0.23) unless
640 otherwise noted as "12" (μ= 13.63 hours, σ = 0.50) or "48" hours (μ= 49.28 hours, σ = 2.94).
641 On the day of the experiment, each set of condition plates was transferred from 4°C to
642 room temperature. After one hour, 4 young adult animals were gently transferred to an empty NGM
643 plate to limit the spread of bacteria from acclimation to condition plates. Animals were then quickly
644 transferred to a condition plate. Animals were transferred using cylindrical plugs excised from clean
645 3% agar [64, 89].
646 Condition plates were subsequently placed face down on a piece of glass suspended above
647 an edge-lit backlight (Advanced Illumination). Recordings were acquired using PixeLink cameras
648 (PL-B741F) combined with Navitar lenses (1-60135 and 1-6044) and Streampix 8 software. Behavior
649 was recorded for one hour at 1024x1024 pixels and 3 frames per second (fps) with spatial resolution
650 of ~33 pixels per mm (μ= 32.68 pixels/mm, σ = 1.70).
651 The assay was repeated over numerous days with every condition assayed on each day when
652 possible. The order of seeding assay plates and recording behavior was randomized for each day to
653 compensate for the potential effects of time on animal age and bacterial density. Further, the average
654 temperature (μ= 21.99°C, σ = 0.95) and humidity (μ= 51.39%, σ = 11.67) during each experiment
655 were recorded. As a result of randomization, animal age, bacterial growth time, temperature, and
656 humidity did not significantly vary between density conditions.
657

658 ***Large, single-patch assay***

659 Plates were prepared as described for the single-density, multi-patch assay with the exception
660 that only one large patch was created by pipetting 20 μL of OP50 solution (OD_{600} = {0, 0.05, 0.1,
661 0.5, 1, 2, 3, 4, 5, 10}) into the center of the 30 mm diameter arena.

662

663 ***Small, single-patch assay***

664 Plates were prepared as described for the single-density, multi-patch assay with the exception
665 that only one small patch was created by pipetting 0.5 μL of OP50 solution (OD_{600} = {0, 0.5, 1, 5,
666 10}) into the center of a 9 mm diameter arena. Given the smaller arena size, only one young adult
667 animal was transferred into the arena. Behavior was recorded for one hour at higher spatial (μ=
668 104.76 pixels/mm, σ = 17.6) and temporal resolution (8 fps). The acquisition set-up was otherwise
669 unaltered except for the removal of a 0.25x Navitar lens (1-6044) from the light path.

670

671 ***Multi-density, multi-patch assay***

672 Plates were prepared as described for the single-density, multi-patch assay with the exception
673 that varying combinations of OD_{600} = {1, 5, 10} (i.e., OD_{600} = {1, 5, 10, 1+5, 1+10, 1+5+10}) were
674 pipetted onto each assay plate in a patterned isometric grid of 18 0.5 μL droplets. Behavior was
675 recorded for two hours. To compensate for the longer duration recordings, NGM agar plates were
676 poured without Bacto™ peptone (BD 211677) to prevent bacterial growth. The result of this
677 change was that the relative density of bacterial patches was ~30% lower as compared to
678 comparable 0.5 μL patches in the single-density, multi-patch assay and the small, single-patch assay
679 (Figure 2 – supplement 2-3). Further, to prevent censorship of our data at the beginning of the
680 recording, we formed a small droplet of S-Complete solution [90] in the middle of the arena where
681 no bacterial patch was placed. Animals were transferred to this droplet using an eyelash pick
682 immediately prior to the assay plate being placed on the imaging set-up. The recording was started
683 once the droplet evaporated and animals were free to crawl about the arena. This process ensured
684 that recordings began prior to an animal's first patch encounter.

685

686 **Bacterial patch location detection**

687 Most bacterial densities tested in these experiments were too dilute to be visible under
688 normal imaging conditions. Therefore, several strategies were employed to accurately detect the
689 location of bacterial patches. First, a small reference dot was cut into the arena and pipetting

690 templates enabling consistent and traceable patch placement. Further, prior to each behavior
691 recording, a "contrast" video was acquired wherein a piece of dark cardstock was passed between
692 the light source and the condition plate (Figure 1 – supplement 1B-D, Video 2). This produced an
693 effect where diffraction of light through the patches provided enough contrast to view the patches.
694 Binary masks of the circular arena and patches were extracted from these videos in MATLAB using
695 the Image Processing Toolbox and further refined manually in Photoshop (Adobe, 2024). Arena
696 masks were used to calculate the scale (pixels/mm) of each image. In early experiments, the
697 "contrast" video was acquired prior to worms being added to the condition plate, which resulted in
698 displacement of the arena within the camera's field-of-view. Image registration using MATLAB's
699 Computer Vision Toolbox was performed to accurately map the patches detected in the "contrast"
700 video onto the behavioral recording.
701
702 **Bacterial patch density estimation**
703 As described above (see Assay preparation and recording), we varied the relative density of
704 bacterial solutions by diluting OP50 in LB and growing patches for different lengths of time. As a
705 result of these procedures, the relative bacterial density throughout the assay was not known and
706 needed to be estimated. To determine the relative density of these bacterial patches, we seeded
707 plates with fluorescently labeled OP50-GFP under identical conditions as in our assays (Figure 2 –
708 supplement 1A). We imaged these bacterial patches for several hours using a Zeiss Axio Zoom.V16.
709 Images were analyzed using the Image Processing Toolbox in MATLAB. After correcting for
710 inconsistent illumination across the field-of-view and normalizing images using matched controls
711 (Figure 2 – supplement 1B-C), we detected the location of each bacterial patch and extracted a
712 fluorescence intensity profile along each patch's radius (Figure 2 – supplement 1D). Consistent with
713 previous studies, we found that even in extremely dilute conditions, bacterial density was greater at
714 the patch edge where actively proliferating bacteria are concentrated [43, 91]. Therefore, we detected
715 the patch edge and computed the peak amplitude of each bacterial patch at all time points assayed
716 (Figure 2 – supplement 1E). We then performed linear regression on the values for each condition
717 to create models of peak amplitude as a function of time. For low density conditions (i.e., OD_{600} =
718 {0.05, 0.1}) of small patches, fluorescent signals could not be detected. We therefore estimated these
719 functions from a multinomial regression of values taken from OD_{600} = {0.5, 1, 2}. Through this
720 process, we used the total time that bacteria were allowed to grow at room temperature for each
721 condition plate to estimate the peak amplitude at each time point (Figure 2 – supplement 3). Finally,

722 to minimize confusion about density conditions between experiments, we computed values for
723 relative density by linearly scaling estimated peak amplitude values so that 0.5 μL patches seeded
724 with OD_{600} = 10 and grown for 1 hour at room temperature would have relative density equal to 10.
725 We labeled each condition using the relative density rounded to one significant digit.
726
727 **Behavioral tracking**
728 WormLab® (MBF Bioscience) was used for tracking animal behavior (Figure 1 – supplement
729 1E-G, Video 3). For each video, we adjusted thresholds for pixel intensity and worm dimensions to
730 enable automatic tracking. WormLab then fit the worm's body at every frame and stitched together a
731 track of each worm across frames. Subsequent manual corrections were required for instances
732 where the software created new worm tracks. This occurred most frequently when animals: 1)
733 encountered the arena border, 2) collided with each other, or 3) overlapped with bubbles or dust
734 particles embedded in the agar. To correct for these discontinuities, we manually "stitched" worm
735 tracks together enabling us to keep track of each animal's location throughout the duration of the
736 experiment. We exported the location of each animal's midpoint for further analysis in MATLAB
737 (Mathworks, 2024a). For small, single-patch assays where higher spatial resolution enabled reliable
738 distinction between the head and tail of the animal, we manually confirmed the head-tail and
739 exported 25 points along the animal's midline (Figure 1 – supplement 2A-C).
740 Animals were excluded from analyses when 1) the animal's location could only be tracked for
741 less than 75% of the video due to the animal escaping the arena and when 2) the location of
742 bacterial patches could not be reliably assessed due to missing or low-quality "contrast" videos (see
743 Bacterial patch location detection).
744
745 **Patch encounter detection**
746 As the head position of animals in our experiments was difficult to track due to low spatial
747 resolution and limited automated detection of head position using WormLab, we instead tracked the
748 midpoint position of the worm's body and estimate patch encounters using a set of measured
749 criteria. To do this, we tracked the behavior of worms in higher resolution (~105 pixels/mm
750 compared to ~33 pixels/mm and 8 fps compared to 3 fps), single patch assays (Figure 1 –
751 supplement 2A-C). We found that when the head of the animal was in contact (i.e., within 1 pixel)
752 with the patch edge (see Bacterial patch location detection), the animal's midpoint was on average
753 0.46024 mm away (Figure 1 – supplement 2D). We therefore defined a patch encounter as the time

754 when an animal's midpoint came within 0.46024 mm of the patch edge. However, this definition led
755 to two types of errors: 1) putative entry events where the animal merely passed by the patch and 2)
756 putative leaving events where the animal did not fully leave the patch.
757 To remove putative entry events where the animal nearly passed by the patch, we defined an
758 additional distance threshold based on the distance between the animal's midpoint and the patch
759 edge for all time points when the head was within the patch (Figure 1 – supplement 2E). The
760 midpoint was almost always (99% of time) within 0.28758 mm of the patch edge. Therefore, we
761 removed patch encounters where the midpoint never got closer than 0.28758 mm from the patch
762 edge. Although this criterion removes most "near miss" events, some events remain where the
763 animal approached the patch, but its head never entered. Further decreasing this threshold (e.g.,
764 midpoint must be on patch) would result in real events being excluded due to the animal taking on
765 specific postures where the midpoint remains outside the patch while feeding within the patch.
766 Therefore, we chose to be more liberal (i.e., more false positive patch encounters than false
767 negatives) in our detection of patch encounters. Subsequent analysis of these putative patch
768 encounters removed the majority of remaining false positives (see Patch encounter classification as
769 sensing or non-sensing).
770 To address putative leaving events and avoid splitting a single patch encounter into multiple
771 encounters, we considered that a lawn leaving event is most frequently defined as an event where all
772 body parts have left the patch [31]. When tracking only the midpoint, it is not possible to ensure that
773 the worm's entire body has exited the patch. Using the criterion that an animal exits a patch when it's
774 midpoint exceeds 0.46024 mm from the patch edge accurately predicts exit events most of the time,
775 but under certain scenarios (e.g., animals maintain an outstretched feeding posture [64]) false leaving
776 events were detected. To exclude these leaving events, we analyzed the variability in the distance
777 from the midpoint to the patch edge during on- and off-patch events (Figure 1 – supplement 2F).
778 We found that on-patch events had low distance variability while off-patch events displayed a
779 bimodal distribution, with some events having high variability as expected, and some events having
780 low variability. We fit a two-component Gaussian mixture model to the off-patch distance variability
781 and found that low variability leaving events could be reliably excluded when the standard deviation
782 of off patch distances was less than 0.13259. We subsequently combined putative patch encounters
783 where variability was below this threshold, resulting in fewer overall encounters.
784
785 **Patch encounter classification as exploration or exploitation**

To classify patch encounters as *exploration* or *exploitation* events, patch encounters were detected (see Patch encounter detection) and two features were computed: 1) duration of patch encounter and 2) average on-patch velocity. Both the duration and velocity features displayed a bimodal distribution with two visible clusters: one with short duration encounters and high on-patch velocity and one with long duration encounters and low on-patch velocity (Figure 2 – supplement 6A). To classify patch encounters into one of these clusters, we used a two-component Gaussian mixture model (GMM) to estimate $p(y_k = 1|\boldsymbol{z}_k)$ where for each encounter k, $\boldsymbol{z}_k$ are the log transforms of the duration and average velocity of the patch encounter, $y_k = 1$ indicates an *exploitation*, and $y_k = 0$ indicates an *exploration*. We optimized the GMM across cross-validated replicates with respect to the regularization value α to minimize the posterior variance given by

$$\sum_k p(y_k = 1|\boldsymbol{z}_k)\, p(y_k = 0|\boldsymbol{z}_k)$$

We found that $\alpha = 0.025$ best separated the *exploration* and *exploitation* clusters (Figure 2 – supplement 6B). The posterior probability of *exploitation* $p(y_k = 1|\boldsymbol{z}_k)$ was subsequently estimated for all encounters (Figure 2 – supplement 6C-D).

Patch encounter classification as sensing or non-sensing

To classify patch encounters as *sensing* or *non-sensing* events, we computed animals' 1) deceleration upon encounter with the patch edge, 2) minimum velocity during the patch encounter, and 3) maximum change in velocity between the peak velocity immediately prior to the start of the patch encounter and the minimum velocity during the encounter (Figure 2 – supplement 7A). Deceleration was defined as the slope of the line fit on an animal's velocity between -1.5 seconds before and 6.5 seconds after the start of an encounter. Minimum velocity was defined as the absolute minimum velocity observed during the duration of the patch encounter. The maximum change in velocity was computed by subtracting the minimum velocity from the peak velocity within 10 seconds of the patch encounter. The combination of these three metrics reveals two non-Gaussian clusters representing encounters where animals sensed the patch (i.e., slow minimum velocity, large changes in velocity) or did not appear to detect it (i.e., maintained fast minimum velocity, with little to no change). We estimated the probability of *sensing* $p(v_k = 1|\boldsymbol{w}_k)$ where for each encounter k, $\boldsymbol{w}_k = (s_k, t_k, u_k)$ are the three velocity-related features (i.e., minimum velocity, deceleration, and maximum change in velocity, respectively), $v_k = 1$ indicates an encounter that was

sensed, and $v_k = 0$ indicates an encounter which did not appear to be *sensed*. Using a semi-supervised approach to quadratic discriminant analysis (QDA), we labeled a subset of all encounters and iteratively estimated labels on the remaining unlabeled data (Figure 2 – supplement 7C-E, Video 4). All encounters with bacteria-free patches (i.e., LB only, relative density 0) were labeled as true negatives $v_k = 0$. Across 1000 replicates, we probabilistically included *exploitation* encounters $y_k = 1$ estimated from the distribution $y_k|\boldsymbol{z}_k \sim \mathrm{Bern}\big(p(y_k = 1|\boldsymbol{z}_k)\big)$ as true positives $v_k = 1$. Using this approach, the conditional probability of *sensing* $p(v_k = 1|\boldsymbol{w}_k)$ was iteratively estimated for all encounters using QDA and averaged across replicates.

Although we found that the two clusters were successfully discriminated by this semi-supervised QDA approach, a small subset of encounters (252 of 20109 encounters) could not be reliably classified in this manner as the onset of the patch encounter was not observed. This type of data censoring occurred when the behavioral recording was started after the animal had already entered the patch. Although we could compute deceleration-related metrics for these encounters with the assumption that the animal entered the patch at the first frame, these measurements are censored with a bias towards lower magnitudes of deceleration. Therefore, to better predict the conditional probabilities of *sensing* for these 252 encounters, we assumed that the minimum velocity on-patch s_k was a reliable metric and marginalized the conditional probabilities over the other two metrics (t_k and u_k) as defined by

$$p(v_k = 1|s_k) = \int_{-\infty}^{\infty}\int_{-\infty}^{\infty} p(v_k = 1 \mid s_k, t_k, u_k)\, p(t_k, u_k \mid s_k)\; dt\, du$$

We numerically integrated using an adaptive quadrature method over the product of the QDA estimated conditional probability distribution and the kernel density estimate of the joint probability distribution. This procedure resulted in a slight increase ($\mu = +0.0615$, $\sigma = 0.1832$) in our estimation of the probability of *sensing* (Figure 2 – supplement 7H).

Altogether, this classification approach resulted in low false positive and false negative rates. Specifically, 3.35% of the time encounters with bacteria-free patches were incorrectly identified as *sensing* while 2.92% of the time *exploitatory* encounters were incorrectly identified as *non-sensing*. Further, this classification removed many of the remaining near miss patch encounters in which animals came close to but did not truly enter the patch (see Patch encounter detection). For all analyses, we excluded near miss encounters where the animal's midpoint never entered the patch and the probability of *sensing* was less than 5% (i.e., $p(v_k = 1|\boldsymbol{w}_k) < 0.05$).

Models of exploitation probability

We consider that the probability of *exploiting* a patch upon any given encounter can be described by a logistic function:

$$p(y_k = 1|\boldsymbol{\beta} \cdot \boldsymbol{x}_k) = \frac{1}{1 + e^{-\boldsymbol{\beta} \cdot \boldsymbol{x}_k}}$$

where $p(y_k = 1|\boldsymbol{\beta} \cdot \boldsymbol{x}_k)$ represents the conditional probability that an animal exploited during patch encounter k; $\boldsymbol{x}_k \in R^n$ is a vector of covariates; and $\boldsymbol{\beta} \in R^n$ is a vector of weights that describes how much each covariate influences the animal's choice. In models compared here, $\boldsymbol{x}_k$ includes a combination of a constant element as well as covariates that may empirically influence the decision to exploit: 1) the log-transformed relative density of the encountered patch k (ρ_k), 2) the duration of time spent off food since departing the last *exploited* patch (τ_s), 3) the log-transformed relative density of the patch encountered immediately before encounter k (ρ_h), and 4) the log-transformed relative density of the last *exploited* patch (ρ_e).

The observations of *exploitation* and *sensation* for our data are derived predictions from classification models (see Patch encounter classification as exploration or exploitation and Patch encounter classification as sensing or non-sensing). As such, the labels for both whether a patch encounter was *sensed* by the animal $p(v_k = 1|\boldsymbol{w}_k)$ and whether the animal *exploited* the patch $p(y_k = 1|\boldsymbol{z}_k)$, are both reported as probabilities rather than direct measurements.

To account for uncertainty in *sensation*, we produced 100 sets of "encounter sampled" observations wherein we probabilistically included *sensed* encounters $v_k = 1$ estimated from the distribution $v_k|\boldsymbol{w}_k \sim \text{Bern}\big(p(v_k = 1|\boldsymbol{w}_k)\big)$. In doing so, we assume that only patch encounters recognized by the animal guide the decision to *exploit* (Figure 4B). After removing *non-sensing* encounters where $v_k = 0$, we defined observations of all covariates (i.e., ρ_k, τ_s, ρ_h, and ρ_e) using only *sensed* encounters.

To account for uncertainty in *exploitation* we modified the standard maximum likelihood. To understand our approach, consider that standard logistic regression models binary observations as realizations of the Bernoulli distribution $y_k|\boldsymbol{x}_k \sim \text{Bern}\big(p(y_k = 1|\boldsymbol{\beta} \cdot \boldsymbol{x}_k)\big)$ and that the likelihood for this model is given by

$$\prod_k p(y_k = 1|\boldsymbol{\beta} \cdot \boldsymbol{x}_k)^{y_k} \left(1 - p(y_k = 1|\boldsymbol{\beta} \cdot \boldsymbol{x}_k)\right)^{1-y_k}$$

However, we do not have direct observations of y_k and cannot evaluate the logistic likelihood directly. Rather, we have posterior probabilities of *exploitation* determined by a classifier, denoted by $p(y_k = 1|\boldsymbol{z}_k)$, where $\boldsymbol{z}_k$ are a set of velocity-related features that are distinct from $\boldsymbol{x}_k$ (see Patch encounter classification as exploration or exploitation). Thus, rather than maximizing the Bernoulli likelihood, we accommodate our uncertainty about y_k by learning the regression parameters that minimize the Kullback-Leibler (KL) divergence between $p(y_k|\boldsymbol{\beta} \cdot \boldsymbol{x}_k)$ and the reference probability distribution $p(y_k|\boldsymbol{z}_k)$ as given by

$$\begin{aligned}
\mathcal{D}_{KL}[p(y_k|\boldsymbol{z}_k)||p(y_k|\boldsymbol{\beta} \cdot \boldsymbol{x}_k)] &\equiv \sum_{y_k} p(y_k|\boldsymbol{z}_k) \log\left[\frac{p(y_k|\boldsymbol{z}_k)}{p(y_k|\boldsymbol{\beta} \cdot \boldsymbol{x}_k)}\right] \\
&= C_{\boldsymbol{\beta}} - \sum_{y_k} p(y_k|\boldsymbol{z}_k) \log[p(y_k|\boldsymbol{\beta} \cdot \boldsymbol{x}_k)] \\
&= C_{\boldsymbol{\beta}} - \sum_{y_k} p(y_k|\boldsymbol{z}_k) \log\left[p(y_k|\boldsymbol{\beta} \cdot \boldsymbol{x}_k)^{y_k} \left(1 - p(y_k|\boldsymbol{\beta} \cdot \boldsymbol{x}_k)\right)^{1-y_k}\right] \\
&= C_{\boldsymbol{\beta}} - p(y_k = 1|\boldsymbol{z}_k) \log[p(y_k|\boldsymbol{\beta} \cdot \boldsymbol{x}_k)] \\
&\quad -\left(1 - p(y_k = 1|\boldsymbol{z}_k)\right) \log[1 - p(y_k|\boldsymbol{\beta} \cdot \boldsymbol{x}_k)] \\
&= C_{\boldsymbol{\beta}} \\
&\quad - \log\left[p(y_k|\boldsymbol{\beta} \cdot \boldsymbol{x}_k)^{p(y_k=1|\boldsymbol{z}_k)}\left(1 - p(y_k|\boldsymbol{\beta} \cdot \boldsymbol{x}_k)\right)^{1-p(y_k=1|\boldsymbol{z}_k)}\right]
\end{aligned}$$

where C_β is a term that is constant with respect to $\boldsymbol{\beta}$, and the second term is equivalent to the logarithm of the logistic likelihood with $p(y_k = 1|\boldsymbol{z}_k)$ replacing y_k. Put plainly, minimizing the sum of the KL divergence between our classifier probabilities and logistic regression probabilities over all encounters k is equivalent to maximizing the logistic likelihood with our classifier-based *exploitation* probabilities $p(y_k = 1|\boldsymbol{z}_k)$ as observations instead of direct measurements of *exploitation* y_k as given by

$$\sum_k \log\left[p(y_k|\boldsymbol{\beta} \cdot \boldsymbol{x}_k)^{p(y_k=1|\boldsymbol{z}_k)}\left(1 - p(y_k|\boldsymbol{\beta} \cdot \boldsymbol{x}_k)\right)^{1-p(y_k=1|\boldsymbol{z}_k)}\right]$$

To train our model, we therefore fit a standard logistic regression GLM where we provided sets of observations of covariates $\boldsymbol{x}_k$ and response variables $p(y_k = 1|\boldsymbol{z}_k)$ for *sensed* encounters.

Exploitation of single-density, multi-patch environments

As described above, we used an "encounter sampling" protocol to generate 100 replicate observations of only *sensed* encounters by removing all encounters that were not *sensed* (i.e., $v_k = 0$) as randomly estimated from the distribution $v_k|\boldsymbol{w}_k \sim \text{Bern}\big(p(v_k = 1|\boldsymbol{w}_k)\big)$ (Figure 4B). For example, we can consider an animal foraging in this single-density, multi-patch environment. Although we detected 10 total encounters $K = k_1, k_2, \ldots, k_{10}$, several of these encounters had low probabilities of sensing $p(v_k = 1|\boldsymbol{w}_k)$ (Figure 4B). We use our "encounter sampling" protocol to simulate *sensation* of the patch during each of these 10 encounters and find that $v_k = 0$ for k_1, k_3, k_6 and k_8. By removing these 4 non-sensed encounters, we generate a new observation comprised of the 6 *sensed* encounters $K_1^* = k_2, k_4, k_5, k_7, k_9, k_{10} = k_{1*}, k_{2*}, \ldots, k_{6*}$. Using only the data related to this new sequence of encounters K_1^*, we generated a vector of covariates (i.e., ρ_k, τ_s, ρ_h, and ρ_e). Importantly, this procedure considers time spent during the *non-sensed* encounters k_1, k_3, k_6 and k_7 the same as time spent searching off patch. We repeated this process 100 times to generate new observations of encounter sequences (i.e., $K_1^*, K_2^*, \ldots, K_{100}^*$). In doing so, we reduced the number of encounters from 6,560 total encounters (as defined in Patch encounter detection) to 2,604-2,698 (μ = 2659.8, σ = 15.9) *sensed* encounters for each of the 100 replicates.

Additionally, we used a "worm sampling" protocol to generate 500 hierarchically bootstrapped replicates [92]. Specifically, we took our vector of 443 animals $A = a_1, a_2, \ldots, a_{443}$ and resampled with replacement (e.g., $A_1^* = a_{317}, a_{88}, \ldots, a_{130} = a_{1*}, a_{2*}, \ldots, a_{443*}$) to generate 500 new samples $A_1^*, A_2^*, \ldots, A_{500}^*$. When combined, the "encounter sampling" and "worm sampling" protocols created 50,000 unique replicates of observations of the covariates $\boldsymbol{x}_k$ and response variables $p(y_k = 1|\boldsymbol{z}_k)$ which were used to estimate the coefficients $\boldsymbol{\beta}$ (Figure 4C). A null distribution of coefficients $\boldsymbol{\beta}^*$ was estimated by shuffling the response variable vector (Figure 4 – supplement 1B). A two-tailed, one-sample bootstrap hypothesis test was used to assess whether our covariate estimates were significantly greater than or less than 0 (i.e., $\boldsymbol{p} = 2 \times \min[P(\boldsymbol{\beta} \leq \boldsymbol{0}), P(\boldsymbol{\beta} \geq \boldsymbol{0})]$).

Exploitation of food-deprived animals in single-density, multi-patch environments

To validate model predictions related to the satiety signal covariate τ_s, a novel data set of well-fed and 3-hour food-deprived animals foraging in single-density, multi-patch environments of

relative density 5 was generated (Figure 4 – supplement 3A-B). The "encounter sampling" protocol described above was used to generate 100 replicates of observations of the covariates $\boldsymbol{x}_k$ and response variables $p(y_k = 1|\boldsymbol{z}_k)$ for this data set. As a result of "encounter sampling", we reduced the number of encounters from 42 total encounters to 30-37 (μ = 34.6, σ = 1.3) *sensed* encounters for food-deprived animals and 235 total encounters to 94-107 (μ = 99.8, σ = 2.1) *sensed* encounters for well-fed animals. Coefficient values $\boldsymbol{\beta}$ were re-estimated in the absence of the satiety signal τ_s (Figure 4 – supplement 3C) using the original single-density, multi-patch data set. Using the mean coefficient values $\boldsymbol{\beta}$ for both models (with and without satiety), we predicted the conditional probabilities of exploiting $p(y_k = 1|\boldsymbol{\beta} \cdot \boldsymbol{x}_k)$ for the new data set for well-fed and food-deprived animals. We subsequently simulated a series of *exploitation* events from a Bernoulli distribution using the estimated (i.e., $y_k|\boldsymbol{x}_k \sim \mathrm{Bern}\big(p(y_k = 1|\boldsymbol{\beta} \cdot \boldsymbol{x}_k)\big)$) and observed (i.e., $y_k|\boldsymbol{z}_k \sim \mathrm{Bern}\big(p(y_k = 1|\boldsymbol{z}_k)\big)$) *exploitation* probabilities. These simulated *exploitations* were used to generate distributions of the probability of an *exploitation* occurring for the first time as a function of the number of encounters (Figure 4 – supplement 3D).

Exploitation of multi-density, multi-patch environments

To validate model predictions related to the prior experience covariates ρ_h and ρ_e, a novel data set of animals foraging on multi-density, multi-patch environments was generated (Figure 4E, Figure 4 - supplement 4A-C). The "encounter sampling" protocol described above was used to generate 100 replicates of observations of the covariates $\boldsymbol{x}_k$ and response variables $p(y_k = 1|\boldsymbol{z}_k)$ for this data set. As a result of "encounter sampling", we reduced the number of encounters from 4,296 total encounters (350-984 total encounters per condition) to 1,702-1,745 (μ = 1,724.6, σ = 9.9) *sensed* encounters. Coefficient values $\boldsymbol{\beta}$ were re-estimated in the absence of the recently encountered and *exploited* patch density terms ρ_h and ρ_e (Figure 4 – supplement 4D) using the original single-density, multi-patch data set. Using the mean coefficient values $\boldsymbol{\beta}$ for both models (with and without prior experience), we predicted the probabilities of *exploiting* $p(y_k = 1|\boldsymbol{\beta} \cdot \boldsymbol{x}_k)$ for the new data set. To generate the heat maps of predicted behavior (Figure 4F), we varied ρ_k and ρ_h as well as ρ_k and ρ_e across a range of values and set the remaining covariate terms to the average values observed in the data set. To generate the heat maps of observed behavior (Figure 4F), we averaged the observed probabilities of *exploiting* $p(y_k = 1|\boldsymbol{z}_k)$ for each pairing of ρ_k and ρ_h as well as ρ_k and ρ_e and linearly interpolated values between these 9 points.

949

950 ***Exploitation of sensory mutants in single-density, multi-patch environments***

951 To test the utility of our model in identifying covariate-specific phenotypes in animals with
952 varied genotypes, a novel data set of wild-type animals and sensory mutants foraging on single-
953 density, multi-patch environments was generated (Figure 4 - supplement 5A-B). The "encounter
954 sampling" and "worm sampling" protocols described above were used to generate 50,000 replicates
955 of observations of the covariates $\boldsymbol{x}_k$ and response variables $p(y_k = 1|\boldsymbol{z}_k)$ for this data set. As a
956 result of "encounter sampling", we reduced the number of encounters from 1,352 total encounters
957 (27-193 total encounters per condition) to 862-894 (μ = 879.4, σ = 7.4) *sensed* encounters. As the
958 number of encounters were significantly less in these data sets as compared to the original single-
959 density, multi-patch data set, we used ridge regression to regularize the magnitude of the covariates.
960 We optimized each model across cross-validated replicates by varying the regularization value λ. We
961 found that $\lambda_{\mathrm{N2}} = 0.0175$, $\lambda_{mec-4} = 0.0223$, and $\lambda_{osm-6} = 0.0614$ maximized the mean log-
962 likelihood of each model (Figure 4 – supplement 5E). Coefficient values $\boldsymbol{\beta}$ were estimated for each
963 of the three strains tested using these values (Figure 4 – supplement 5D). To assess whether the
964 magnitude of coefficients significantly differed between wild-type and mutant models, we conducted
965 a two-sample test of the mean of differences as given by

$$Z = \frac{\mu_{\mathrm{mutant}} - \mu_{\mathrm{N2}}}{\sqrt{\sigma^2_{\mathrm{mutant}} + \sigma^2_{\mathrm{N2}}}}$$

966 where μ and σ are the mean and standard deviation, respectively, of the distribution of a covariate
967 across replicates. Statistical significance was calculated as a left-tailed test $\phi(Z)$ for the density
968 coefficients (β_k, β_h, and β_e) and a two-tailed test $\phi(-|Z|)$ for the other coefficients (β_0 and β_s)
969 where ϕ is the standard normal cumulative distribution function.

References

1. Lee D (2013). Decision making: From neuroscience to psychiatry. *Neuron* **78** (2): 233-248. https://doi.org/10.1016/j.neuron.2013.04.008.

2. Budaev S, Jørgensen C, Mangel M, Sigrunn E, and Giske J (2019). Decision-making from the animal perspective: Bridging ecology and subjective cognition. *Frontiers in Ecology and Evolution* **7**, 164. https://doi.org/10.3389/fevo.2019.00164.

3. Mobbs D, Trimmer PC, Blumstein DT, and Dayan P (2018). Foraging for foundations in decision neuroscience: Insights from ethology. *Nature Reviews Neuroscience* **19** (7): 419-427. https://doi.org/10.1038/s41583-018-0010-7.

4. Gold JI, and Shadlen MN (2007). The neural basis of decision making. *Annual Review of Neuroscience* **30**: 535-574. https://doi.org/10.1146/annurev.neuro.29.051605.113038.

5. Stephens DW (2008). Decision ecology: Foraging and the ecology of animal decision making. *Cognitive, Affective, & Behavioral Neuroscience* **8** (4): 475-484. https://doi.org/10.3758/CABN.8.4.475.

6. Hall-McMaster S, and Luyckx F (2019). Revisiting foraging approaches in neuroscience. *Cognitive, Affective, & Behavioral Neuroscience* **19**: 225-230. https://doi.org/10.3758/s13415-018-00682-z.

7. Schoener TW (1971). Theory of feeding strategies. *Annual Review of Ecology and Systematics* **2**: 369-404. https://doi.org/10.1146/annurev.es.02.110171.002101.

8. Pyke GH, Pulliam HR, and Charnov EL (1977). Optimal foraging: A selective review of theory and tests. *The Quarterly Review of Biology* **52** (2): 137-154. https://doi.org/10.1086/409852.

9. Stephens DW, and Krebs JR. (1986). Foraging Theory (Princeton University Press).

10. Stephens DW, Brown JS, and Ydenberg RC. (2007). Foraging: Behavior and Ecology (University of Chicago Press). 10.7208/9780226772653.

11. Nonacs P (2000). State dependent behavior and the Marginal Value Theorem. *Behavioral Ecology* **12** (1): 71-83. https://doi.org/10.1093/oxfordjournals.beheco.a000381.

12. Hills TT (2010). Animal foraging and the evolution of goal-directed cognition. *Cognitive Science* **30** (1): 3-41. https://doi.org/10.1207/s15516709cog0000_50.

13. Calhoun AJ, and Hayden BY (2015). The foraging brain. *Current Opinion in Behavioral Sciences* **5**: 24-31. https://doi.org/10.1016/j.cobeha.2015.07.003.

14. Charnov EL (1976). Optimal foraging, the marginal value theorem. *Theoretical Population Biology* **9** (2): 129-136. https://doi.org/10.1016/0040-5809(76)90040-x.

1002 15. Haley JA, and Chalasani SH (2024). *C. elegans* foraging as a model for understanding the neuronal
1003 basis of decision-making. *Cellular and Molecular Life Sciences* **81**, 252.
1004 https://doi.org/10.1007/s00018-024-05223-1.

1005 16. Brenner S (1974). The genetics of *Caenorhabditis elegans*. *Genetics* **77** (1): 71-94.
1006 https://doi.org/10.1093/genetics/77.1.71.

1007 17. Faumont S, and Lockery SR (2006). The awake behaving worm: Simultaneous imaging of
1008 neuronal activity and behavior in intact animals at millimeter scale. *Journal of Neurophysiolovy*
1009 **95**: 1976-1981. https://doi.org/10.1152/jn.01050.2005.

1010 18. Boulin T, and Hobert O (2012). From genes to function: The *C. elegans* genetic toolbox. *Wiley*
1011 *Interdisciplinary Review Developmental Biology* **1** (1): 114-137. https://doi.org/10.1002/wdev.1.

1012 19. Samuel BS, Rowedder H, Braendle C, Félix M-A, and Ruvkun G (2016). *Caenorhabditis elegans*
1013 responses to bacteria from its natural habitats. *PNAS* **113** (27): E3941-E3949.
1014 https://doi.org/10.1073/pnas.1607183113.

1015 20. White JG, Southgate E, Thomson JN, and Brenner S (1986). The structure of the nervous
1016 system of the nematode *Caenorhabditis elegans*. *Philisophical Transactions of the Royal Society B* **314**
1017 (1165): 1-340. https://doi.org/10.1098/rstb.1986.0056.

1018 21. de Bono M, and Maricq AV (2005). Neuronal substrates of complex behaviors in *C. elegans*.
1019 *Annual Review of Neuroscience* **28**: 451-501.
1020 https://doi.org/10.1146/annurev.neuro.27.070203.144259.

1021 22. Colbert HA, and Bargmann CI (1995). Odorant-specific adaptation pathways generate olfactory
1022 plasticity in *C. elegans*. *Neuron* **14** (4): 803-812. https://doi.org/10.1016/0896-6273(95)90224-
1023 4.

1024 23. Zhang Y, Lu H, and Bargmann CI (2005). Pathogenic bacteria induce aversive olfactory learning
1025 in *Caenorhabditis elegans*. *Nature* **438**: 179-184. https://doi.org/10.1038/nature04216.

1026 24. Ardiel EL, and Rankin CH (2010). An elegant mind: Learning and memory in *Caenorhabditis*
1027 *elegans*. *Learning & Memory* **17**: 191-201. https://doi.org/10.1101/lm.960510.

1028 25. Calhoun AJ, Tong A, Sharpee TO, and Chalasani SH (2015). Neural mechanisms for evaluating
1029 environmental variability in *Caenorhabditis elegans*. *Neuron* **86**: 428-441.
1030 https://doi.org/10.1016/j.neuron.2015.03.026.

1031 26. Bendesky A, Tsunozaki M, Rockman MV, Kruglyak L, and Bargmann CI (2011). Catecholamine
1032 receptor polymorphisms affect decision-making in *C. elegans*. *Nature* **472** (7343): 313-318.
1033 https://doi.org/10.1038/nature09821.

1034 27. Faumont S, Lindsay TH, and Lockery SR (2012). Neuronal microcircuits for decision making in
1035 *C. elegans*. *Current Opinion in Neurobiology* **22** (4): 580-591.
1036 https://doi.org/10.1016/j.conb.2012.05.005.

1037 28. Iwanir S, Brown AS, Nagy S, Najjar D, Kazakov A, Lee KS, Zaslaver A, Levine E, and Biron D
1038 (2016). Serotonin promotes exploitation in complex environments by accelerating decision-
1039 making. *BMC Biology* **14** (9). https://doi.org/10.1186/s12915-016-0232-y.

1040 29. Tanimoto Y, Yamazoe-Umemoto A, Fujita K, Kawazoe Y, Miyanishi Y, Yamazaki SJ, Fei X,
1041 Busch KE, Gengyo-Ando K, Nakai J, Iino Y, Iwasaki Y, Hashimoto K, and Kimura KD
1042 (2017). Calcium dynamics regulating the timing of decision-making in *C. elegans*. *eLife* **6**:
1043 e21629. https://doi.org/10.7554/eLife.21629.

1044 30. Ji N, Madan GK, Fabre GI, Dayan A, Baker CM, Kramer TS, Nwabudike I, and Flavell SW
1045 (2021). A neural circuit for flexible control of persistent behavioral states. *eLife* **10**: e62889.
1046 https://doi.org/10.7554/eLife.62889.

1047 31. Scheer E, and Bargmann CI (2023). Sensory neurons couple arousal and foraging decisions in *C.*
1048 *elegans*. *eLife* **12**: RP88657. https://doi.org/10.7554/eLife.88657.1.

1049 32. Petersen C, Dirksen P, and Schulenburg H (2015). Why we need more ecology for genetic
1050 models such as *C. elegans*. *Trends in Genetics* **31** (3): 120-127.
1051 https://doi.org/10.1016/j.tig.2014.12.001.

1052 33. Volgin AD, Yakovlev OV, Demin KA, de Abreu MS, Rosemberg DB, Meshalkina DA,
1053 Alekseeva PA, Friend AJ, Amstislavskaya TG, and Kalueff AV (2018). Understanding the
1054 role of environmental enrichment in zebrafish neurobehavioral models. *Zebrafish* **15** (5): 425-
1055 432. https://doi.org/10.1089/zeb.2018.1592.

1056 34. Kempermann G (2019). Environmental enrichment, new neurons and the neurobiology of
1057 individuality. *Nature Reviews Neuroscience* **20** (4): 235-245. https://doi.org/10.1038/s41583-
1058 019-0120-x.

1059 35. Guisnet A, Maitra M, Pradhan S, and Hendricks M (2021). A three-dimensional habitat for *C.*
1060 *elegans* environmental enrichment. *PLoS One* **16** (1): e0245139.
1061 https://doi.org/10.1371/journal.pone.0245139.

1062 36. Shtonda BB, and Avery L (2006). Dietary choice behavior in *Caenorhabditis elegans*. *Journal of*
1063 *Experimental Biology* **209** (1): 89-102. https://doi.org/10.1242/jeb.01955.

1064 37. Hills T, Brockie PJ, and Maricq AV (2004). Dopamine and glutamate control area-restricted
1065 search behavior in *Caenorhabditis elegans*. *Journal of Neuroscience* **24** (5): 1217-1225.
1066 https://doi.org/10.1523/JNEUROSCI.1569-03.2004.

1067 38. Calhoun AJ, Chalasani SH, and Sharpee TO (2014). Maximally informative foraging by
1068 *Caenorhabditis elegans*. *eLife* **3**: e04220. https://doi.org/10.7554/eLife.04220.001.

1069 39. Gray JM, Hill JJ, and Bargmann CI (2005). A circuit for navigation in *Caenorhabditis elegans*. *PNAS*
1070 **102** (9): 3184-3191. https://doi.org/10.1073/pnas.0409009101.

1071 40. Milward K, Busch KE, Murphy RJ, de Bono M, and Olofsson B (2011). Neuronal and molecular
1072 substrates for optimal foraging in *Caenorhabditis elegans*. *PNAS* **108** (51): 20672-20677.
1073 https://doi.org/10.1073/pnas.1106134109.

41. Olofsson B (2014). The olfactory neuron AWC promotes avoidance of normally palatable food following chronic dietary restriction. *Journal of Experimental Biology* **217** (10): 1790-1798. https://doi.org/10.1242/jeb.099929.

42. Pradhan S, Quilez S, Homer K, and Hendricks M (2019). Environmental programming of adult foraging behavior in *C. elegans*. *Current Biology* **29**: 2867-2879. https://doi.org/10.1016/j.cub.2019.07.045.

43. Gloria-Soria A, and Azevedo RBR (2008). *npr-1* regulates foraging and dispersal strategies in *Caenorhabditis elegans*. *Current Biology* **18** (21): 1694-1699. https://doi.org/10.1016/j.cub.2008.09.043.

44. Madirolas G, Al-Asmar A, Gaouar L, Marie-Louise L, Garza-Enríquez A, Rodríguez-Rada V, Khona M, Dal Bello M, Ratzke C, Gore J, and Pérez-Escudero A (2023). *Caenorhabditis elegans* foraging patterns follow a simple rule of thumb. *Communications Biology* **6**, 841. https://doi.org/10.1038/s42003-023-05220-3.

45. Fujiwara M, Sengupta P, and McIntire SL (2002). Regulation of body size and behavioral state of *C. elegans* by sensory perception and the EGL-4 cGMP-dependent protein kinase. *Neuron* **36** (6): 1091-1102. https://doi.org/10.1016/s0896-6273(02)01093-0.

46. Sawin ER, Ranganathan R, and Horvitz HR (2000). *C. elegans* locomotory rate is modulated by the environment through a dopaminergic pathway and by experience through a serotonergic pathway. *Neuron* **26** (3): 619-631. https://doi.org/10.1016/S0896-6273(00)81199-X.

47. Fawcett TW, McNamara JM, and Houston AI (2012). When is it adaptive to be patient? A general framework for evaluating delayed rewards. *Behavioural Processes* **89** (2): 128-136. https://doi.org/10.1016/j.beproc.2011.08.015.

48. Susini I, Safryghin A, HIllemann F, and Wascher CAF (2021). Delay of gratification in non-human animals: A review of inter-specific variation in performance. *bioRxiv*. https://doi.org/10.1101/2020.05.05.078659.

49. Constantino SM, and Daw ND (2015). Learning the opportunity cost of time in a patch-foraging task. *Cognitive, Affective, & Behavioral Neuroscience* **15**: 837-853. https://doi.org/10.3758/s13415-015-0350-y.

50. Carter EC, Pedersen EJ, and McCullough ME (2015). Reassessing intertemporal choice: Human decision-making is more optimal in a foraging task than in a self-control task. *Frontiers in Psychology* **6**, 95. https://doi.org/10.3389/fpsyg.2015.00095.

51. Hayden BY (2018). Why has evolution not selected for perfect self-control? *Philisophical Transactions of the Royal Society B* **374** (1766). https://doi.org/10.1098/rstb.2018.0139.

52. Stephens DW, and Anderson D (2001). The adaptive value of preference for immediacy: When shortsighted rules have farsighted consequences. *Behavioral Ecology* **12** (3): 330-339. https://doi.org/10.1093/beheco/12.3.330.

1110 53. Ferguson TS (1967). Sequential Decision Problems. In Mathematical Statistics: A Decision
1111 Theoretic Approach, Z.W. Birnbaum, and E. Lukacs, eds. (Academic Press).

1112 54. Robbins H (1970). Optimal stopping. *The American Mathematical Monthly* **77** (4): 333-343.
1113 https://doi.org/10.2307/2316139.

1114 55. Mischel W, and Ebbesen EB (1970). Attention in delay of gratification. *Journal of Personality and*
1115 *Social Psychology* **16** (2): 329-337. https://doi.org/10.1037/h0029815.

1116 56. Rosati AG, Stevens JR, Hare B, and Hauser MD (2007). The evolutionary origins of human
1117 patience: Temporal preferences in chimpanzees, bonobos, and human adults. *Current Biology*
1118 **17** (19): 1663-1668. https://doi.org/10.1016/j.cub.2007.08.033.

1119 57. Schnell AK, Boeckle M, Rivera M, Clayton NS, and Hanlon RT (2021). Cuttlefish exert self-
1120 control in a delay of gratification task. *Proceedings of the Royal Society B: Biological Sciences* **288**,
1121 1946. https://doi.org/10.1098/rspb.2020.3161.

1122 58. Range F, Brucks D, and Virányi Z (2020). Dogs wait longer for better rewards than wolves in a
1123 delay of gratification task: But why? *Animal Cognition* **23** (3): 443-453.
1124 https://doi.org/10.1007/s10071-020-01346-7.

1125 59. Hillemann F, Bugnyar T, Kotrschal K, and Wascher CAF (2014). Waiting for better, not for
1126 more: Corvids respond to quality in two delay maintenance tasks. *Animal Behaviour* **90**: 1-10.
1127 https://doi.org/10.1016/j.anbehav.2014.01.007.

1128 60. Miller R, Frohnwieser A, Schiestl M, McCoy DE, Gray RD, Taylor AH, and Clayton NS (2020).
1129 Delayed gratification in New Caledonian crows and young children: Influence of reward type
1130 and visibility. *Animal Cognition* **23** (1): 71-85. https://doi.org/10.1007/s10071-019-01317-7.

1131 61. Pujol N, Link EM, Liu LX, Kurz CL, Alloing G, Tan M-W, Ray KP, Solari R, Johnson CD, and
1132 Ewbank JJ (2001). A reverse genetic analysis of components of the Toll signaling pathway in
1133 *Caenorhabditis elegans*. *Current Biology* **11** (11): 809-821. https://doi.org/10.1016/S0960-
1134 9822(01)00241-X.

1135 62. Melo JA, and Ruvkun G (2012). Inactivation of conserved *C. elegans* genes engages pathogen-
1136 and xenobiotic-associated defenses. *Cell* **149** (2): 452-466.
1137 https://doi.org/10.1016/j.cell.2012.02.050.

1138 63. Pradel E, Zhang Y, Pujol N, Matsuyama T, Bargmann CI, and Ewbank JJ (2007). Detection and
1139 avoidance of a natural product from the pathogenic bacterium *Serratia marcescens* by
1140 *Caenorhabditis elegans*. *PNAS* **104** (7): 2295-2300. https://doi.org/10.1073/pnas.0610281104.

1141 64. Quach KT, and Chalasani SH (2022). Flexible reprogramming of *Pristionchus pacificus* motivation
1142 for attacking *Caenorhabditis elegans* in predator-prey competition. *Current Biology* **32**: 1-14.
1143 https://doi.org/10.1016/j.cub.2022.02.033.

1144 65. Pribadi A, Rieger MA, Rosales K, Reddy KC, and Chalasani SH (2023). Dopamine signaling
1145 regulates predator-driven changes in *Caenorhabditis elegans'* egg laying behavior. *eLife* **12**:
1146 e83957. https://doi.org/10.7554/eLife.83957.

1147 66. Busch KE, and Olofsson B (2012). Should I stay or should I go? *Worm* **1** (3): 182-186.
1148 https://doi.org/10.4161/worm.20464.

1149 67. Krebs JR, and Inman AJ (1992). Learning and foraging: Individuals, groups, and populations. *The*
1150 *American Naturalist* **140**: S63-S84. https://doi.org/10.1086/285397.

1151 68. Frézal L, and Félix M-A (2015). *C. elegans* outside the Petri dish. *eLife* **4**: e05849.
1152 https://doi.org/10.7554/eLife.05849.

1153 69. Matty MA, Lau HE, Haley JA, Singh A, Chakraborty A, Kono K, Reddy KC, Hansen M, and
1154 Chalasani SH (2022). Intestine-to-neuronal signaling alters risk-taking behaviors in food-
1155 deprived *Caenorhabditis elegans*. *PLoS Genetics* **18** (5): e1010178.
1156 https://doi.org/10.1371/journal.pgen.1010178.

1157 70. Ezcurra M, Tanizawa Y, Swoboda P, and Schafer WR (2011). Food sensitizes *C. elegans*
1158 avoidance behaviors through acute dopamine signaling. *EMBO Journal* **30** (6): 1110-1122.
1159 https://doi.org/10.1038/emboj.2011.22.

1160 71. Anderson JL, Albergotti L, Ellebracht B, Huey RB, and Phillips PC (2011). Does
1161 thermoregulatory behavior maximize reproductive fitness of natural isolates of *Caenorhabditis*
1162 *elegans*. *BMC Evolutionary Biology* **11**, 157. https://doi.org/10.1186/1471-2148-11-157.

1163 72. Petersen C, Dirksen P, Prahl S, Strathmann EA, and Schulenburg H (2014). The prevalence of
1164 *Caenorhabditis elegans* across 1.5 years in selected North German locations: The importance of
1165 substrate type, abiotic parameters, and *Caenorhabditis* competitors. *BMC Ecology* **6** (14), 4.
1166 https://doi.org/10.1186/1472-6785-14-4.

1167 73. Fraune S, and Bosch TCG (2010). Why bacteria matter in animal development and evolution.
1168 *BioEssays* **32** (7): 571-580. https://doi.org/10.1002/bies.200900192.

1169 74. Dirksen P, Assié A, Zimmerman J, Zhang F, Tietje A-M, Marsh SA, Félix M-A, Shapira M,
1170 Kaleta C, Schulenburg H, and Samuel BS (2020). CeMbio - The *Caenorhabiditis elegans*
1171 microbiome resource. *G3 Genes|Genomes|Genetics* **10** (9): 3025-3039.
1172 https://doi.org/10.1534/g3.120.401309.

1173 75. Ding SS, Muhle LS, Brown AEX, Schumacher LJ, and Endres RG (2020). Comparison of
1174 solitary and collective foraging strategies of *Caenorhabditis elegans* in patchy food distributions.
1175 *Philosophical Transactions of the Royal Society B* **375**, 37520190382.
1176 https://doi.org/10.1098/rstb.2019.0382.

1177 76. Lipton J, Kleemann G, Ghosh R, Lints R, and Emmons SW (2004). Mate searching in
1178 *Caenorhabditis elegans*: A genetic model for sex drive in a simple invertebrate. *Journal of*
1179 *Neuroscience* **24** (34): 7427-7434. https://doi.org/10.1523/JNEUROSCI.1746-04.2004.

1180 77. Barrios A, Nurrish S, and Emmons SW (2008). Sensory regulation of *C. elegans* male mate-
1181 searching behavior. *Current Biology* **18** (23): 1865-1871.
1182 https://doi.org/10.1016/j.cub.2008.10.050.

1183 78. Matsuura T, Sato T, and Shingai R (2005). Interactions between *Caenorhabditis elegans* individuals
1184 during chemotactic responses. *Zoological Science* **22** (10): 1095-1103.
1185 https://doi.org/10.2108/zsj.22.1095.

1186 79. Gray J, and Lissmann HW (1964). The locomotion of nematodes. *Journal of Experimental Biology*
1187 **41**: 135-154. https://doi.org/10.1242/jeb.41.1.135.

1188 80. Croll NA (1975). Behavioural analysis of nematode movement. *Advances in Parasitology* **13**: 71-122.
1189 https://doi.org/10.1016/s0065-308x(08)60319-x.

1190 81. Croll NA (1975). Components and patterns in the behavior of the nematode *Caenorhabditis*
1191 *elegans*. *Journal of Zoology* **176** (2): 159-176. https://doi.org/10.1111/j.1469-
1192 7998.1975.tb03191.x.

1193 82. You Y-j, Kim J, Raizen DM, and Avery L (2008). Insulin, cGMP, TGF-beta signals regulate food
1194 intake and quiescence in *C. elegans*: A model for satiety. *Cell Metabolism* **7** (3): 249-257.
1195 https://doi.org/10.1016/j.cmet.2008.01.005.

1196 83. Prevedel R, Yoon Y-G, Hoffmann M, Pak N, Wetzstein G, Kato S, Schrödel T, Raskar R,
1197 Zimmer M, Boyden ES, and Vaziri A (2014). Simultaneous whole-animal 3D imaging of
1198 neuronal activity using light-field microscopy. *Nature Methods* **11**: 727=730.
1199 https://doi.org/10.1038/nmeth.2964.

1200 84. Nguyen JP, Shipley FB, Linder AN, Plummer GS, Liu M, Setru SU, Shaevitz JW, and Leifer AM
1201 (2015). Whole-brain calcium imaging with cellular resolution in freely behaving *Caenorhabditis*
1202 *elegans*. *PNAS* **113** (8): E1074-E1081. https://doi.org/10.1073/pnas.1507110112.

1203 85. Venkatachalam V, Ji N, Wang X, Clark C, Mitchell JK, Klein M, Tabone CJ, Florman J, Ji H,
1204 Greenwood J, Chisholm AD, Srinivasan J, Alkema M, Zhen M, and Samuel ADT (2015).
1205 Pan-neuronal imaging in roaming *Caenorhabditis elegans*. *PNAS* **113** (8): E1082-E1088.
1206 https://doi.org/10.1073/pnas.1507109113.

1207 86. Voleti V, Patel KB, Li W, Perez Campos C, Bharadwaj S, Yu H, Ford C, Casper MJ, Yan RW,
1208 Liang W, Wen C, Kimura KD, Targoff KL, and Hillman EMC (2019). Real-time volumetric
1209 microscopy of *in vivo* dynamics and large-scale samples with SCAPE 2.0. *Nature Methods* **16**
1210 (10): 1054-1062. https://doi.org/10.1038/s41592-019-0579-4.

1211 87. Hallinen KM, Dempsey R, Scholz M, Yu X, Linder AN, Randi F, Sharma AK, Shaevitz JW, and
1212 Leifer AM (2021). Decoding locomotion from population neural activity in moving *C.*
1213 *elegans*. *eLife* **10**: e66135. https://doi.org/10.7554/eLife.66135.

1214 88. Labrousse A, Chauvet S, Couillault C, Kurz CL, and Ewbank JJ (2000). *Caenorhabditis elegans* is a
1215 model host for *Salmonella typhimurium*. *Current Biology* **10** (23): 1543-1545.
1216 https://doi.org/10.1016/S0960-9822(00)00833-2.

1217 89. Quach KT, Hughes GA, and Chalasani SH (2024). Interdependence between SEB-3 and NLP-
1218 49 peptides shifts across predator-induced defensive behavioral modes in *Caenorhabditis*
1219 *elegans*. *eLife* **13**: RP98262. https://doi.org/10.7554/eLife.98262.1.

1220 90. Sulston JE, and Brenner S (1974). The DNA of *Caenorhabditis elegans*. *Genetics* **77** (1): 95-104.
1221 https://doi.org/10.1093/genetics/77.1.95.

1222 91. Hallatschek O, Hersen P, Ramanathan S, and Nelson DR (2007). Genetic drift at expanding
1223 frontiers promotes gene segregation. *PNAS* **104** (50): 19926-19930.
1224 https://doi.org/10.1073/pnas.0710150104.

1225 92. Saravanan V, Berman GJ, and Sober SJ (2020). Application of the hierarchical bootstrap to
1226 multi-level data in neuroscience. *Neurons, Behavior, Data analysis, and Theory* **3** (5).
1227

1228 **Figures**

1229 **Figure 1: *C. elegans* forage in a patchy environment with an explore-then-exploit strategy.**

1230

1231 (A) An example animal's midbody location (colored to represent time in the experiment) as it
1232 forages in an environment bounded by a large (30 mm diameter) arena containing 19 small (~1.8
1233 mm diameter) bacterial patches (gray). Each patch was made by pipetting ~0.5 μL of OP50 *E. coli*
1234 diluted to OD_{600} ~10 and grown at room temperature for ~1 hour. (B) Distance between the
1235 example animal's midbody position and the nearest patch edge (positive indicates inside patch) is
1236 plotted (black) for every time point. Putative encounters with a bacterial patch are indicated (gray).
1237 (C) Patch encounters (colored to represent the duration of the encounter) for 50 individuals
1238 foraging in these environments are plotted. (D) The number of total and unique patch encounters
1239 for each animal are shown. (E) Duration for each patch encounter was computed and classified as
1240 either short (0-2 minutes) or long (2-60 minutes) using a Gaussian mixture model. The distributions
1241 of all observed short and long encounters are plotted with duration binned logarithmically. (F) The
1242 observed start time of each patch encounter is shown for all short and long duration encounters.
1243 Long duration encounters occur significantly later (one-tailed Mann-Whitney U-Test). (G) The
1244 probability of residing on patch was computed for all worms across time (black) and compared to
1245 the probability of residing on patch if patch locations were semi-randomly permuted (pink).
1246 Smoothed median values are plotted with bootstrap-derived 2.5% and 97.5% quantiles shown in
1247 shaded regions. Time points where observed probabilities of residing on patch significantly exceed
1248 permuted probabilities are indicated by a black line (one-tailed Fisher's exact test with Benjamini-
1249 Hochberg correction). (H) The track of the example animal in (A) is replotted with color used to
1250 represent the animal's instantaneous velocity at each time point. (I) Velocity of the example animal
1251 over time is plotted (black) alongside patch encounters (gray) as previously identified in (B).
1252 Example encounters – one early, short duration (green) and one late, long duration (blue) – are
1253 indicated. (J,K) A 60-second time window surrounding the start of these example encounters is
1254 enlarged. (L) Velocity trajectories were aligned to patch entry for every encounter. Mean encounter-
1255 aligned (black/gray) and randomly-aligned (pink) trajectories are plotted for each animal (light) and
1256 across all animals (dark). (M) Deceleration upon encounter with the patch edge is plotted for every
1257 encounter and grouped by duration type. Deceleration was significantly lower for encounter-aligned
1258 as compared to randomly-aligned trajectories (pink) for all duration types (one-tailed Mann-Whitney
1259 U-Tests with Bonferroni Correction). (N) Mean velocity as a function of the distance from the edge
1260 of bacterial patches (computed for 50 μm bins) is shown for every animal (gray) and across all
1261 animals (black). (O) Each animal's mean velocity during time spent on and off (midpoint at least -
1262 0.46 mm from patch edge) patch is shown. Velocity on patch was significantly slower than off patch
1263 (one-tailed paired-sample *t*-test). Sample data for one animal (worm #1) are shown in (A-C,H-K).
1264 Summary data for all animals (N = 50 worms) and encounters (N = 419 total encounters) are shown
1265 in (D-G,L-O). Violin plots in (D,F,M,O) give the KDE and quartiles for each measure. Asterisks
1266 denote statistical significance (***$p<0.001$). See also Figure 1 – supplement 1-5 and Video 1-4.

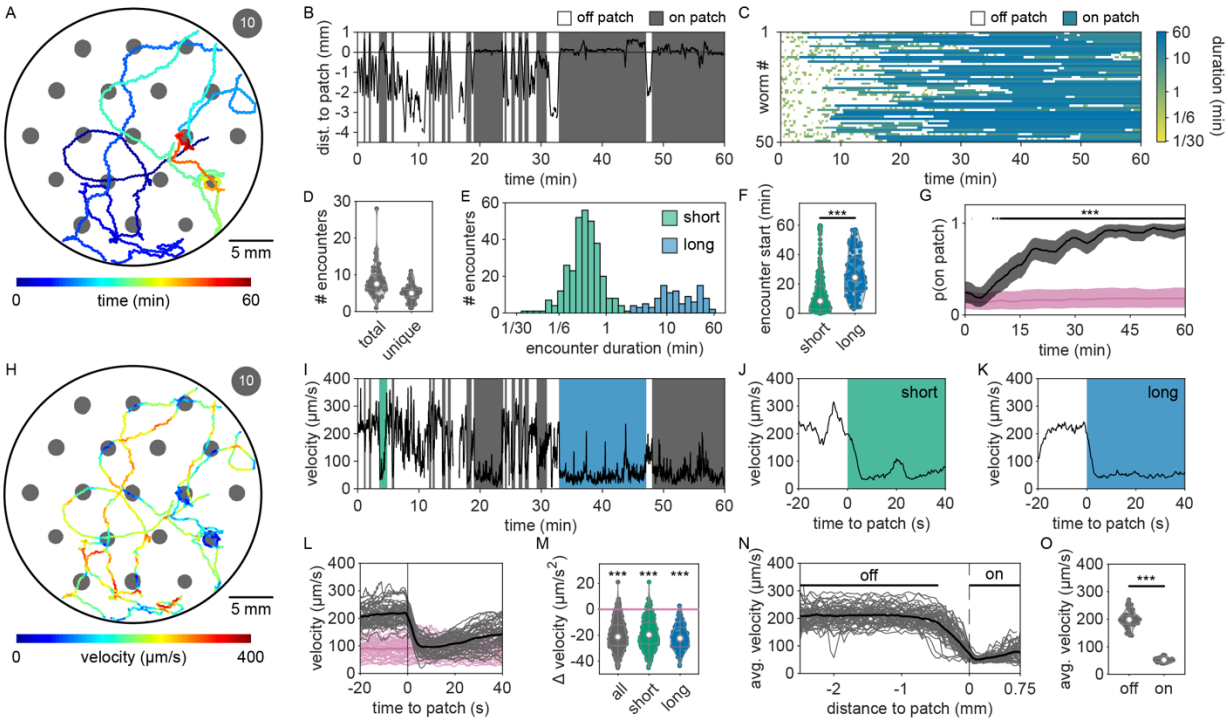
A
10
5 mm
0
time (min)
60
B
off patch
on patch
dist. to patch (mm)
time (min)
C
off patch
on patch
worm #
time (min)
duration (min)
D
encounters
total
unique
E
encounters
short
long
encounter duration (min)
F
encounter start (min)
short
long
G
p(on patch)
time (min)
H
10
5 mm
0
velocity (µm/s)
400
I
velocity (µm/s)
time (min)
J
short
velocity (µm/s)
time to patch (s)
K
long
velocity (µm/s)
time to patch (s)
L
velocity (µm/s)
time to patch (s)
M
Δ velocity (µm/s²)
all
short
long
N
off
on
avg. velocity (µm/s)
distance to patch (mm)
O
avg. velocity (µm/s)
off
on

1267

1268 **Figure 2: The timing of the switch from explore-to-exploit is density-dependent.**
1269
1270 (A) The relative density (as estimated by fluorescently-labeled OP50-GFP) is shown for small (~1.8
1271 mm diameter) bacterial patches made by pipetting ~0.5 μL droplets of OP50 *E. coli* diluted in LB to
1272 a range of optical densities (OD_{600} = {0, 0.05, 0.1, 0.5, 1, 2, 3, 4, 5, 10} and controlling growth time
1273 at room temperature (hours = {1, 12, 48}). For (A-G,L-O), gray-scale color saturation is
1274 proportional to the relative density of each condition and corresponds to labels in (A). (B) The
1275 mean velocities of animals foraging in environments containing patches matching one of the 12
1276 bacterial densities are plotted as a function of the distance from the edge of bacterial patches
1277 (computed for 50 μm bins). (C) Animals' average on-patch velocity is plotted as a function of the
1278 relative density of bacteria. Compared to animals foraging amongst bacteria-free patches containing
1279 only LB (relative density 0), animals foraging on bacterial patches with relative density of 0.5 or
1280 greater display significantly slower on-patch velocities (one-tailed Mann-Whitney U-Tests with
1281 Bonferroni Correction). (D) The midbody location (colored to represent time in the experiment) of
1282 example animals foraging in environments containing patches (gray) of relative density 0, 1, 5, 10,
1283 and 200 are shown. (E) The total time each animal spent on patch is plotted as a function of the
1284 relative density of bacteria. Time on patch increased monotonically with increasing bacterial density
1285 (Kendall's τ correlation, $p<0.001$) following a sigmoidal trend. (F) Smoothed median values of the
1286 probability of worms residing on patch over time for each density condition are plotted. Time
1287 points where observed probabilities of residing on patch either match (pink) or significantly exceed
1288 (gray) the probability of residing on patch if patch locations were semi-randomly permuted are
1289 indicated (one-tailed Fisher's exact test with Benjamini-Hochberg correction). (G) A KDE of the
1290 distribution of encounter durations is plotted for each density condition. (H) For each encounter,
1291 the average velocity of the animal during the encounter and the duration of that encounter are
1292 plotted on a double-logarithmic plot with color representing the probabilities of clustering
1293 classification as *search* (orange), *sample* (green), or *exploit* (blue). Contours showing the first, second,
1294 and third standard deviation of the GMM used to classify *explore* and *exploit* encounters are shown as
1295 shaded ellipses with saturation corresponding to standard deviation. KDEs for distributions of
1296 average on-patch velocity and encounter duration are plotted for each encounter type. (I) For each
1297 encounter, the minimum on-patch velocity and maximum change in velocity are plotted. Contours
1298 showing the separation of *sensing* and *non-sensing* encounters as estimated by semi-supervised QDA
1299 are indicated. A KDE for the distribution of the maximum change in velocity is plotted for each
1300 encounter type. (J) Features used to classify encounters as *search*, *sample*, or *exploit* are summarized.
1301 (K) KDEs of the distributions of animals' velocities are shown for all timepoints during search off
1302 and on patch as well as during sample and exploit encounters. (L) Ethograms of patch encounters
1303 (colored to represent the probability of classification as *search*, *sample*, and *exploit*) are shown for 443
1304 individuals. (M) The average proportion of each encounter type over time is plotted. (N) Time
1305 elapsed and (O) number of encounters occurring prior to the first *exploitation* event are plotted for
1306 every animal (blue). In the event that no *exploitation* event occurred, the maximum observed time and
1307 encounters are plotted (red-orange). Both time and encounter number before *exploitation* decrease
1308 monotonically with increasing patch density (Kendall's τ correlation, $p<0.001$) following a sigmoidal
1309 trend. Summary data for all animals (N = 443 total worms; N = 20-50 worms per condition) and
1310 encounters (N = 6,560 total encounters; N = 46-876 encounters per condition) are shown in (A-
1311 C,E-I,K-O). Asterisks denote statistical significance (***$p<0.001$). See also Figure 2 – supplement 1-
1312 7 and Video 5-6.

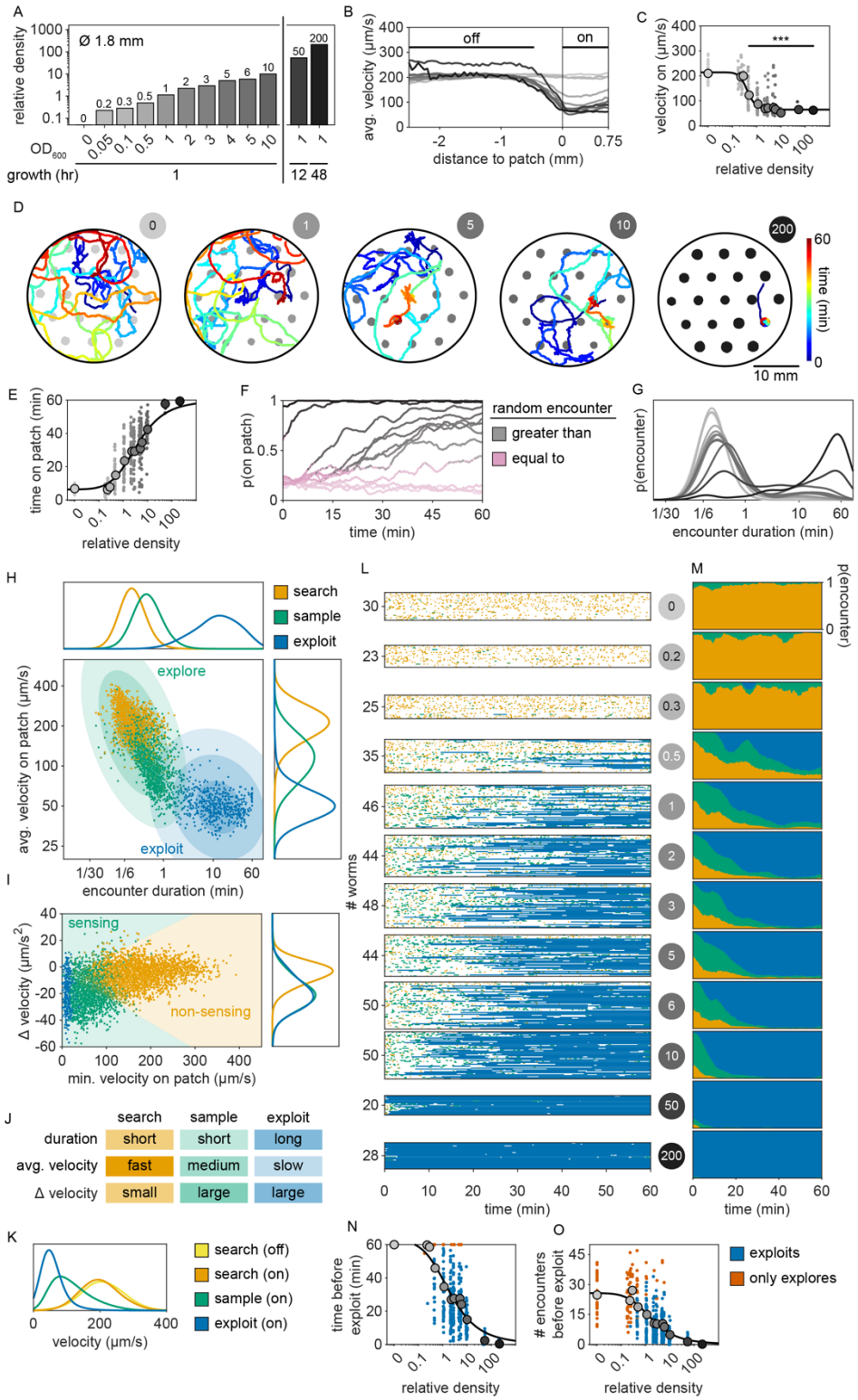
A
relative density
Ø 1.8 mm
OD600
growth (hr)
B
avg. velocity (µm/s)
off
on
distance to patch (mm)
C
velocity on (µm/s)
relative density
D
time (min)
10 mm
E
time on patch (min)
relative density
F
p(on patch)
random encounter
greater than
equal to
time (min)
G
p(encounter)
encounter duration (min)
H
search
sample
exploit
explore
avg. velocity on patch (µm/s)
encounter duration (min)
I
sensing
non-sensing
Δ velocity (µm/s²)
min. velocity on patch (µm/s)
J
search
sample
exploit
duration
avg. velocity
Δ velocity
short
long
fast
medium
slow
small
large
large
K
velocity (µm/s)
search (off)
search (on)
sample (on)
exploit (on)
L
worms
time (min)
M
p(encounter)
time (min)
N
time before exploit (min)
relative density
O
encounters before exploit
relative density
exploits
only explores

1313

1314 **Figure 3: *C. elegans* explore first even when only one patch is available.**
1315
1316 (A) Relative density of large (~8.3 mm diameter) and (B) small (~1.8 mm diameter) bacterial patches
1317 was varied by pipetting 20 μL and 0.5 μL, respectively, droplets of OP50 *E. coli* diluted in LB to a
1318 range of optical densities (OD_{600} = {0, 0.05, 0.1, 0.5, 1, 2, 3, 4, 5, 10} and controlling growth time at
1319 room temperature (hours = {1, 48}). (C) Large patches were formed in the center of 30 mm arenas
1320 while small patches were formed in the center of 9 mm arenas. (D-E) The midbody location
1321 (colored to represent time in the experiment) of example animals foraging in environments
1322 containing a single (D) large or (E) small patch (gray) are shown. (F-G) Ethograms of patch
1323 encounters (colored to represent the probability of classification as *search*, *sample*, and *exploit*) for (F)
1324 144 individuals (8-15 per condition) foraging on a single large patch and (G) 191 individuals (27-38
1325 per condition) foraging on a single small patch are shown. (H-I) Time elapsed prior to the first
1326 *exploitation* event (blue) for animals foraging on (H) large and (I) small patches is plotted for every
1327 animal. When *exploitation* was not observed, time elapsed in the experiment is plotted (red-orange).
1328 Animals in large and small patch environments *exploited* higher density patches significantly earlier
1329 (Kendall's τ correlation, $p < 0.001$) following a sigmoidal trend. See also Figure 3 – supplement 1-2.

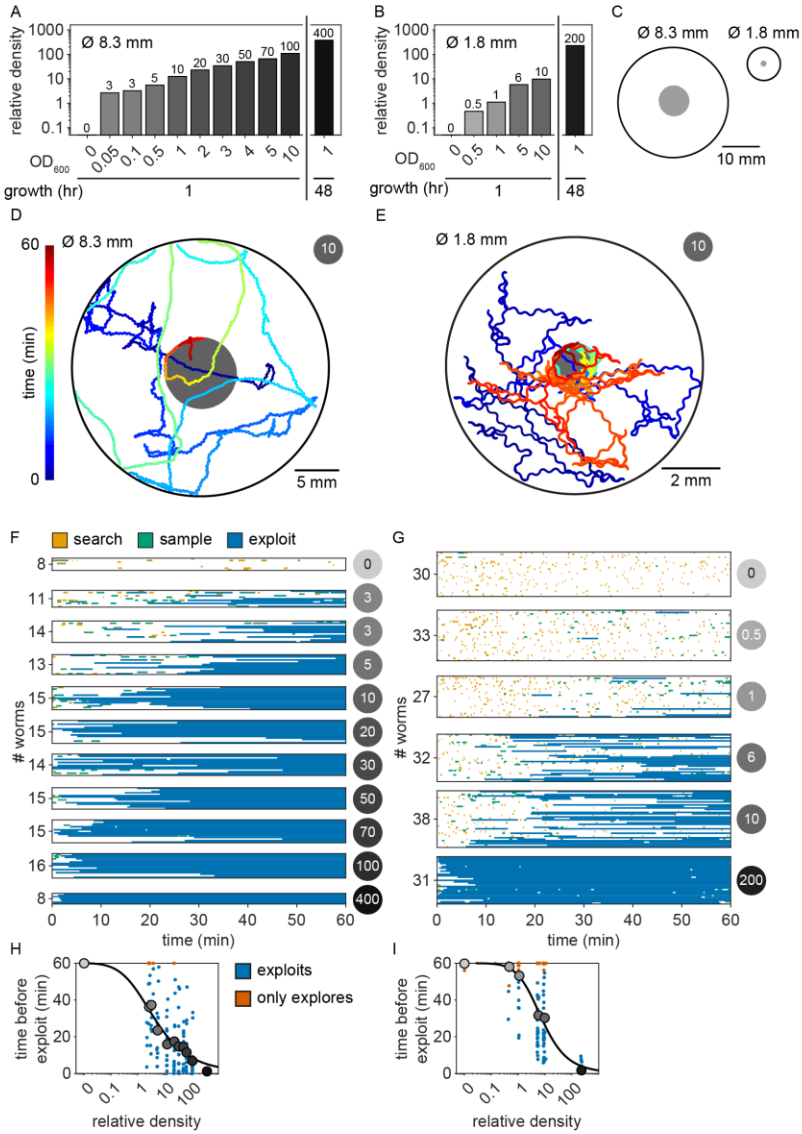
A
relative density
Ø 8.3 mm
OD600
growth (hr)
B
Ø 1.8 mm
C
Ø 8.3 mm
Ø 1.8 mm
10 mm
D
Ø 8.3 mm
time (min)
5 mm
E
Ø 1.8 mm
2 mm
F
search
sample
exploit
worms
time (min)
G
H
time before exploit (min)
exploits
only explores
relative density
I

1330

Figure 4: Exploitation decisions are driven by available sensory information, satiety, and prior experience.

(A) Schematic of the covariates $\boldsymbol{x}_k$ used in our logistic regression model to predict the probability of *exploiting* a patch upon any given encounter $p(y_k = 1|\boldsymbol{\beta} \cdot \boldsymbol{x}_k)$. $\boldsymbol{x}_k$ includes the relative density of the encountered patch k (ρ_k), the duration of time spent off food since departing the last *exploited* patch (τ_s), the relative density of the patch encountered immediately before encounter k (ρ_h), and the relative density of the last *exploited* patch (ρ_e). (B) To account for uncertainty in our classification of sensation, we produced 100 sets of observations wherein we probabilistically included *sensed* encounters ($v_k = 1$) estimated from the distribution $v_k|\boldsymbol{w}_k \sim \mathrm{Bern}\big(p(v_k = 1|\boldsymbol{w}_k)\big)$ where $p(v_k = 1|\boldsymbol{w}_k)$ is the probability that the patch was *sensed* as estimated in Figure 2I. To account for uncertainty in our classification of *exploitation*, we substitute the response variable y_k with our estimate of the probability that the patch was *exploited* $p(y_k = 1|\boldsymbol{z}_k)$ as estimated in Figure 2H, a procedure analogous to including *exploitations* ($y_k = 1$) estimated from the distribution $y_k|\boldsymbol{z}_k \sim \mathrm{Bern}\big(p(y_k = 1|\boldsymbol{z}_k)\big)$. A schematic of these procedures is shown (see Models of exploitation probability). (C) Coefficient values for each covariate in the GLM were estimated across 50000 replicates (500 replicates of hierarchically bootstrapped animals in combination with 100 sets of probabilistically *sensed* encounters). All coefficients are significantly greater than or less than 0 (two-tailed, one-sample bootstrap hypothesis tests with Bonferroni correction). (D) Using observed $p(y_k = 1|\boldsymbol{z}_k)$ and estimated $p(y_k = 1|\boldsymbol{\beta} \cdot \boldsymbol{x}_k)$ probabilities of *exploitation*, *exploitation* events were simulated from a Bernoulli distribution. Distributions of the probability of first *exploiting* as a function of the number of encounters as estimated by the model with covariates added one-by-one and as observed are shown for animals foraging in single-density, multi-patch environments of relative density 1 or 10. (E) A schematic of multi-density, multi-patch assays where animals foraged in environments containing small (~1.8 mm diameter) bacterial patches (gray) of varying combinations of OP50 *E. coli* with relative densities 1, 4, and 7 is shown. (F) The probability of exploitation as estimated with ($p(y_k = 1|\beta_0 + \beta_k\rho_k + \beta_s\tau_s + \beta_h\rho_h + \beta_e\rho_e)$) and without ($p(y_k = 1|\beta_0 + \beta_k\rho_k + \beta_s\tau_s)$) the history-dependent terms and as observed $p(y_k = 1|\boldsymbol{z}_k)$ is shown for every pairing of current patch density (ρ_k) combined with the density of recently encountered (ρ_h) or *exploited* (ρ_e) patches. Heat maps for observed values were interpolated between the 9 patch density pairings tested. (G) *Exploitation* events were simulated from the distribution $y_k|\boldsymbol{z}_k \sim \mathrm{Bern}\big(p(y_k = 1|\boldsymbol{z}_k)\big)$ and used to calculate the probability of observing *exploitation* for the first time as a function of the number of encounters for N2, *mec-4*, and *osm-6* animals foraging in single-density, multi-patch environments of relative density 1 or 10. (H) Coefficient values for each covariate were estimated using ridge regression models for each strain across 50000 replicates. A subset of these coefficients significantly varied between wild-type and mutant strains (mean of differences tests with Benjamini-Hochberg correction). Summary data for all animals (N = 443 total worms; N = 20-50 worms per condition) and encounters (μ = 2659.8, σ = 15.9) in the single-density, multi-patch assay are shown in (C,D). Summary data for all animals (N = 198 total worms; N = 20-40 worms per condition) and *sensed* encounters (μ = 1,724.6, σ = 9.9) in the multi-density, multi-patch assay are shown in (F). Summary data for all wild-type and mutant animals (N = 221 total worms; N = 14-44 worms per condition) and encounters (N = 1,352 total encounters) in a single-density, multi-patch assay are shown in (G,H). Violin plots in (C,H) show the KDE and quartiles for each measure. Asterisks denote statistical significance († $p_{unadjusted}$<0.05; *p<0.05; **p<0.01; ***p<0.001). See also Figure 4 – supplement 1-5.

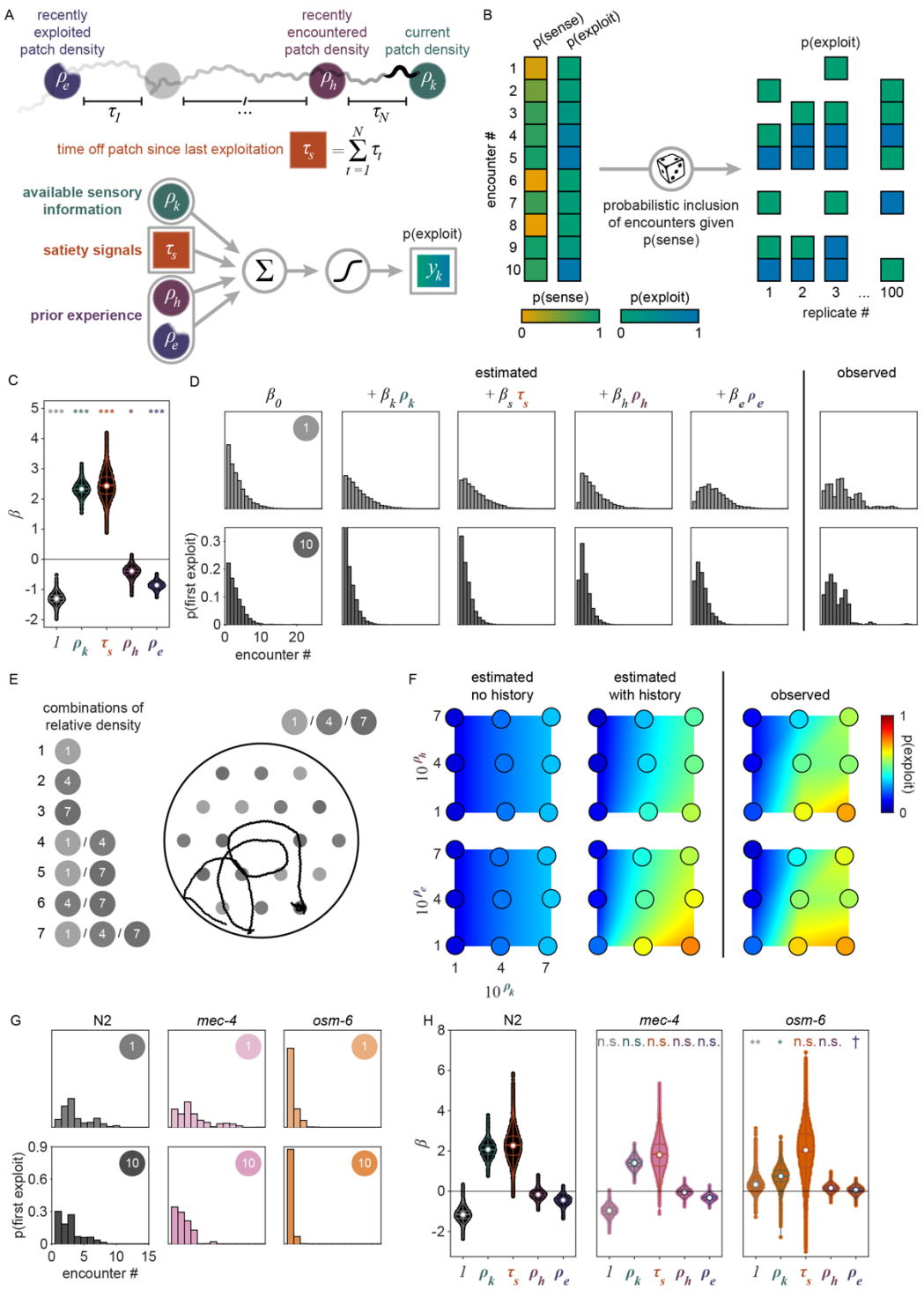
A
recently exploited patch density
recently encountered patch density
current patch density
time off patch since last exploitation
available sensory information
satiety signals
prior experience
p(exploit)
B
p(sense)
p(exploit)
encounter #
probabilistic inclusion of encounters given p(sense)
replicate #
C
D
estimated
observed
p(first exploit)
encounter #
E
combinations of relative density
F
estimated no history
estimated with history
observed
p(exploit)
G
N2
mec-4
osm-6
p(first exploit)
encounter #
H
N2
mec-4
osm-6

1376

Figure Supplements

Figure 1 – supplement 1: Assay preparation, arena and patch detection, and behavioral tracking.

(A) Graphic describing the steps to prepare assay plates. Created with BioRender. (B) Example frames from a "contrast video" showing how a piece of dark cardstock passed between the light source and the assay plate enables visualization of dilute bacterial patches. (C) An image of the bacterial patches is generated from the "contrast video". (D) Masks of the arena (black) and bacterial patches (gray) were constructed using image processing techniques and, when applicable, subsequent manual corrections (see Bacterial patch location detection). Arena masks were used to calculate the image scale in pixels/mm. (E) Example frame from a behavior video containing four adult *C. elegans* is shown. (F) WormLab was used to identify the midbody location of animals in each frame (see Behavioral tracking). An inset shows detection of one of the four worms. (G) An example animal's tracked location as it forages in this environment is plotted with color used to represent time (dark blue = 0 mins; dark red = 60 mins).

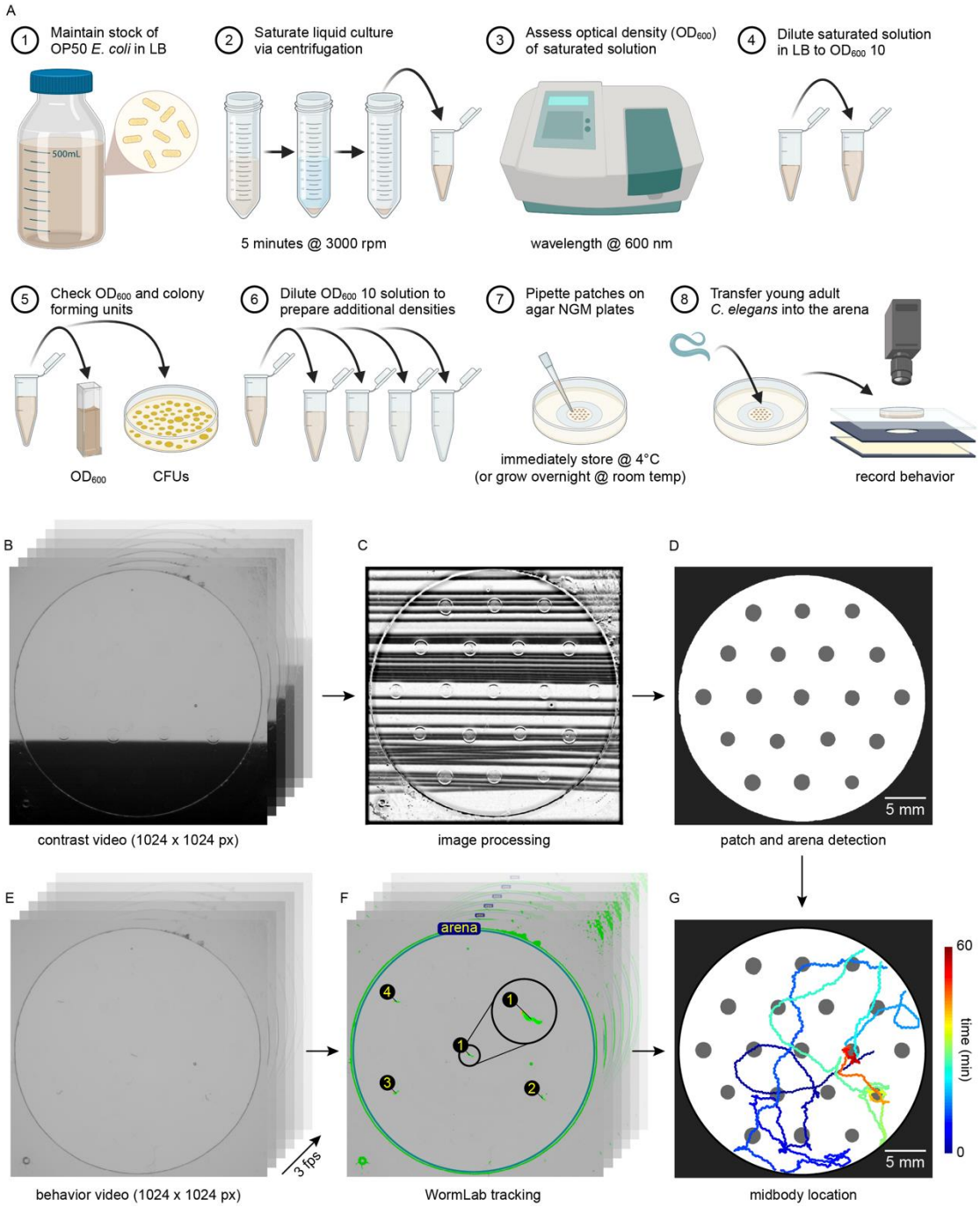
A
1 Maintain stock of OP50 E. coli in LB
500mL
2 Saturate liquid culture via centrifugation
5 minutes @ 3000 rpm
3 Assess optical density (OD600) of saturated solution
wavelength @ 600 nm
4 Dilute saturated solution in LB to OD600 10
5 Check OD600 and colony forming units
OD600
CFUs
6 Dilute OD600 10 solution to prepare additional densities
7 Pipette patches on agar NGM plates
immediately store @ 4°C
(or grow overnight @ room temp)
8 Transfer young adult C. elegans into the arena
record behavior
B
contrast video (1024 x 1024 px)
C
image processing
D
5 mm
patch and arena detection
E
3 fps
behavior video (1024 x 1024 px)
F
arena
WormLab tracking
G
60
time (min)
0
5 mm
midbody location

1392

Figure 1 – supplement 2: Defining a patch encounter using high resolution behavioral recordings.

(A) Example frame from a behavior video containing one adult *C. elegans* is shown. (B) WormLab was used to track the body of the animal in each frame (see Behavioral tracking). (C) An example image showing the center spline of the example animal as well as the location of the bacterial patch (gray) and arena (black). The inset shows the animal's center spline and bacterial patch superimposed on top of the raw image. (D) Example body postures/orientations (black) of an animal during frames when its head is on the patch edge. The distance (blue lines) between the head (black dot) and midpoint (blue dot) of the animal was calculated. A histogram of this head-to-midpoint distance is plotted, and the median value (blue) is indicated (sample size: 220 animals; 74839 frames). The median head-to-midpoint distance was subsequently used as a threshold for detection of patch encounter and leaving events. For one example animal, the distance between the head (black) or midbody (blue) position and the nearest patch edge (positive = inside patch; negative = outside patch) is plotted for every time point. The edge of the patch (solid black line) and threshold for encounter detection (dashed -.- black line) are indicated. Putative patch encounter (green) and leaving (red) events are shown. (E) Example body postures/orientations of an animal when its head is on the patch. The distance between the midpoint of the animal and the patch edge (blue lines) was calculated. A histogram of this midpoint-to-patch distance is plotted, and the 1st percentile (blue) is indicated (sample size: 220 animals; 1571163 frames). This value is used a threshold for excluding putative encounters where the animal's midpoint never comes within 0.28768 mm of the patch edge. A 1.5 minute time window of the example animal's position in (D) is shown. The edge of the patch (solid line), threshold for encounter detection (dashed -.- line), and threshold for encounter exclusion (dashed – line) are indicated. Example putative encounters are shown. The first two sets of enter and exit events were excluded. The third set shown was included. The included encounter is shaded in gray. (F) The standard deviation of the distance between the location of the patch edge and the midpoint of the animal was calculated for every putative on-patch encounter and off-patch event (sample size: 220 animals; 2945 putative on-patch events; 2725 putative off-patch events). A subset of putative off-patch events had low standard deviations matching those of on-patch events. A one-dimensional Gaussian mixture model was fit to the off-patch standard deviation values and a threshold was set where the posterior probability of events falling in the high or low variance cluster was 0.5. A 1.5 minute time window of the example animal's position in (D) is shown. Examples of two excluded off-patch events and one included event are shown.

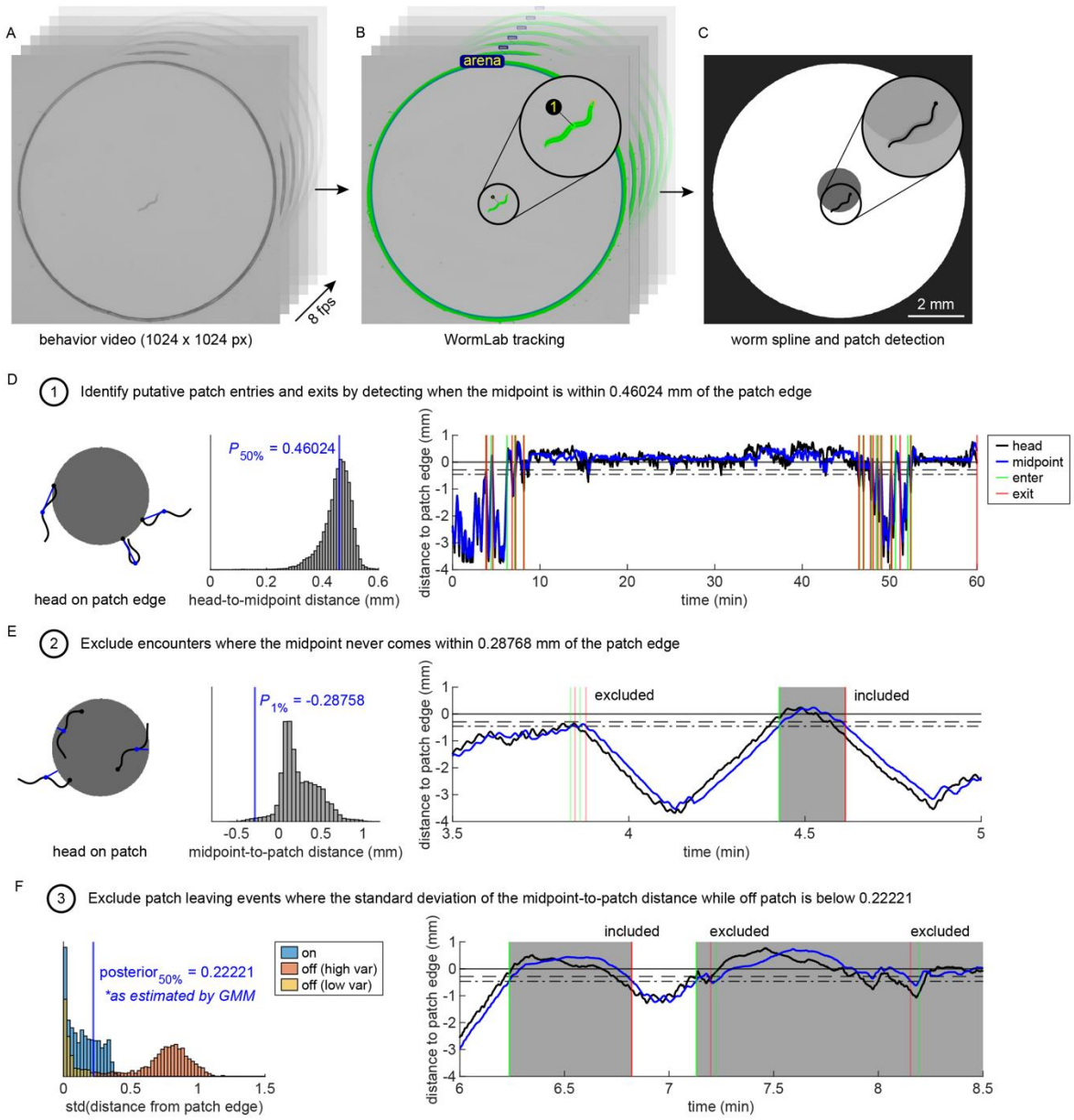
A
B
C
arena
8 fps
2 mm
behavior video (1024 x 1024 px)
WormLab tracking
worm spline and patch detection
D
1 Identify putative patch entries and exits by detecting when the midpoint is within 0.46024 mm of the patch edge
head on patch edge
P50% = 0.46024
head-to-midpoint distance (mm)
distance to patch edge (mm)
time (min)
head
midpoint
enter
exit
E
2 Exclude encounters where the midpoint never comes within 0.28768 mm of the patch edge
head on patch
P1% = -0.28758
midpoint-to-patch distance (mm)
excluded
included
F
3 Exclude patch leaving events where the standard deviation of the midpoint-to-patch distance while off patch is below 0.22221
posterior50% = 0.22221
*as estimated by GMM
on
off (high var)
off (low var)
std(distance from patch edge)
included
excluded
excluded

1426

Figure 1 – supplement 3: Classifying encounters based on duration using a Gaussian mixture model.

(A) As in Figure 1E, duration for each patch encounter (N = 419 events; 50 worms) was computed and classified as either short or long using a Gaussian mixture model (GMM). The distributions of all observed short and long encounters are plotted with duration binned logarithmically. The probability density functions for the two component Gaussians are shown. (B) The posterior probabilities for classification as short or long are sorted for all encounters, highlighting the low posterior variance of the GMM. (C) Given that some patch encounters were not fully observed (i.e., ~22% of animals were already on patch at the start of the recording and ~96% of animals were on patch when the recording ended), we identified that ~14% of observed patch durations were left-censored (i.e., having actual duration ≥ observed duration). Thus, to confirm findings in Figure 1E-F, we re-classified only non-censored observations where both the entry and exit of a patch encounter were observed. As in Figure 1C, patch encounters for 50 individuals foraging in these patchy environments are plotted across time. Encounters that were uncensored (pink) and censored (gray) are indicated. (D) The distribution of the duration of only fully observed (uncensored) encounters (N = 360 events; 50 worms) is plotted. The component Gaussians for a GMM fitting this subset of data are shown. (E) Sorted posterior probabilities for the uncensored model are shown. (F) The observed start time of each uncensored patch encounter is shown for all short and long duration encounters. Long duration encounters occur significantly later (Mann-Whitney U-Test, ***p<0.001). Violin plots show the KDE and quartiles for each duration type. (G) Posterior probabilities for classification in the long duration cluster are shown for the two models. The uncensored data model results in a slight increase in posterior probabilities of long duration classification, but ultimately affected classification of only one of the 419 encounters.

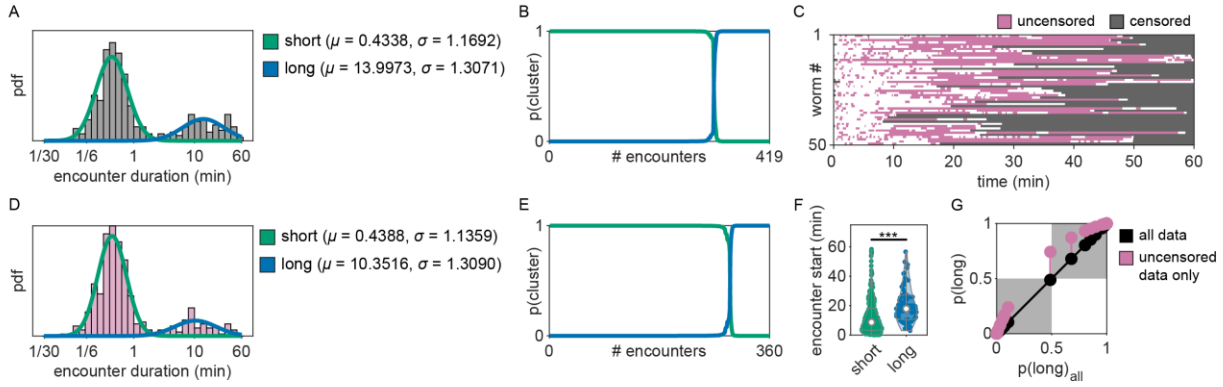

1453 **Figure 1 – supplement 4: Permuting patches to test for significance of the observed time-**
1454 **dependent increase in patch residence.**
1455
1456 (A) Locations of bacterial patches (dark gray) are shown with the threshold for putative encounters
1457 (light gray) set at 0.46024 mm as described in Figure 1 – supplement 2 and Patch encounter
1458 detection. (B) Patches were permuted via randomized rotation and translation with the restriction
1459 that patches could not overlap with other patches nor with the arena. (C,D) Midbody location of the
1460 animal over time was overlaid on the original and semi-randomly permuted patches. (E,F) On patch
1461 events were subsequently identified. This permutation procedure was repeated for 1000 replicates
1462 for every worm tested. Smoothed median values of the probability of worms residing on patch over
1463 time was compared for every time point in Figure 1G, 2F and Figure 2 – supplement 5.
1464

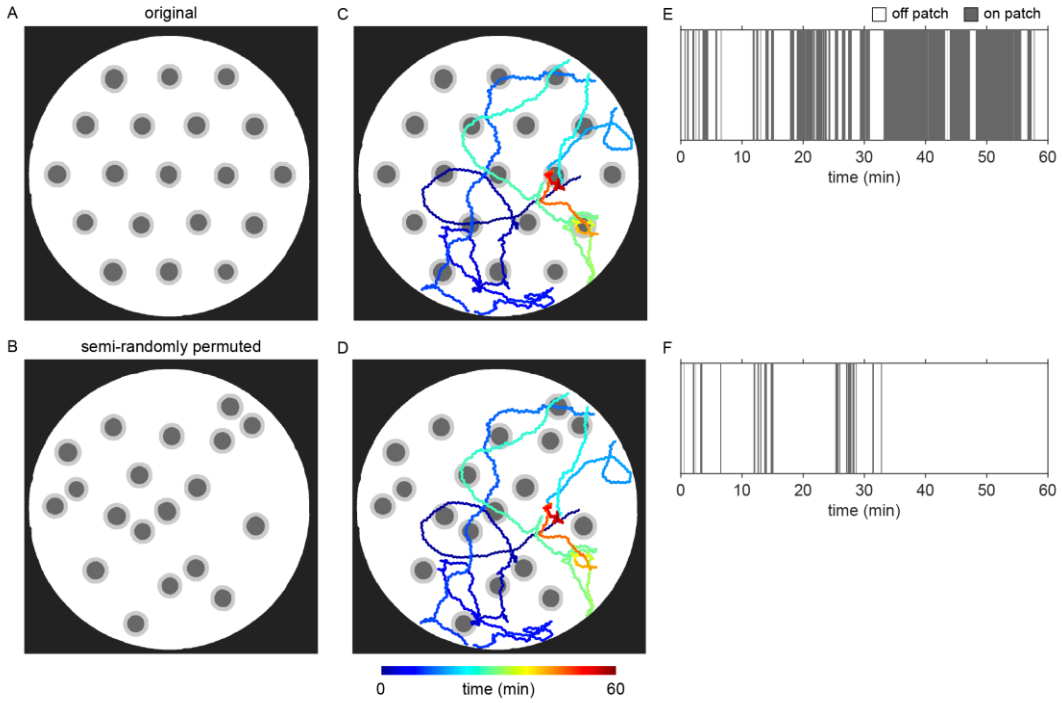

1465

Figure 1 – supplement 5: Analyzing deceleration upon encounter with a patch.

(A) To quantify the magnitude of slow-down upon encounter with the patch edge, we averaged the velocity trajectories across encounters and found the velocity reached a maximum at 1.5 seconds before (green) and a minimum at 6 seconds after (red) the start of the encounter (gray). (B,C) Subsequently, for every encounter, a line (blue) was fit to the animal's velocity (black) for that 8 second time window surrounding the start of the encounter. Deceleration was defined as the slope of this line. Examples matching (B) the short duration encounter in Figure 1J and (C) the long duration encounter in Figure 1K are shown.

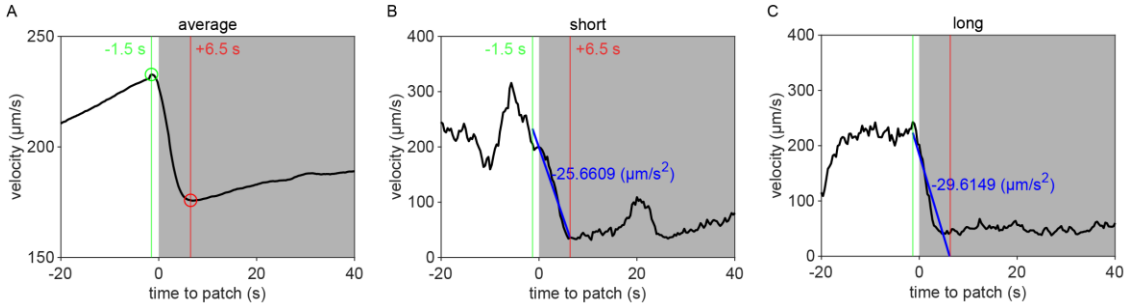

1477 **Figure 2 – supplement 1: Obtaining intensity profiles for fluorescent bacterial patches.**
1478
1479 (A) Fluorescently labeled OP50-GFP bacterial patches were seeded onto agar plates under
1480 conditions matching those in the experimental assay. Small patches (0.5 μL) were pipetted in an
1481 isometric grid (6 mm center-to-center spacing) on a 16 x 25 mm rectangular template comparable to
1482 the one used in behavioral assays. Large patches (20 or 200 μL) were seeded directly onto agar plates.
1483 Brightfield and fluorescence images were acquired for every condition at multiple time points of
1484 bacterial growth. The fluorescence intensity profile of these images was obtained. (B) Due to
1485 uneven illumination within the field-of-view of our imaging system, matched fluorescence images of
1486 an empty agar plate were acquired at each time point. These "background" images were smoothed
1487 using a two-dimensional averaging filter to remove noise. (C) Fluorescence images of the bacterial
1488 patches were normalized to these background images. (D) Locations of bacterial patches within the
1489 template were automatically detected using image processing techniques. Each patch was then
1490 radially segmented in bins of equal area. The mean pixel intensity value for each bin was computed
1491 and used to create an intensity profile of the patch. (E) The patch border and peak were detected
1492 using signal processing techniques. Specifically, the patch border was identified by finding a peak in
1493 the curvature κ of the edge profile. Border amplitude was defined as the magnitude of the
1494 difference between the patch border and peak. Relative border amplitude was defined as the border
1495 amplitude divided by the exposure time. A line was fit to the values of relative border amplitude
1496 across numerous time points and experiment days (5 replicates shown as varying color points).

A

1 Brightfield and fluorescence images were acquired of OP50-GFP bacterial patches seeded uniformly using a template.

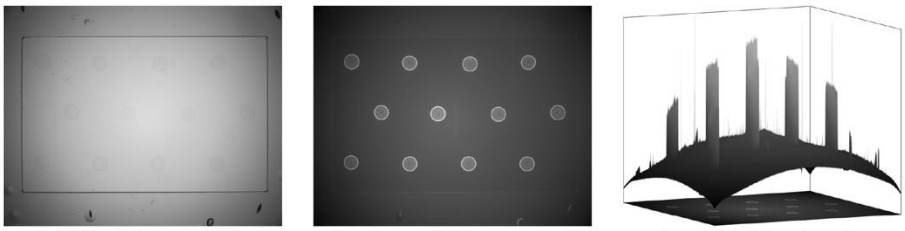

brightfield (2208 x 2752 px) | fluorescence (3000 ms exposure) | fluorescence intensity profile

B

2 As the diffusion of light in our imaging system resulted in uneven illumination of the field-of-view, matched fluorescence images of an empty agar plate were acquired for each time point. This "background" image was smoothed using a 2D averaging filter.

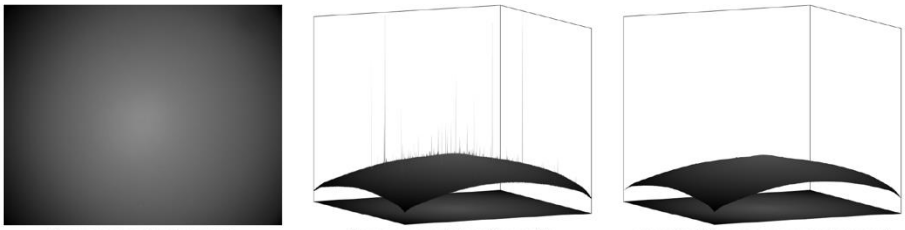

fluorescence background | fluorescence intensity profile | smoothed fluorescence background

C

3 Fluorescence images of the OP50-GFP bacterial patches were normalized to the smoothed background, removing the majority of the illumination-dependent spatial variance in signal intensity.

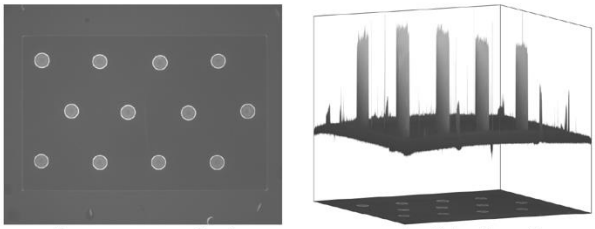

fluorescence normalized | normalized intensity profile

D

4 Arena (16 x 25 mm) and bacterial patch locations were automatically detected via image processing techniques. Each patch was radially segmented in bins of equal area to compute an intensity profile of the patch.

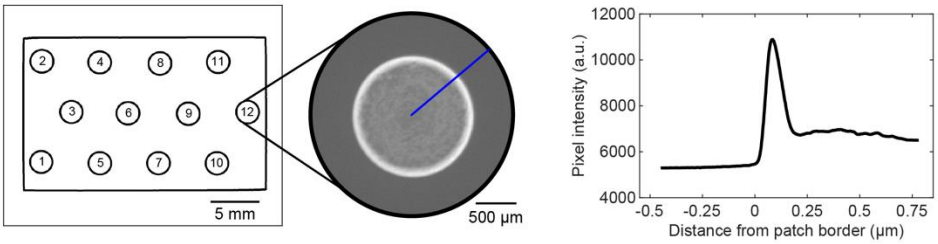

E

5 Using the profiles curvature and maximum value, the patch border and peak were detected. Border amplitude was defined as the difference in magnitude between the peak and border pixel intensities. Border amplitude was divided by exposure time to compute a relative border amplitude that could be compared across time points and patch densities.

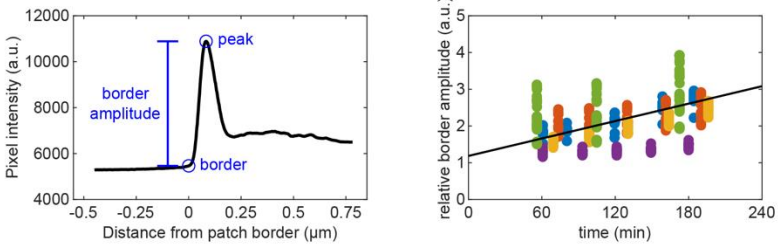

1497

1498 **Figure 2 – supplement 2: Example fluorescence profiles of bacterial patches under varied**
1499 **growth conditions.**
1500
1501 Fluorescently-labeled OP50-GFP bacterial patches were imaged as described in Figure 2 –
1502 supplement 1 and Bacterial patch density estimation. Inverted images (darker saturation = more
1503 bacteria) are shown here to highlight the range of bacterial densities tested in these experiments. All
1504 patches are shown on the same spatial scale and using one of the two linear saturation scales: 1)
1505 regular – normalized to show variance in high density patches; 2) augmented (~22x) – normalized to
1506 show variance in low density patches). Each patch shown is labeled with the optical density (OD_{600})
1507 at time of seeding and the amount of time bacteria was grown for at room temperature (i.e., 1, 12,
1508 or 48 hours). (A) An example large (200 μL) bacterial patch of the type that animals experienced
1509 immediately prior to the assays in this paper. (B) Example small (0.5 μL) bacterial patches of greatest
1510 density. (C) Example small (0.5 μL) bacterial patches of lower density. The saturation of each image
1511 has been uniformly augmented to ~22x darker to the extent that the OD_{600} 10 (1H) bacterial patch is
1512 the same patch as the one in B. (D) Example small (0.5 μL) bacterial patches of lower density seeded
1513 on NGM agar plates lacking peptone. (E) Example medium (20 μL) bacterial patches of greater
1514 density. (F) Example medium (20 μL) bacterial patches of lowest density. The OD_{600} 1 (1H) bacterial
1515 patch is the same patch as the one shown in E, but ~22x darker.

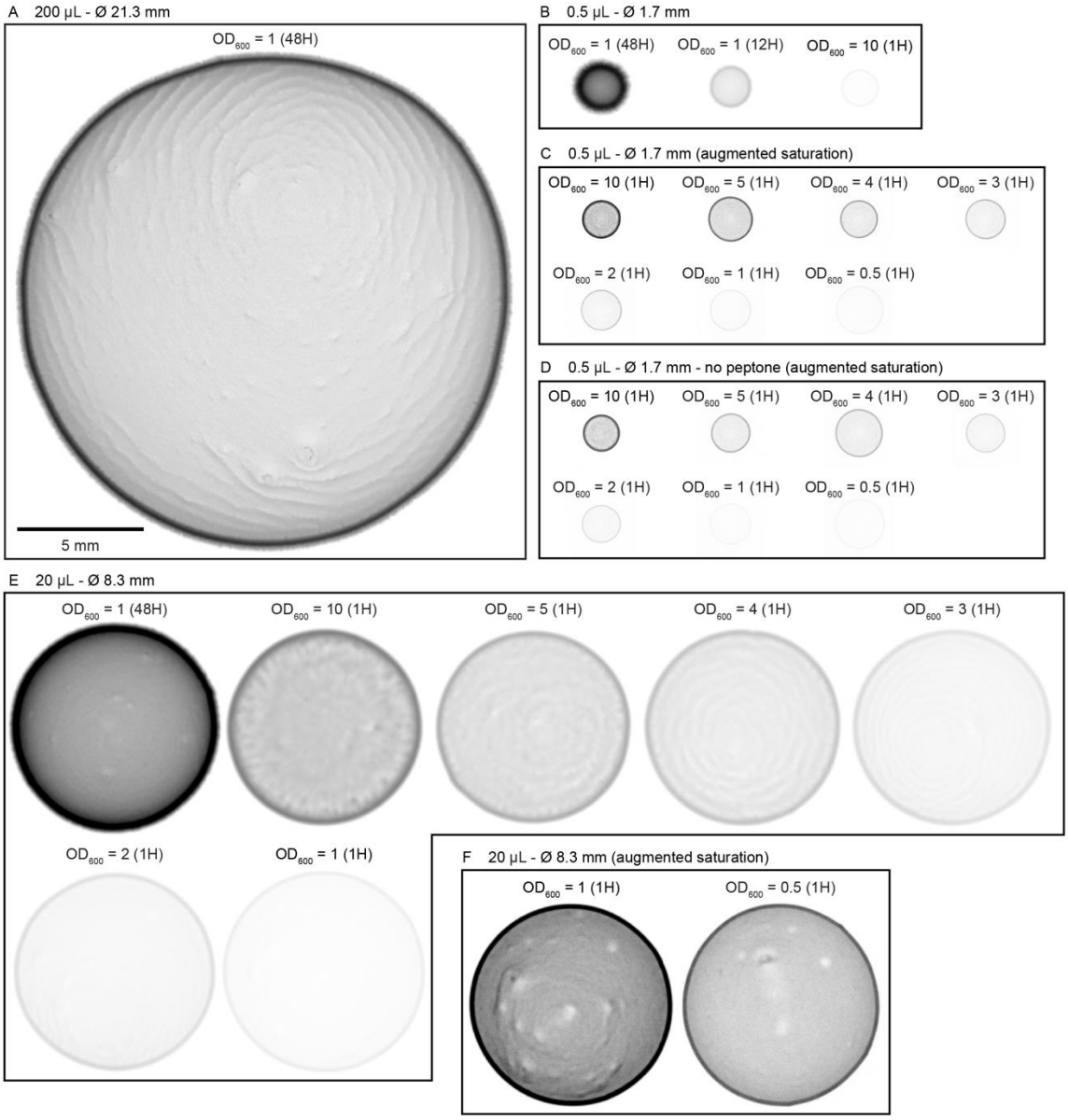
A 200 µL - Ø 21.3 mm
OD600 = 1 (48H)
5 mm
B 0.5 µL - Ø 1.7 mm
OD600 = 1 (48H)
OD600 = 1 (12H)
OD600 = 10 (1H)
C 0.5 µL - Ø 1.7 mm (augmented saturation)
OD600 = 10 (1H)
OD600 = 5 (1H)
OD600 = 4 (1H)
OD600 = 3 (1H)
OD600 = 2 (1H)
OD600 = 1 (1H)
OD600 = 0.5 (1H)
D 0.5 µL - Ø 1.7 mm - no peptone (augmented saturation)
OD600 = 10 (1H)
OD600 = 5 (1H)
OD600 = 4 (1H)
OD600 = 3 (1H)
OD600 = 2 (1H)
OD600 = 1 (1H)
OD600 = 0.5 (1H)
E 20 µL - Ø 8.3 mm
OD600 = 1 (48H)
OD600 = 10 (1H)
OD600 = 5 (1H)
OD600 = 4 (1H)
OD600 = 3 (1H)
OD600 = 2 (1H)
OD600 = 1 (1H)
F 20 µL - Ø 8.3 mm (augmented saturation)
OD600 = 1 (1H)
OD600 = 0.5 (1H)

1516

1517 **Figure 2 – supplement 3: Quantifying the relative density of bacterial patches across**
1518 **conditions and time points.**
1519
1520 (A) Relative density of OP50-GFP bacterial patches matched to all assay conditions in this paper are
1521 shown. Relative density represents the relative border amplitude (as defined in Figure 2 –
1522 supplement 1 and Bacterial patch density estimation) normalized to the mean density of patches
1523 seeded with 0.5 μL of OD_{600} = 10 grown for 1 hour on plates with peptone (blue asterisk). In this
1524 manner, the bacterial patches experienced by animals in Figure 1 have been set to an average relative
1525 density of 10. Violin plots show the KDE and quartiles for each condition. (B) Linear fits for the
1526 relative density of bacterial patches in each condition as a function of time are plotted. Saturation of
1527 each line corresponds to the relative density as depicted in (A). For each experimental plate, the
1528 relative density of bacterial patches was estimated by applying the coefficients from these linear
1529 regressions to the total amount of time the bacteria was grown at room temperature.
1530

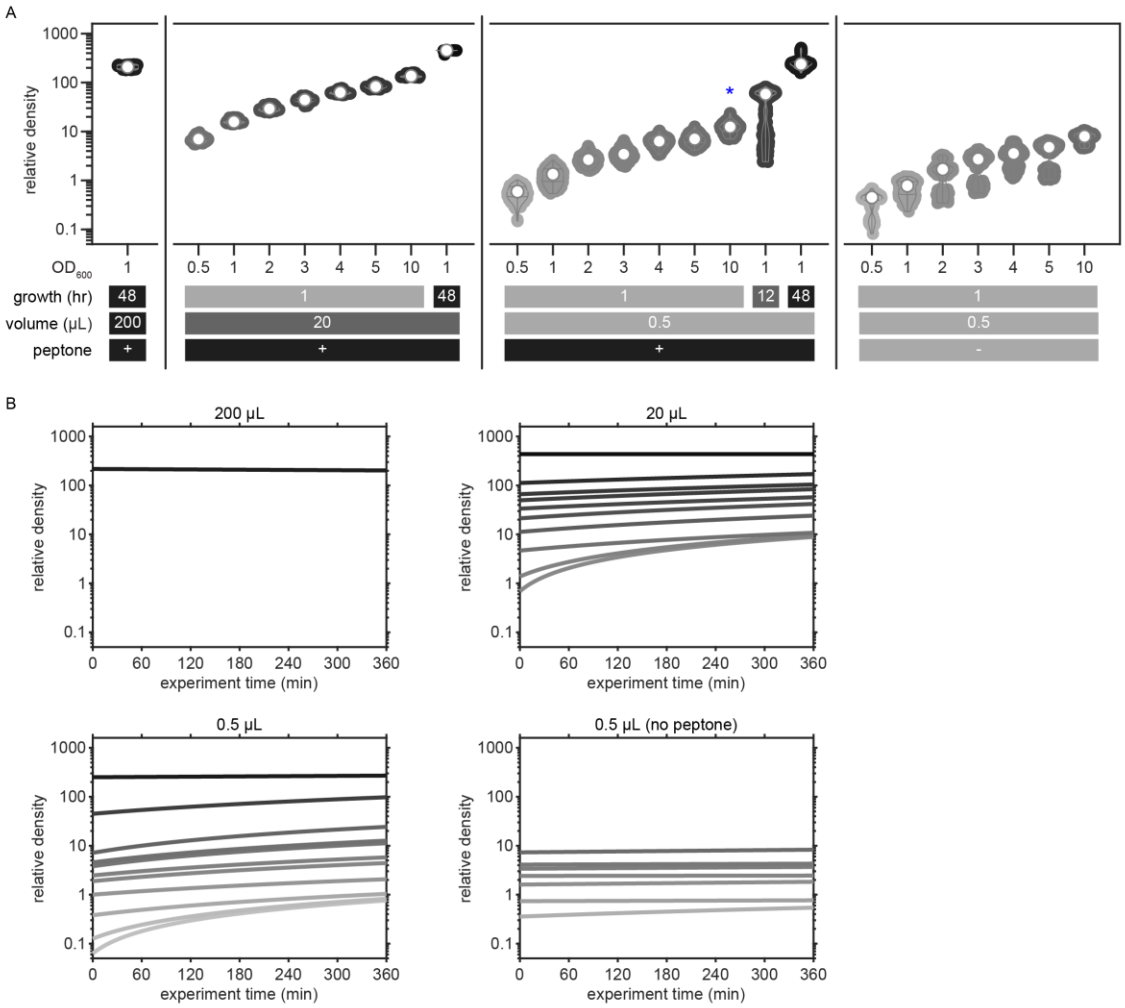

1531

Figure 2 – supplement 4: Example traces of animals foraging in environments with varying bacterial density.

Traces showing the midbody location of 12 example animals as they forage within a 30 mm arena are plotted with color used to represent time (dark blue = 0 mins; dark red = 60 mins). Locations of bacterial patches are indicated in gray. The relative density of bacterial patches in each environment is noted. Animals shown foraging on relative density 0, 1, 5, 10, and 200 are the same as those in Figure 2D.

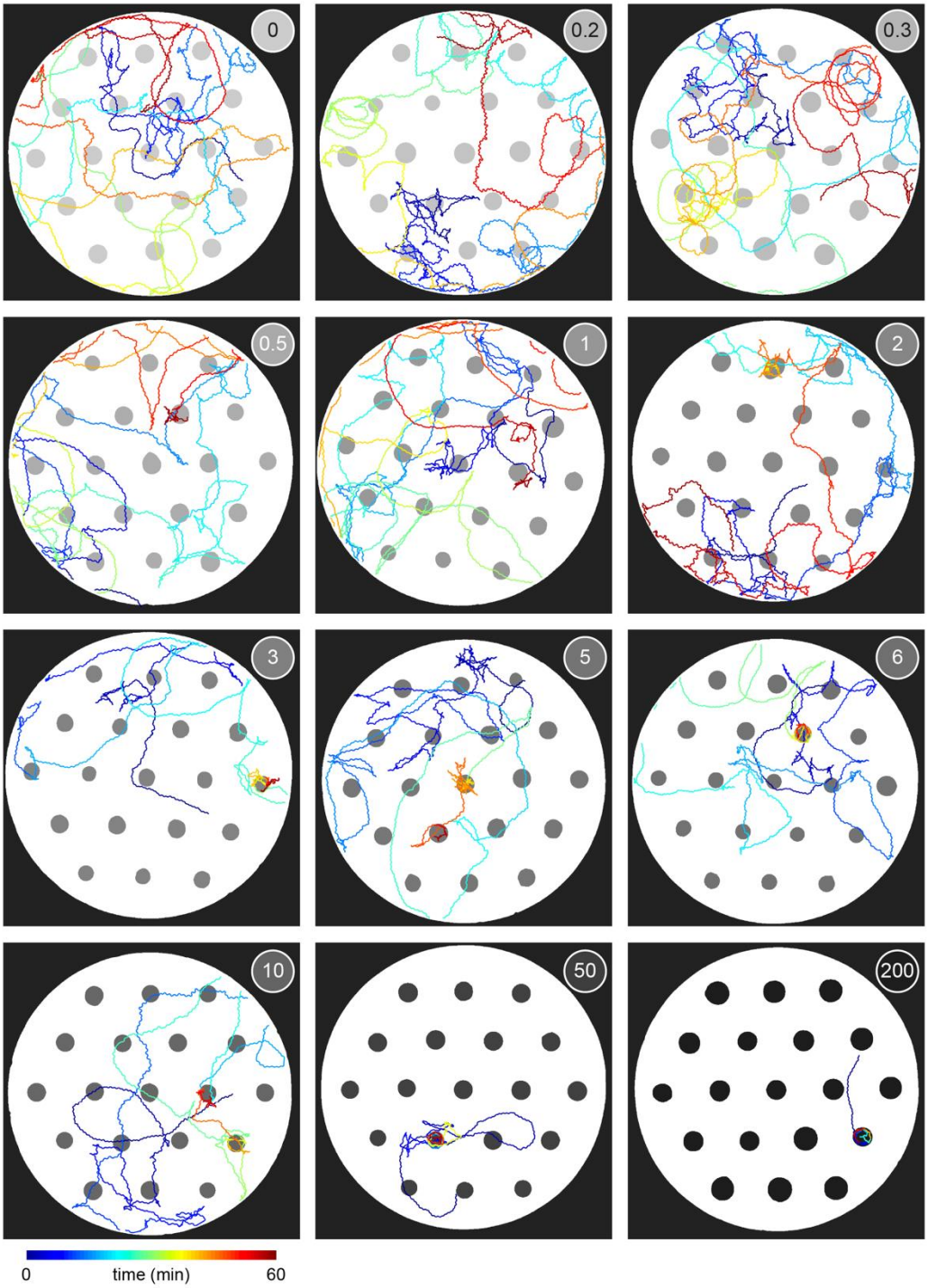

1541

1542 **Figure 2 – supplement 5: Time- and density-dependent increase in patch residence.**
1543
1544 Probability of residing on patch was computed for all worms across time (black) and compared to
1545 the probability of residing on patch for semi-randomly permuted patch locations (pink) as described
1546 in Figure 1 – supplement 4. Smoothed median values are plotted with bootstrap-derived 2.5% and
1547 97.5% quantiles shown in shaded regions. Time points where observed probabilities of residing on
1548 patch significantly exceed permuted probabilities are indicated by a black line (one-tailed Fisher's
1549 Exact Tests with Benjamini-Hochberg correction, ***$p < 0.001$). The smoothed median values for
1550 observed data are shown in Figure 2F. Data for relative density 10 match those in Figure 1G.
1551

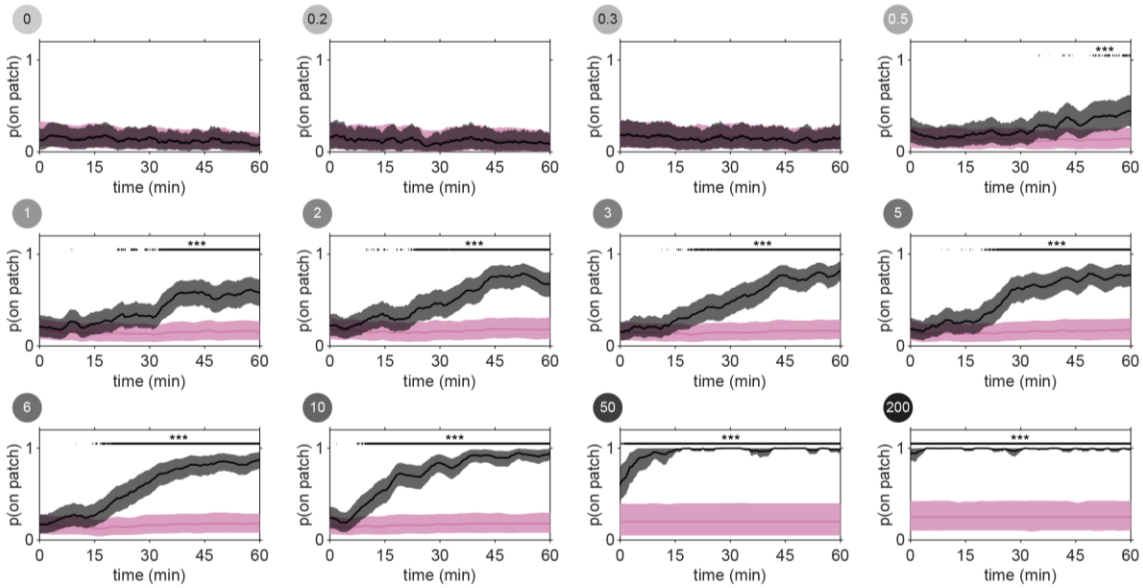

1552

Figure 2 – supplement 6: Classifying encounters as exploration or exploitation.

(A) The average velocity of the animal during an encounter and the duration of that encounter are plotted for each encounter as visualized on a double-logarithmic plot. Contours showing the first, second, and third standard deviation of the two-dimensional Gaussian mixture model (GMM) are shown as shaded ellipses with saturation corresponding to standard deviation. Encounters for all data in the paper are individually plotted as in Figure 2H but with color representing the posterior probability of clustering classification as *explore* (green) or *exploit* (blue). (B) Posterior variance of the data as defined in Patch encounter classification as *exploration* or *exploitation* was calculated for 1000 replicates of GMMs with varied regularization value α. The classifier with minimum posterior variance (i.e., $\alpha = 0.025$) was used. (C) The posterior probabilities for classification as *explore* (green) or *exploit* (blue) are sorted for all encounters, highlighting the low posterior variance of the GMM. (D) Posterior probabilities for only the data in Figure 2 are shown.

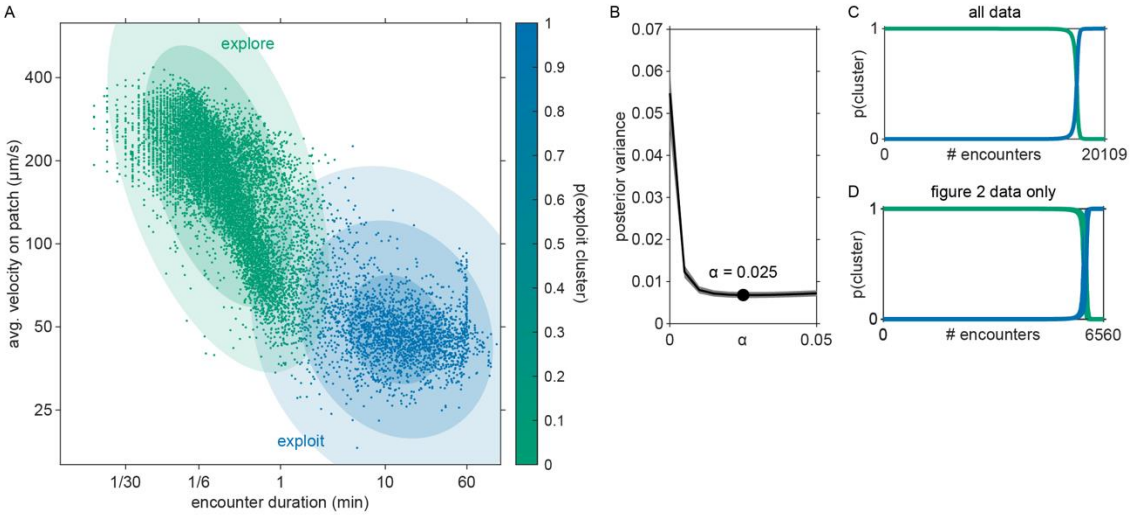

Figure 2 – supplement 7: Classifying encounters as sensing or non-sensing.

(A) Minimum velocity (min. velocity on patch), maximum change in velocity (max. Δ velocity), and deceleration (Δ velocity) were calculated as described in Patch encounter classification as sensing or non-sensing. (B) Maximum change in velocity for every density condition is shown. Violin plots show the KDE and quartiles for each condition. (C) Deceleration upon encounter and minimum on-patch velocity during the encounter are plotted for each encounter. A three-dimensional parabolic boundary between *sensing* and *non-sensing* clusters was fit using semi-supervised QDA and a subset of labeled data (blue circles = sensing, dark orange circles = non-sensing). Regions identified by the classifier as *non-sensing* or *sensing* are indicated by colored contours (orange = *non-sensing*, green = *sensing*). Encounters for all data in the paper are individually plotted as in Figure 2I but with color representing the conditional probability of clustering classification as *non-sensing* (orange) or *sensing* (green). (D) Maximum change in velocity and minimum on-patch velocity during the encounter are plotted for each encounter in the paper as in (C). (E) Minimum velocity on patch, maximum change in velocity, and deceleration are shown for every encounter in the paper. See Video 5 for three-dimensional rotation of this plot. (F) The probabilities for classification as *sense* (green) or *non-sense* (orange) are sorted for all encounters. (G) Probabilities for only the data in Figure 2 are shown. (H) For a subset of encounters that were censored (i.e., recording did not observe animals entering the patch), probabilities of *sensing* were estimated using the semi-supervised QDA approach as well as via marginalization over the conditional probabilities using only the observed minimum velocity on patch. Marginalized probabilities were used for these values as described in Patch encounter classification as sensing or non-sensing.

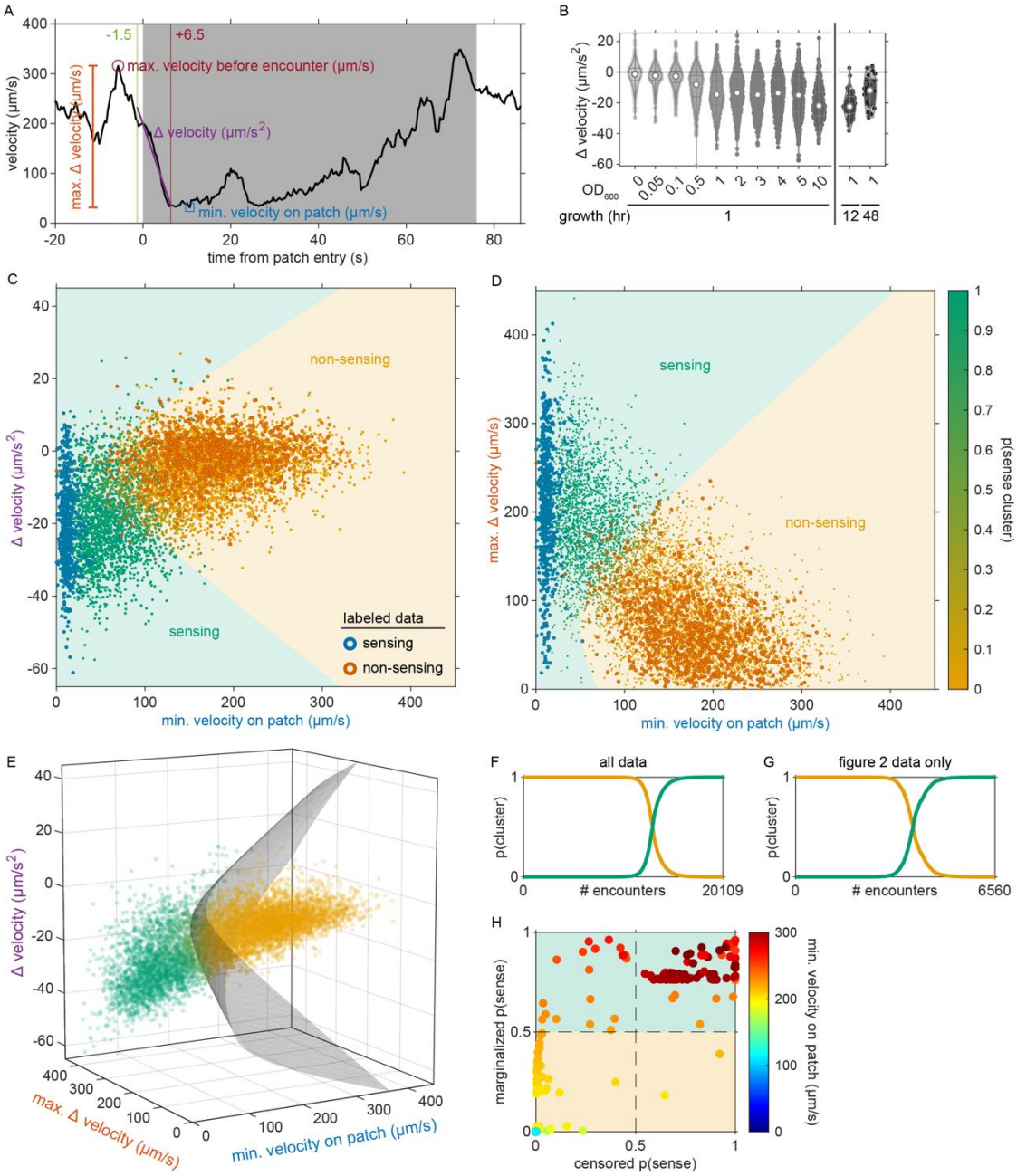
A
-1.5
+6.5
max. velocity before encounter (μm/s)
max. Δ velocity (μm/s)
Δ velocity (μm/s²)
min. velocity on patch (μm/s)
velocity (μm/s)
time from patch entry (s)
B
Δ velocity (μm/s²)
OD600
growth (hr)
C
non-sensing
sensing
labeled data
sensing
non-sensing
Δ velocity (μm/s²)
min. velocity on patch (μm/s)
D
sensing
non-sensing
max. Δ velocity (μm/s)
min. velocity on patch (μm/s)
p(sense cluster)
E
Δ velocity (μm/s²)
max. Δ velocity (μm/s)
min. velocity on patch (μm/s)
F
all data
p(cluster)
# encounters
G
figure 2 data only
p(cluster)
# encounters
H
marginalized p(sense)
censored p(sense)
min. velocity on patch (μm/s)

1590

Figure 3 – supplement 1: Example traces of animals foraging in environments with one large bacterial patch.

Example traces showing the midbody location of 11 animals as they forage within a 30 mm arena are plotted with color used to represent time (dark blue = 0 mins; dark red = 60 mins). Location of bacterial patches are indicated in gray. The relative density of bacterial patches in each environment is noted. The animal shown foraging on relative density 10 is the same as that in Figure 3D.

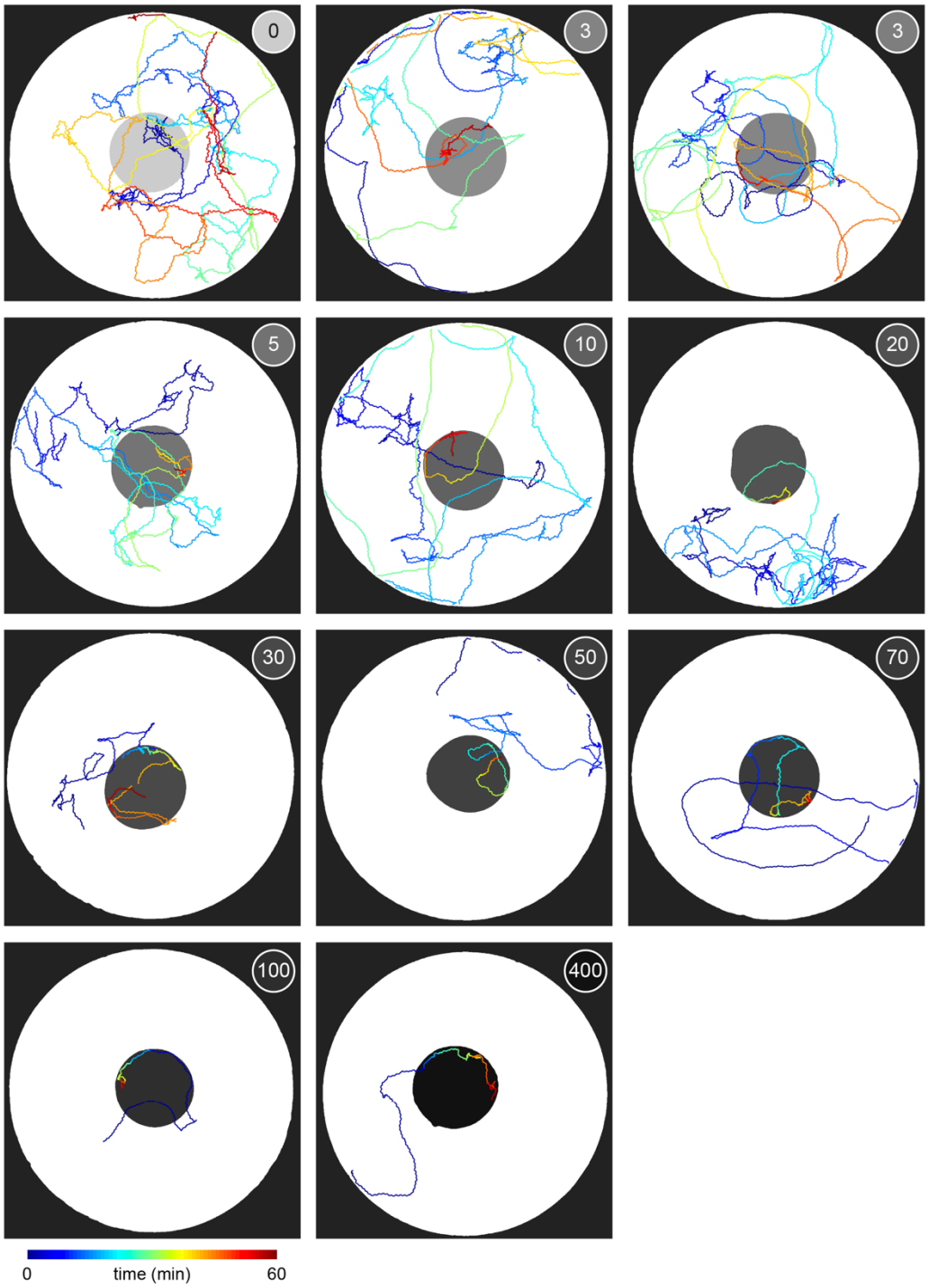

Figure 3 – supplement 2: Example traces of animals foraging in environments with one small bacterial patch.

Example traces showing the midbody location of 6 animals as they forage within a 9 mm arena are plotted with color used to represent time (dark blue = 0 mins; dark red = 60 mins). Location of bacterial patches are indicated in gray. The relative density of bacterial patches in each environment is noted. The animal shown foraging on relative density 10 is the same as that in Figure 2E.

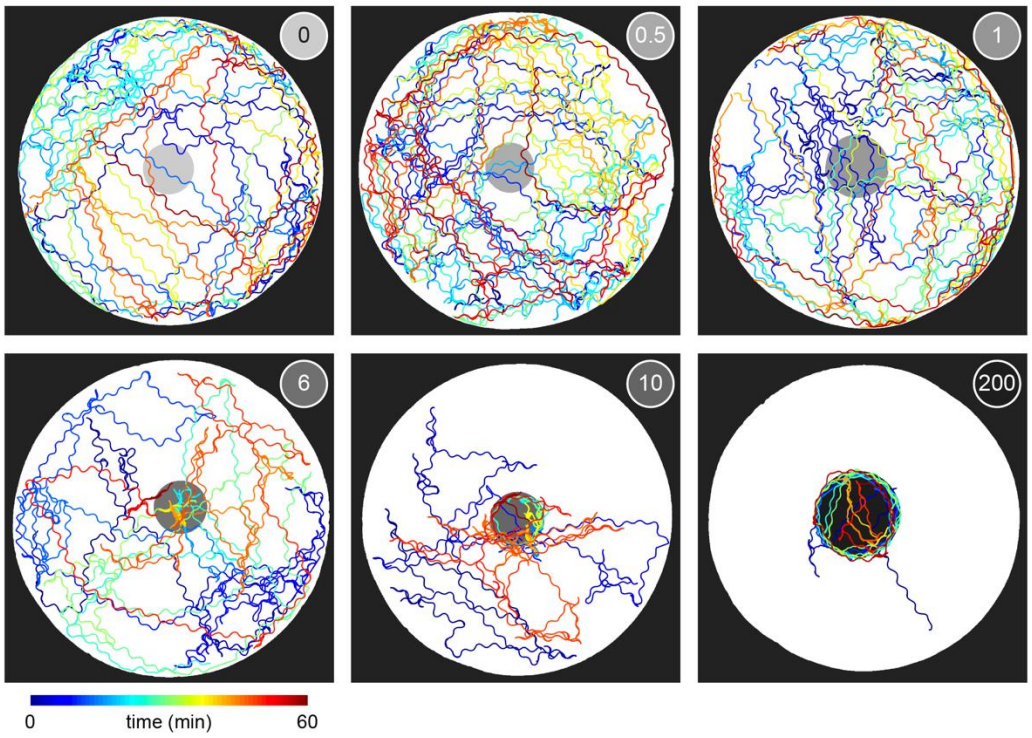

Figure 4 – supplement 1: Model selection for nested GLMs.

(A) Values of log-likehood, Aikake Information Criterion (AIC), and Bayesian Information Criterion (BIC) were computed for 50,000 replicates of the linear regression model described in Models of exploitation probability. Each of these metrics is plotted here across 100 replicates of "encounter samples" (i.e., we removed encounters where the animal likely did not *sense* the encounter $v_k = 0$ as estimated from the distribution $v_k|\boldsymbol{w}_k \sim \text{Bern}\big(p(v_k = 1|\boldsymbol{w}_k)\big)$) and 500 replicates of hierarchically bootstrapped "worm samples" (i.e., we resampled animals with replacement and included all encounters of the resampled animals). Values for each metric at each replicate are colored to match their respective color bar. Metrics were computed for the addition of each covariate to the model. Lower AIC and BIC values for the full model ((i.e., $\boldsymbol{\beta} \cdot \boldsymbol{x}_k = \beta_0 + \beta_k \rho_k + \beta_s \tau_s + \beta_h \rho_h + \beta_e \rho_e$), represent better model performance even with penalization for increasing the number of parameters. (B) Coefficients $\boldsymbol{\beta}^*$ for the null distribution (i.e., observations of the response variable $p(y_k = 1|\boldsymbol{z}_k)$ shuffled relative to the covariates $\boldsymbol{x}_k$) are plotted. Only β_0 was significantly greater than or less than 0 (two-tailed, one-sample bootstrap hypothesis tests with Bonferroni correction). Violin plots show the KDE and quartiles for each covariate across the 50,000 replicates. Asterisks denote statistical significance (*p<0.05; **p<0.01; ***p<0.001). These $\boldsymbol{\beta}^*$ represent the null distribution for the $\boldsymbol{\beta}$ in Figure 4C.

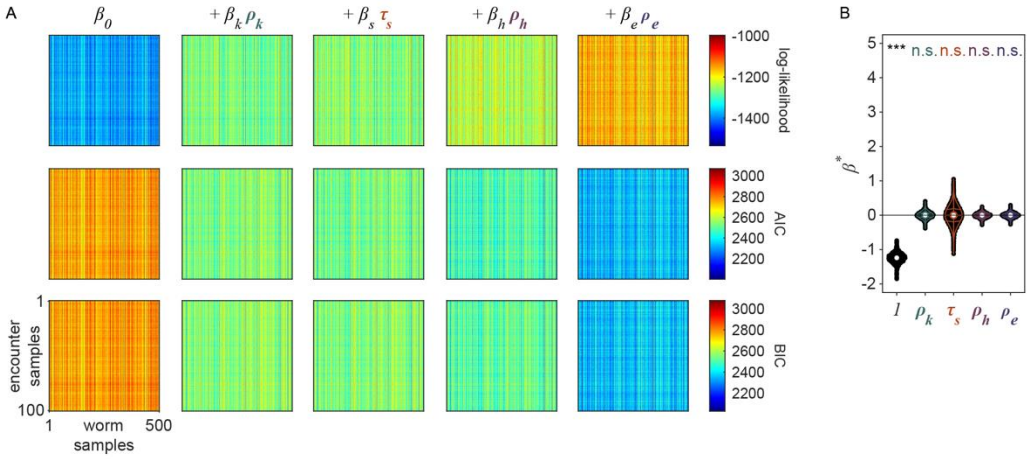

Figure 4 – supplement 2: Probability of first exploitation as a function of the number of encounters.

Histograms of the probability of first *exploiting* as a function of the number of encounters as estimated by the models and as observed are shown for animals foraging in single-density, multi-patch environments of all 12 density conditions. *Exploitation* events were simulated from a Bernoulli distribution with probability estimated by the model $y_k \,|\boldsymbol{x}_k \sim \mathrm{Bern}\big(p(y_k = 1|\boldsymbol{\beta} \cdot \boldsymbol{x}_k)\big)$ where covariates were added one at time as well as from the observed probabilities estimated by the Gaussian mixture model classification $y_k|\boldsymbol{z}_k \sim \mathrm{Bern}\big(p(y_k = 1|\boldsymbol{z}_k)\big)$ in Figure 2H. Histograms for relative density 1 and 10 are the same as those in Figure 4D.

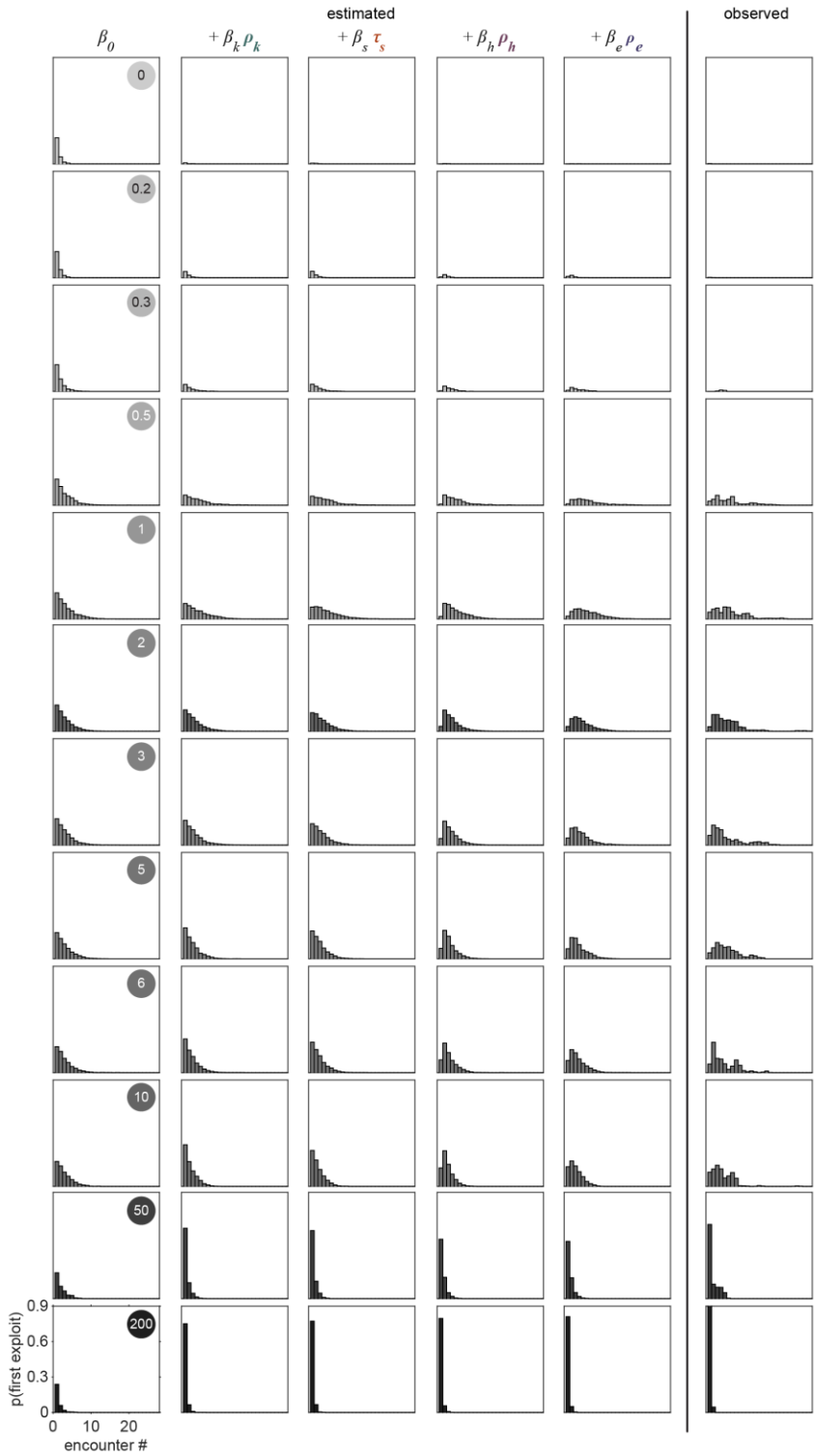
estimated
observed
β_0
$+\beta_k \rho_k$
$+\beta_s \tau_s$
$+\beta_h \rho_h$
$+\beta_e \rho_e$
0
0.2
0.3
0.5
1
2
3
5
6
10
50
200
p(first exploit)
0.9
0.6
0.3
0
0
10
20
encounter #

1638

Figure 4 – supplement 3: Exploitation decision of food-deprived animals is well-predicted by the model.

(A) Schematic of experiments used to test satiety's influence on the decision to *exploit*. As in all experiments, animals were acclimated to high density (relative density ~200) patches for ~24 hours. Well-fed animals were then removed from these acclimation plates, cleaned of bacteria, and then immediately transferred to the assay plate with relative density 5. Food-deprived animals moved about a bacteria-free arena for 3 hours prior to the assay. Examples of animal behavior while foraging in acclimation-like, bacteria-free, and single-density, multi-patch environments of relative density 5 are shown. (B) Patch encounters for 28 food-deprived and 28 well-fed individuals are plotted across time. Each encounter is colored to match its probability of classification as *search* (orange), *sample* (green), and *exploit* (blue). (C) Coefficient values were re-estimated across 50000 replicates as in Figure 4C for a model with the satiety term removed (i.e., $p(y_k = 1|\beta_0 + \beta_k\rho_k + \beta_h\rho_h + \beta_e\rho_e)$). All coefficients are significantly greater than or less than 0 (two-tailed, one-sample bootstrap hypothesis tests with Bonferroni correction; ***p<0.001). Violin plots show the KDE and quartiles for each measure. (D) Histograms of the probability of first *exploiting* as a function of the number of encounters are shown for food-deprived and well-fed animals. Model predictions of *exploitation* events were simulated from a Bernoulli distribution $y_k|\boldsymbol{x}_k \sim \mathrm{Bern}\big(p(y_k = 1|\boldsymbol{\beta}\cdot\boldsymbol{x}_k)\big)$ where the coefficient values $\boldsymbol{\beta}$ corresponded to those previously estimated for our linear regression model with (Figure 4C) and without (Figure 4 – supplement 3C) the satiety term using the data set shown in Figure 2 (i.e., the 443 well-fed animals foraging in one of 12 density conditions). Observed *exploitations* were simulated from a Bernoulli distribution using the probability of *exploitation* estimated by our GMM classifier $y_k|\boldsymbol{z}_k \sim \mathrm{Bern}\big(p(y_k = 1|\boldsymbol{z}_k)\big)$ in Figure 2H. Summary data for all animals (N = 56 total worms; N = 28 worms per condition) and encounters (N = 277 total encounters; N = 42-235 encounters per condition) are shown in (B,D).

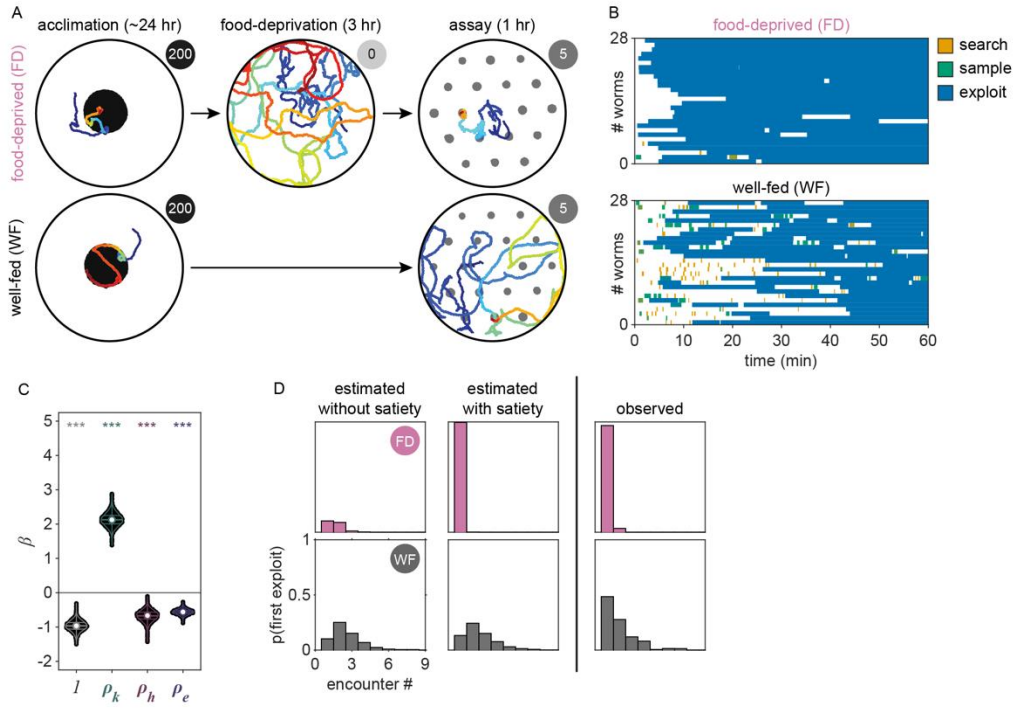

Figure 4 – supplement 4: Example traces and classified behavior of animals foraging in environments with multiple patch densities.

(A) Example traces showing the midbody location of 7 animals as they forage within a 30 mm arena are plotted with color used to represent time (dark blue = 0 mins; dark red = 60 mins). Locations of bacterial patches are indicated in gray with saturation indicating the relative density. Environments contained combinations of patches with relative density 1, 4, and 7 as noted. (B) Patch encounters for 200 individuals (20-40 per condition) are plotted across time. Each encounter is colored to match its relative density. (C) Patch encounters are colored to match their probability of classification as *search* (orange), *sample* (green), and *exploit* (blue). (D) Coefficient values were re-estimated across 50000 replicates as in Figure 4C for a model with the history-dependent terms removed (i.e., $p(y_k = 1|\beta_0 + \beta_k\rho_k + \beta_s\tau_s)$). All coefficients are significantly greater than or less than 0 (two-tailed, one-sample bootstrap hypothesis tests with Bonferroni correction; **p<0.01; ***p<0.001). Violin plots show the KDE and quartiles for each measure. Summary data for all animals (N = 198 total worms; N = 20-40 worms per condition) and encounters (N = 3,493 total encounters; N = 282-795 encounters per condition) are shown in (B,C).

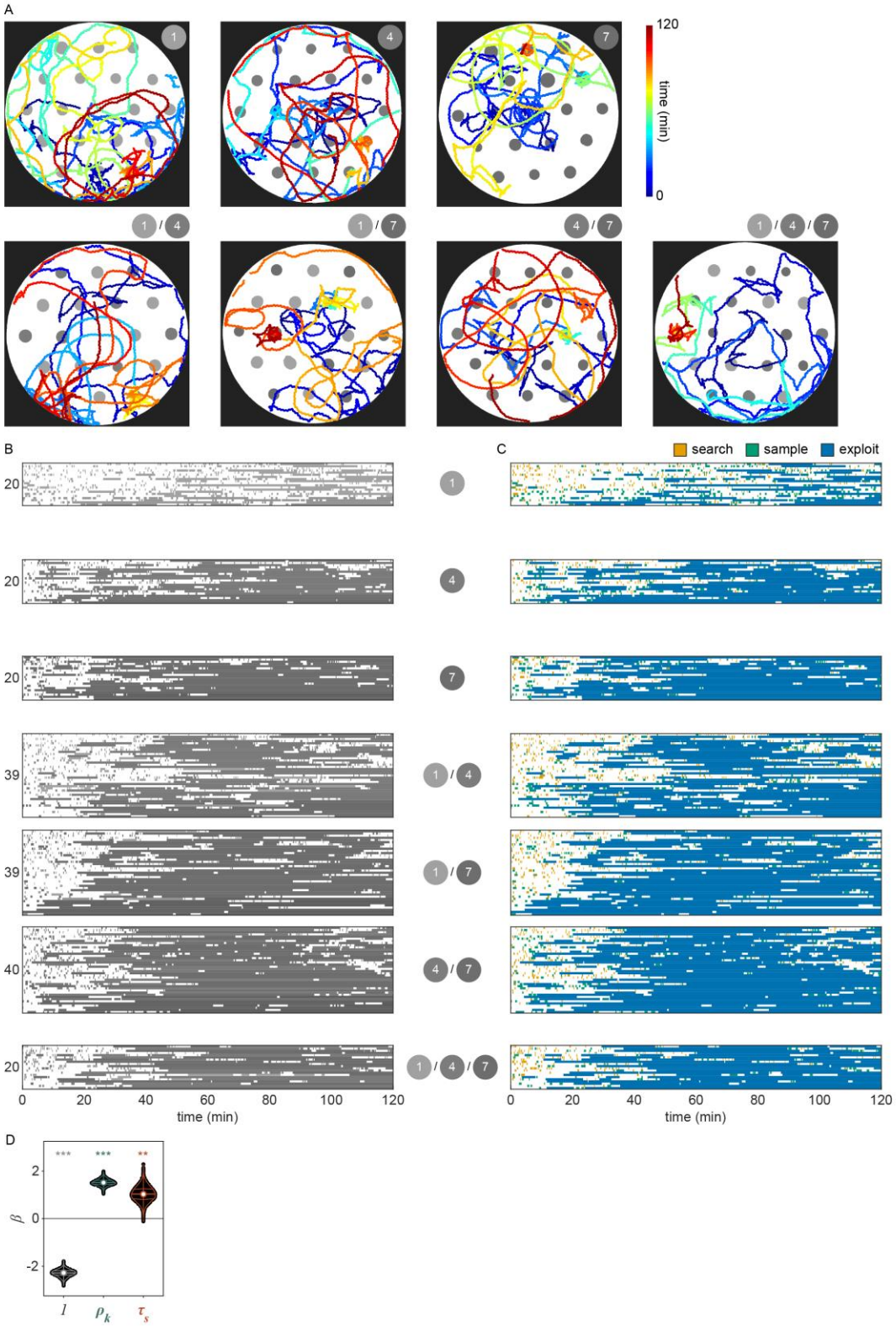
A
120
time (min)
0
1
4
7
1 / 4
1 / 7
4 / 7
1 / 4 / 7
B
C
search
sample
exploit
20
39
40
0
20
40
60
80
100
120
time (min)
D
***
***
**
2
0
-2
β
1
ρ_k
τ_s

Figure 4 – supplement 5: Example traces and classified behavior of animals with chemosensory or mechanosensory deficiencies.

(A) Example traces showing the midbody location of 9 animals as they forage within a 30 mm arena are plotted with color used to represent time (dark blue = 0 mins; dark red = 60 mins Location of bacterial patches are indicated in gray. The relative density of bacterial patches in each environment is noted. 3 strains of *C. elegans* were tested (grey = N2, pink = *mec-4*, orange = *osm-6*) across 3 conditions of relative density (1, 5, and 10). (B) Patch encounters for 76 individuals (16-44 per density condition) of each strain are plotted across time. Each encounter is colored to match its probability of classification as *search* (orange), *sample* (green), and *exploit* (blue). (C) Histograms of the probability of first *exploiting* as a function of the number of encounters are shown for each strain and density condition. Observed *exploitations* were simulated from a Bernoulli distribution using the posterior probability of *exploitation* defined by our GMM classifier $y_k|\boldsymbol{z}_k \sim Bern\big(p(y_k = 1|\boldsymbol{z}_k)\big)$ in Figure 2H. Histograms of each strain for relative density conditions 1 and 10 are the same as those in Figure 4G. (D) Coefficients $\boldsymbol{\beta}^*$ for the null distribution (i.e., observations of the response variable $p(y_k = 1|\boldsymbol{z}_k)$ were shuffled relative to the covariates $\boldsymbol{x}_k$) are plotted. Violin plots show the KDE and quartiles for each covariate across the 50,000 replicates. These $\boldsymbol{\beta}^*$ represent the null distribution for the $\boldsymbol{\beta}$ in Figure 4H. (E) The ridge regression parameter λ was optimized for each strain to maximize the mean log-likelihood of the model. Summary data for all animals (N = 221 total worms; N = 14-44 worms per condition) and encounters (N = 1,352 total encounters; N = 27-193 encounters per condition) are shown in (B,C).

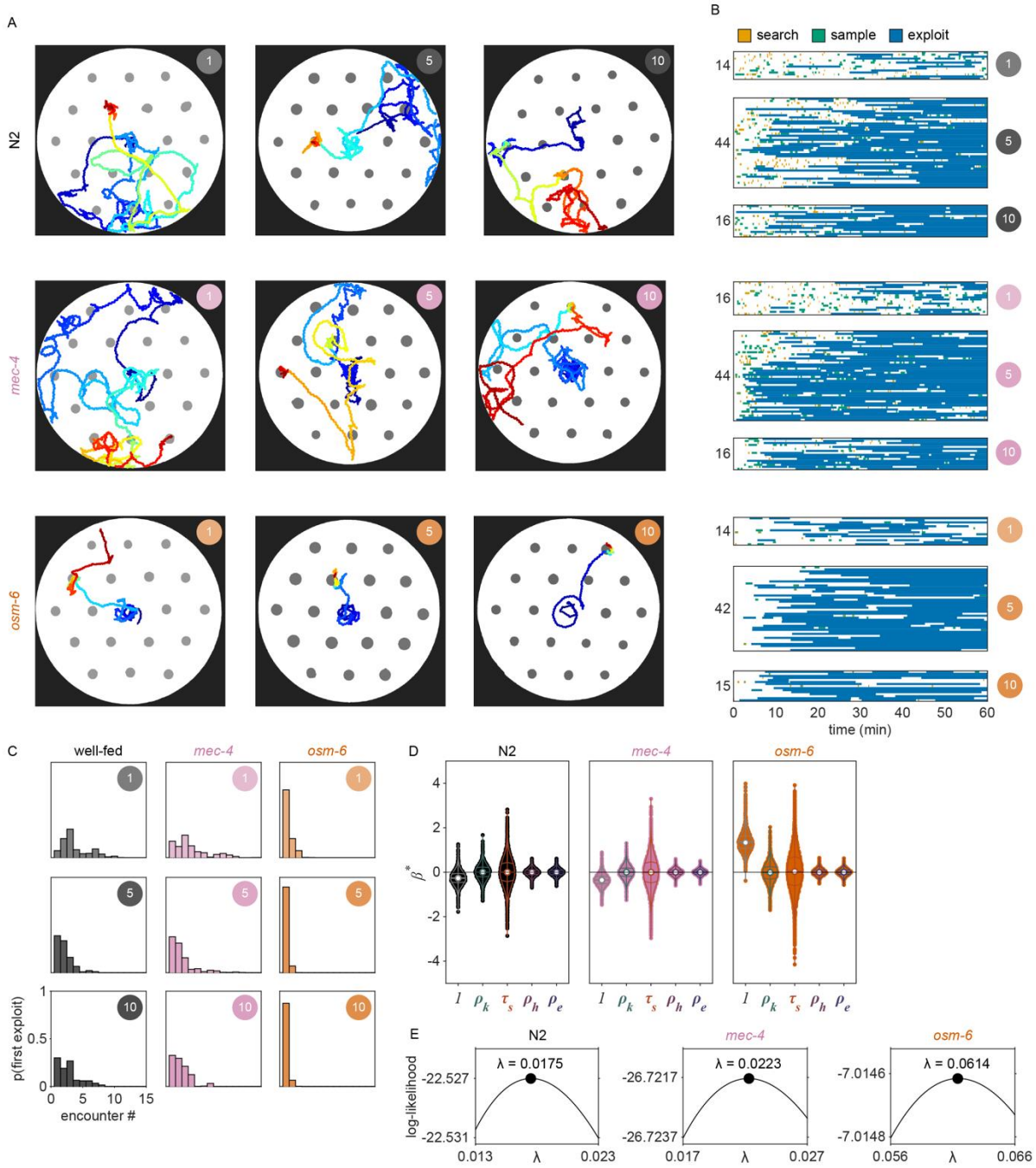
A
N2
mec-4
osm-6
B
search
sample
exploit
time (min)
C
well-fed
mec-4
osm-6
p(first exploit)
encounter #
D
N2
mec-4
osm-6
E
N2
mec-4
osm-6
log-likelihood
λ = 0.0175
λ = 0.0223
λ = 0.0614

1704

Video Legends

Video 1. *C. elegans* foraging in a patchily distributed environment.
Four adult *C. elegans* forage for one hour in a 30 mm arena containing an isometric grid of small, low density bacterial patches.

Video 2. Visualizing dilute bacterial patches using diffraction of light.
A piece of dark cardstock passed between the light source and the assay plate enables visualization of dilute bacterial patches.

Video 3. Tracking the midbody location of an animal foraging in a patchily distributed environment.
The midbody location of one of the four animals shown in Video 1 is shown as the animal forages for one hour in a 30 mm arena containing an isometric grid of small, low density bacterial patches. The animal shown corresponds to the example animal observed in Figure 1A-B,H-K.

Video 4. Tracking the entire body of a foraging animal.
The position of the entire body of an animal is shown as the animal forages for one hour in a 9 mm arena containing one small, low density bacterial patch. The head is indicated by a small dot. The animal shown corresponds to the example animal observed in Figure 3D.

Video 5. Classifying encounters as *sensing* based on quantification of slow-down.
Three metrics quantifying the magnitude of slow-down upon patch encounter were computed. A semi-self-supervised quadratic discriminant analysis was trained on a subset of labeled data and used to classify all encounters as *sensing* (green) or *non-sensing* (orange). Data correspond with Figure 2I and Figure 2 – supplement 7C-E.

Video 6. Foraging behavior of an animal with encounters labeled as *search*, *sample*, or *exploit*.
The midbody location of the animal in Video 3 is shown and labeled by the probability of classification as *searching* (i.e., off patch *exploration* and patch encounters that were not *sensed*), *sampling* (i.e., patch encounters that were *sensed*, but not *exploited*), and *exploiting* at every time point. The animal shown corresponds to the example animal observed in Figure 1A-B,H-K.